HEINRICH HEINE
UNIVERSITÄT DÜSSELDORF

Molecular analysis of small Ras-related GTPase genes with potential tumor suppressor function in human gliomas

Inaugural-Dissertation

zur Erlangung des Doktorgrades

der Mathematisch-Naturwissenschaftlichen Fakultät

der Heinrich-Heine-Universität Düsseldorf

vorgelegt von

Natalie Schmidt

aus Berkeley/CA/USA

Düsseldorf, Mai 2011

Aus dem Institut für Neuropathologie
der Heinrich-Heine-Universität Düsseldorf

(Direktor: Prof. Dr. Guido Reifenberger)

Gedruckt mit der Genehmigung der
Mathematisch-Naturwissenschaftlichen Fakultät der
Heinrich-Heine-Universität Düsseldorf

Referent: Prof. Dr. G. Reifenberger

Korreferent: Prof. Dr. D. Willbold

Tag der mündlichen Prüfung: 05.07.2011

Results of this doctoral thesis are going to be published in the following original paper:

Schmidt N, Windmann S, Reifenberger G, Riemenschneider MJ. DNA hypermethylation and histone modifications downregulate the candidate tumor suppressor gene *RRP22* on 22q12 in human gliomas. *Brain Pathol* 2011 (in press)

Contents

Abbreviations

A	diffuse astrocytoma
AA	anaplastic astrocytoma
AO	anaplastic oligodendroglioma
AOA	anaplastic oligoastrocytoma
APS	ammoniumpersulfat
ATCC	American Tissue Culture Collection
BSA	bovine serum albumine
bp	base pairs
°C	degree Celsius
cDNA	complementary DNA
CpG	Cytosin-phosphatidyl-Guanin
DEPC	diethylpyrocarbonate
DPBS	Dulbecco's Phosphate Buffered Saline
DMEM	Dulbecco's Modified Eagle Medium
DMSO	dimethylsulfoxid
DNA	desoxyribonucleic acid
dNTP	desoxyribonucleoside-5'-triphosphat
DTT	dithiothreitol
EDTA	ethylendiamintetraacetat
ELISA	enzyme linked immunosorbent assay
FACS	fluorescence activated cell sorting
FCS	fetal calf serum
GFP	green fluorescent protein
GBM	glioblastoma (multiforme)

GITC	guanidinium isothiocyanate
h	hour
HEPES	2-[4-(2-hydroxyethyl)piperazin-1-yl]ethanesulfonic acid
IgG	Immunoglobulin G
kb	kilobase
kDa	kilo-Dalton
LOH	loss of heterozygosity
M	molar
NB	non-neoplastic brain tissue
mA	milli-ampere
min	minute
ml	milliliter
mRNA	messenger ribonucleic acid
µl	microliter
O	oligodendroglioma
OA	oligoastrocytoma
PAGE	polyacrylamide gel electrophoresis
PBS	phosphate buffered saline
PCR	polymerase chain reaction
PI	propidium iodide
PMSF	phenylmethanesulfonyl fluoride
RNA	ribonucleic acid
rpm	rotation per minute
RT	room temperature
RT-PCR	reverse transcription - polymerase chain reaction

SD	standard deviation
SDS	sodium dodecyl sulfate
sec	second
shRNA	small hairpin RNA
SSCP	single strand conformation polymorphism
T	tumor
Taq	*Thermus aquaticus*
TBE	Tris-borate-EDTA
TBS-T	Tris-buffered saline with Tween 20
TE	Tris-EDTA
TEMED	N-N-N-N-Tetraethylmethyldiamine
Tris	Tris(hydroxymethyl)aminomethane
U	unit
v/v	volume in volume
V	voltage
W	watt
w/v	weight in volume
WHO	World Health Organization

1 Introduction

1.1 Gliomas: Incidence, epidemiology, clinical behavior

Primary tumors of the central nervous system (CNS) account for about 2-3 % of all cancers. In pediatric patients, primary CNS tumors represent the second most common tumor type after the acute leukemias and the most common cause of cancer-related death (Riemenschneider and Reifenberger 2009b).

Gliomas are the most common primary brain tumors (around 50 %). Gliomas are histologically classified according to the WHO (World Health Organisation) classification of tumors of the central nervous system in its latest edition from 2007 (Louis et al 2007a). Classification is mainly based on histological and immunohistochemical features, however, genetic alterations become increasingly important for differential diagnostic purposes and improved prognostic assessment (Louis et al 2007b, Riemenschneider et al 2010).

Males have a slightly higher incidence rate of gliomas, with an estimated male/female ratio of 1.26 (Ohgaki and Kleihues 2005). Interestingly, secondary glioblastomas develop more frequently in women (m/f: 0.65) while primary glioblastomas are more common in men (m/f: 1.33) (Ohgaki and Kleihues 2007). The overall survival of glioma patients depends on patient age and clinical status, extent of tumor resection, as well as the histological tumor type and WHO malignancy grade. For example, in case of diffuse astrocytic gliomas, patients with WHO grade II tumors usually survive for more than 5 years after diagnosis, while patients with WHO grade III tumors have a median survival of 2-3 years and patients with glioblastomas WHO grade IV usually succumb to their disease within 12-15 month after diagnosis (Louis et al 2007b, Ohgaki and Kleihues 2005). Most gliomas develop spontaneously and only a small proportion of cases are linked to genetic syndromes caused by inherited rare mutations. Familial retinoblastoma (*RB1* mutation), neurofibromatosis 1 (*NF1* mutation) and 2 (*NF2* mutation), and Li-Fraumeni syndrome (*TP53* mutation) have been associated with increased risk for gliomas (Schwartzbaum et al 2006). Therapy also depends on the type and WHO grade of the tumor. Surgery is effective in relieving mass effect, reducing tumor volume, removing the necrotic tumor core (Grossman and Batara 2004)

and is also offered as salvage therapy in some patient with recurrent malignant glioma (Mitchell et al 2005). Chemotherapy with procarbazine/lomustine/vincristine (PCV), temozolomide or carmustine, and radiotherapy are standard therapies for malignant gliomas of WHO grade III or IV (Henson 2006, Norden and Wen 2006). Patients with WHO grade II gliomas usually do not receive adjuvant radio- or chemotherapy, unless they demonstrate progressive tumor growth. In contrast, patients with anaplastic gliomas (WHO grade III) either receive radiotherapy or alkylating chemotherapy (Wick and Weller 2009), while glioblastoma patients are treated with radiotherapy plus concomitant and adjuvant temozolomide (Stupp et al 2005). Epigenetic silencing of the O6-methylguanine-DNA methyltransferase (*MGMT*) gene has been shown to prolong overall survival in malignant glioma patients treated with combined radiochemotherapy or chemotherapy alone by decreasing DNA repair activity (Hegi et al 2005, Weller et al 2009, Wick and Weller 2009). In patients with anaplastic oligodendroglial tumors, losses of the chromosomal arms 1p and 19q have been linked to better response to radiotherapy and/or chemotherapy with temozolomide or PCV as well as longer overall survival (Cairncross et al 2006, van den Bent et al 2006, Wick and Weller 2009). Moreover, mutations in the isocitrate dehydrogenase gene 1 (*IDH1*) have been reported as powerful independent prognostic marker for patients with anaplastic gliomas (van den Bent et al 2010, Wick and Weller 2009) and glioblastomas (Sanson et al 2009, Weller et al 2009).

1.1.1 WHO classification of gliomas

According to the WHO classification of tumors of the central nervous system (Louis et al 2007a) gliomas are divided into four main groups: astrocytic gliomas, oligodendroglial tumors, mixed oligoastrocytic gliomas and ependymal tumors (Figure 1).

In addition to tumor classification, gliomas are also assigned to a defined malignancy grade (WHO grade). Cellular and nuclear atypia, cellularity, mitotic activity, microvascular proliferation and necrosis are important features considered in the WHO grading of gliomas, which ranges from WHO grade I (benign) to WHO grade IV (highly malignant). WHO grade I tumors grow slowly and well circumscribed. Therefore, they are usually cured by complete surgical resection. WHO grade II gliomas also grow slowly but show an infiltrative growth in the adjacent brain parenchyma, making complete surgical resection impossible in most patients. Thus, patients with WHO grade II gliomas have a high risk for tumor relapse and malignant progression. WHO

grade III gliomas are characterized by cytological and histological features of anaplasia, in particular elevated mitotic activity, increased tumor cell density, as well as cellular and nuclear atypia. WHO grade IV gliomas (glioblastomas) additionally demonstrate areas of tumor necrosis and pronounced microvascular proliferation on a background of a highly cellular and pleomorphic glioma with high mitotic and proliferative activity (Louis et al 2007a).

1.1.2 Molecular pathology of gliomas

1.1.2.1 Astrocytic gliomas

Astrocytic gliomas are the most common group of primary central nervous system tumors and account for up to two third of all tumors of glial origin (Riemenschneider and Reifenberger 2009a). The just recently identified gene *IDH1* (isocitrate dehydrogenase 1) is mutated in about 70 % of diffuse astrocytomas (Balss et al 2008). Trisomy 7 or gains of 7q also occur in diffuse astrocytomas in about 50 % of the cases (Perry et al 1997, Schrock et al 1996). In addition, the *TP53* tumor suppressor gene at 17p13.1 is mutated in about 60 % of WHO grade II tumors and mutation frequency does not increase in recurrences, suggesting that *TP53* mutations are an early event in astrocytic gliomas (Louis et al 2007a). Tumors without *TP53* mutations exhibit $p14^{ARF}$ promoter hypermethylation at chromosome 9p21, which regulates MDM2-mediated degradation of p53 (Watanabe et al 2007). Furthermore, the *MGMT* (O-6-methylguanine-DNA methyltransferase) gene at 10q26 also has been reported as being silenced in more than 50 % of diffuse astrocytomas by promoter hypermethylation, with one study reporting on an association with *TP53* mutation (Watanabe et al 2007). Another common alteration is the overexpression of *PDGFRA* (platelet-derived growth factor receptor alpha) and its ligand *PDGFalpha*, which leads to an autocrine growth stimulation of the tumor cells (Hermanson et al 1992). Further genomic imbalance in diffuse astrocytomas (WHO grade II) are allelic losses on the chromosomal arms 22q, 19q, 13q, 10p, 1p and Xp and gains on the chromosomal arms 5p, 9q and 19p as well as deletions on chromosome 6 and amplification of genes on chromosome arm 8q (Louis et al 2007a, Reifenberger and Collins 2004) (Figure 1).

Anaplastic astrocytomas (WHO grade III) exhibit similar genetic alterations, like gains on chromosome 7, allelic losses on chromosome 17p, *TP53* and *IDH1* mutations. Additional genetic alterations are allelic losses on chromosome 22q, 19q, 11p, 10q, 9p, 6q and, rarely, *PTEN* (phosphatase and tensin homolog) mutation (Louis et al 2007a,

Riemenschneider and Reifenberger 2009a). Furthermore, deletions on chromosome arm 9p targeting the cell-cycle regulatory genes *p14^{ARF}*, *CDKN2A* and *CDKN2B* (cyclin-dependent kinase inhibitor 2A and 2B) at 9p21 occur in a subset of WHO grade III astrocytomas (Riemenschneider and Reifenberger 2009a) (Figure 1).

Glioblastomas (WHO grade IV) reveal the most complex chromosomal, genetic and epigenetic aberrations affecting many tumor suppressor genes and oncogenes. The most common alterations are monosomy 10 and trisomy 7 (Bigner and Vogelstein 1990). Primary glioblastomas (arising de novo, 95 %) and secondary glioblastomas (arising from lower-grade precursor lesions, 5 %) exhibit different genetic aberrations (Ohgaki and Kleihues 2007). Primary glioblastomas show frequent *EGFR* amplification (36 %), *PTEN* and *TP53* mutations (30 %) as well as *CDK4* (cyclin-dependent kinase 4) and *MDM2* or *MDM4* (murine double minute 2 or 4) amplification. *CDKN2A*, *CDKN2B*, *p14^{ARF}*, *RB1* (retinoblastoma 1) deletions and *NDRG2* hypermethylation are also found in primary glioblstomas (Louis et al 2007a, Riemenschneider and Reifenberger 2009a, Tepel et al 2008). Secondary glioblastomas bear *TP53* and *IDH1* mutation in more than 60 % of cases as well as allelic losses on chromosome arms 19q, 13q and 10q. *RB1* promoter hypermethylation and *PDGFRA* overexpression were also reported in secondary glioblastomas (Ohgaki and Kleihues 2007). In addition, *MGMT* and *EMP3* (epithelial membrane protein 3) gene silencing is more common in secondary glioblastomas while *EGFR* amplification, *PTEN* mutation and *NDRG2* hypermethylation are rare events (Louis et al 2007a, Riemenschneider and Reifenberger 2009a, Tepel et al 2008) (Figure 1).

1.1.2.2 Oligodendroglial tumors

The most characteristic molecular alterations in oliogodendroglial tumors are combined losses of chromosome arms 1p and 19q in over 80 % of the cases (Reifenberger et al 1994). An unbalanced t(1;19)(q10;p10) translocation serves as the mechanism responsible for the frequent co-deletions of both chromosome arms (Griffin et al 2006, Jenkins et al 2006). WHO grade II and III oligodendrogliomas share the high frequency of *IDH1* mutations (about 70 % of cases) with diffuse and anaplastic astrocytomas (Balss et al 2008). Furthermore, *CDKN2A*, *p14^{ARF}*, *CDKN2B* (Wolter et al 2001) and *MGMT* promoter methylation (Mollemann et al 2005) as well as *EGFR* and *PDGFR* overexpression have been reported in oligodendrogliomas of WHO grade II (Di Rocco et al 1998, Reifenberger and Louis 2003) (Figure 1).

Anaplastic oligodendrogliomas exhibit losses of chromosome arms 1p and 19q in about the same frequency as oligodendrogliomas of WHO grade II. In addition, these tumors carry deletions on chromosome arm 9p and/or chromosome 10 (Fallon et al 2004) as well as *CDKN2A*, *CDKN2B* and *p14^{ARF}* alterations in one third of the cases (Jeuken et al 2004). *PTEN* and *TP53* mutations as well as *CDK4*, *EGFR* and *PDGFRA* amplification are rare findings in anaplastic oligodendroglial tumors (Riemenschneider and Reifenberger 2009a) (Figure 1).

1.1.2.3 Mixed oligoastrocytic gliomas

These tumors exhibit histologically two distinct tumor cell populations with oligodendroglial or astrocytic features. Around 50 % of the cases show allelic losses on 1p and 19q and 30 % of these tumors reveal genetic alterations associated with diffuse astrocytomas, such as *TP53* mutations and allelic losses on 17p (Reifenberger and Louis 2003) (Figure 1).

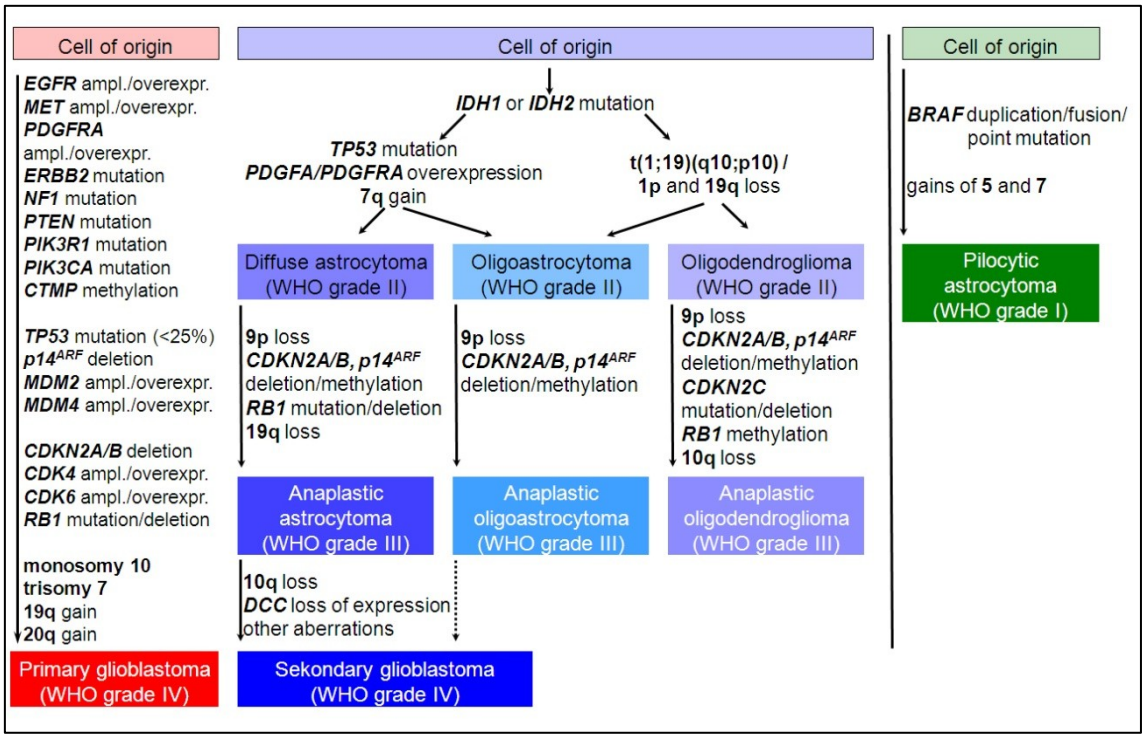

Figure 1: Summary of the most frequent molecular alterations in astrocytic, oligodendroglial and oligoastrocytic gliomas (Riemenschneider et al 2010).

1.2 Small GTPase genes of the Ras-family

Small GTPases (guanine nucleotide binding proteins) are 20-29 kDa proteins that share homologies, motifs and structure. Over 150 GTPase genes have been identified in mammalian genomes. The gene products are involved in signal transduction pathways coordinating vital cell processes, such as transcription, protein biosynthesis, membrane trafficking, cell shape, cell migration, endocytosis, cell survival, cell cycle progression, differentiation and senescence (Rajalingam et al 2007, Wennerberg et al 2005, Wittinghofer and Nassar 1996).

GTPases are monomeric proteins that can be present in two different conformational states: the active form is bound to GTP (guanosine-5'-triphosphate) whereas the inactive form is bound to GDP (guanosine-5'-diphosphate) (Hall 1990). The so-called 'switch regions' are regions that change their conformation structure from the activated to the inactivated state: Switch region I (amino acid 30-38) and switch region II (amino acid 59-67) form interaction surfaces for effector molecules in a GTP-dependent manner (Wennerberg et al 2005, Wittinghofer and Nassar 1996). The intrinsic GTPase activity is usually very slow and can be stimulated by GTPase activating proteins (GAPs) (Bernards and Settleman 2004). GAPs increase the GTP hydrolysis and change the active, GTP-bound form to an inactive, GDP-bound form. Guanine nucleotide exchanging factors (GEFs) (Schmidt and Hall 2002) catalyze the reaction in the opposite direction. GEFs replace the GDP by GTP and can therefore activate GTPases (Wittinghofer and Nassar 1996) (Figure 2).

The carboxy-terminal domain of small GTPases consists of the CAAX tetrapeptide sequence (C = cystein; A = aliphatic amino acid; X = any amino acid). The C-terminal of GTPases is mostly posttranslational modified by lipids. These modifications dictate the interaction with distinct membranes, which is critical for GTPase function (Cox and Der 2002).

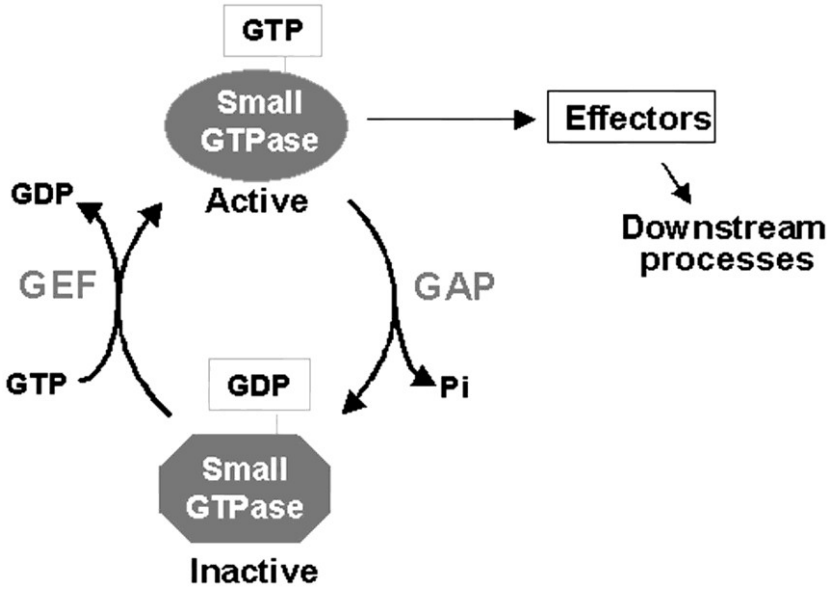

Figure 2: Regulartory cycle of small GTPases. Guanine nucleotide exchange factors (GEF) are stimulated by extracellular stimuli and convert the inactive, GDP-bound form of GTPases into the active, GTP-bound form. GTP-bound GTPases can bind to downstream effectors and can regulate downstream signaling. The GTPase activating proteins (GAPs) stimulate GTP hydrolysis to reset active GTPases to their inactive form (Nielsen et al 2008).

Small GTPases, also called Ras superfamily GTPases, are divided into 5 subgroups on the basis of sequence and functional similarities: Ras, Rho, Rab, Arf and Ran (Rajalingam et al 2007, Wennerberg et al 2005). These subfamilies are related to the well-known oncogene *Ras* (Hall 1990). *Ras* was first identified as retroviral oncogene in the 1960/70s from the genome of Harvey and Kirsten rat sarcoma virus (Malumbres and Barbacid 2003). Approximately 20 % of all cancers exhibit *Ras* mutations, with mutations being detectable in up to 90 % of the cases in special tumor entities (Rajalingam et al 2007).

Most members of the GTPase superfamily exhibit oncogenic characteristics, however, certain members of the Ras superfamily have been suggested as tumor suppressor genes, including *RRP22*, *RHOB*, *RASL11A*, *RERG* and *ARHI/DIRAS3* (Elam et al 2005, Finlin et al 2001, Forget et al 2002, Louro et al 2004, Riemenschneider et al 2008).

1.2.1 Ras-related protein on chromosome 22 (RRP22)

The *RRP22* gene was first characterized in 1996 and maps to the chromosomal band 22q12 that often shows allelic losses in human tumors, including gliomas (Zucman-Rossi et al 1996). The *RRP22* gene belongs to the Ras-subgroup of the Ras superfamily of GTPases (Wennerberg et al 2005) and is expressed in two transcript variants. Transcript variant 1 is composed of three exons with the entire 612 bp coding region from exon 1 to exon 3, whereas transcript variant 2 is expressed from two exons with the complete 348 bp coding region in exon 1 and 2 (Figure 3). One and the same potential CpG island is associated with both *RRP22* transcript variants which includes 232 CpG sites and spans the transcription and translation start site as well as the entire coding sequence (http://genome.ucsc.edu/) (Figure 3). The *RRP22* gene encodes either a small 22.5 kDa GTPase protein (transcript variant 1) or an even smaller 12.5 kDa GTPase protein (transcript variant 2).

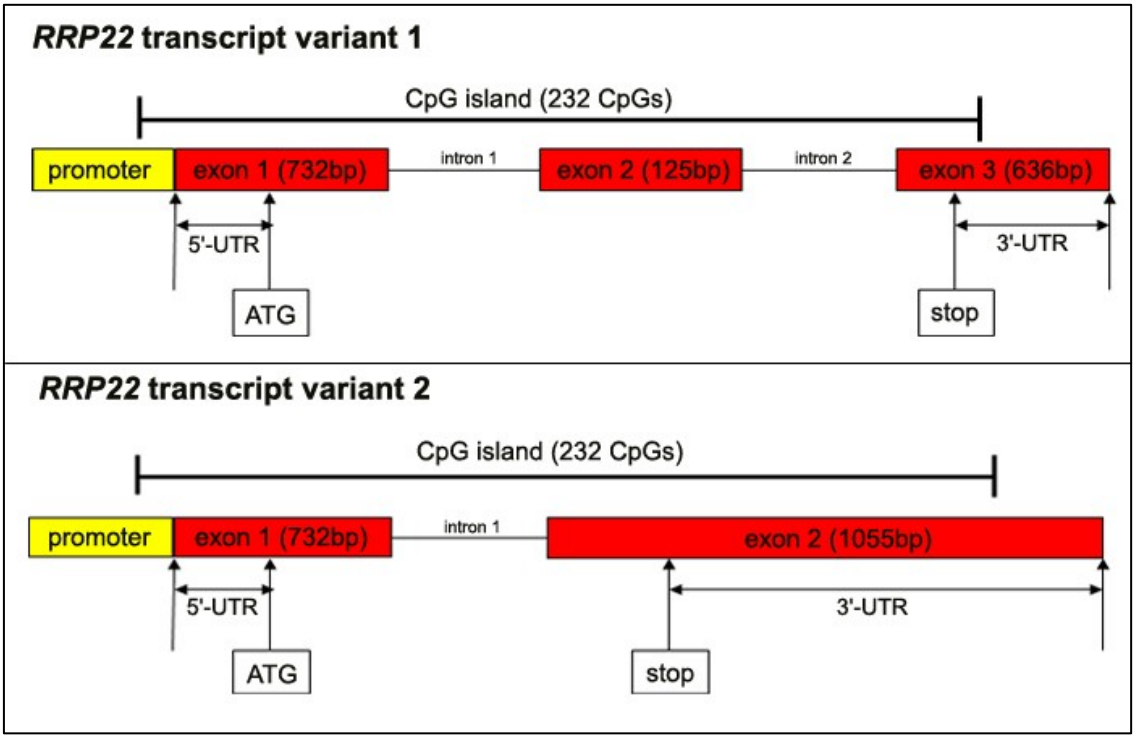

Figure 3: Schematic drawing of the genetic locus of *RRP22* on chromosome 22q12.2. The *RRP22* gene can generate two different isoforms. Isoform a consists of three exons, whereas isoform b contains only 2 exons. Both transcript variants underly transcriptional regulation by the same CpG island with 232 CpG sites.

RRP22 expression appears to be strictly limited to the central nervous system (Zucman-Rossi et al 1996). While further bibliographic data on the role of *RRP22* in human tumors is sparse (Sayagues et al 2007), two studies in gliomas reported RRP22 to suppress tumor cell growth, promote caspase-independent cell death, decrease invasiveness and inhibit the growth in soft agar, thereby supporting a tumor suppressor function (Chen et al 2011, Elam et al 2005). Moreover, Chen et al. (Chen et al 2011) showed that the *RRP22* mRNA expression level decreases with increasing malignancy in glioma patients, and Elam et al. (Elam et al 2005) pointed to a role of promoter hypermethylation as a potential cause for the inactivation of *RRP22* in glioblastoma cell lines. However, the relevance of *RRP22* and its potential inactivation mechanisms in primary human glioma tissue samples *in vivo* had not been investigated.

1.2.2 Ras-homolog gene family member B (RHOB)

In contrast to *RRP22*, the role of the *RHOB* gene on 2p24 in the pathogenesis of human gliomas is far better established. *RHOB* belongs to the Rho-subgroup of the Ras superfamily of GTPases (Wennerberg et al 2005). There are three different Rho isoforms: *RhoA*, *RhoB* and *RhoC*. Despite the high homology among these isoforms, they exhibit different cellular functions (Kanai et al 2010). RhoB is described as a negative regulator of cell survival and thus might fuction as a tumor suppressor, whereas RhoA and RhoC are involved in malignant progression of various tumors by regulating cell motility and centrosome duplication (Kanai et al 2010, Karlsson et al 2009, Wennerberg et al 2005). The transcripts of *RHOB* originate from just one exon, which includes the entire 591 bp coding region. An associated CpG island includes 158 CpG sites and spans the transcription and translation start site as well as the entire coding sequence (http://genome.ucsc.edu/) (Figure 4). The *RHOB* gene encodes a small 22.1 kDa GTPase protein.

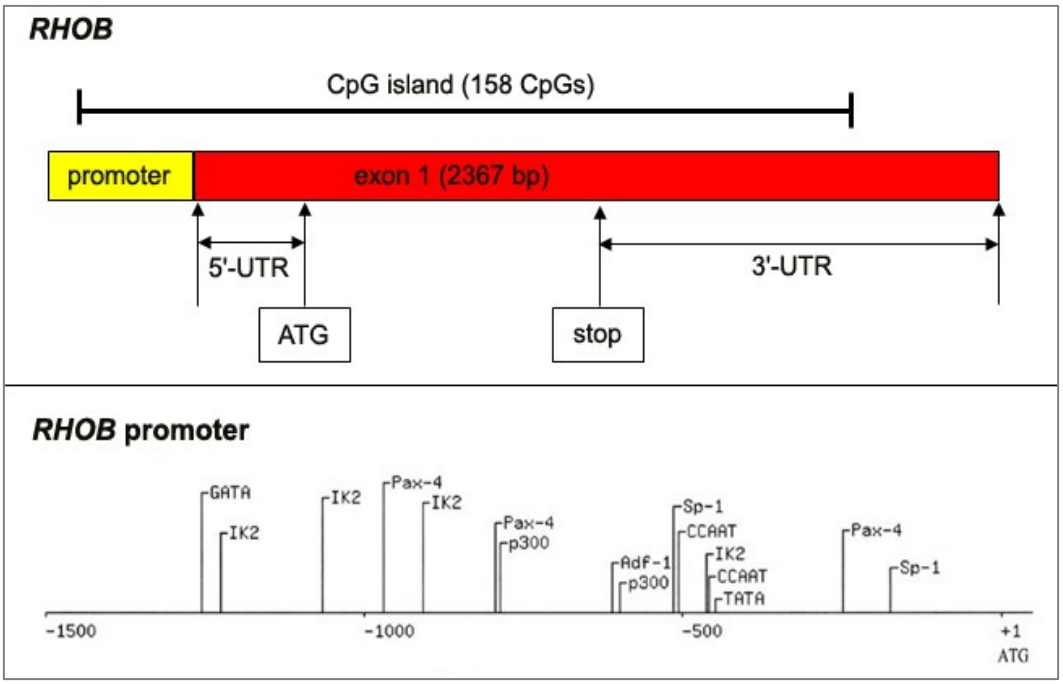

Figure 4: Schematic drawing of the *RHOB* locus on chromosome band 2p24.1. The *RHOB* gene generates one transcript including one single exon (upper figure). The *RHOB* promoter (lower figure) is well described with potential binding sites for transcription factors. The inverted CCAAT box (5'-ATTGG-3') at position -451 relative to the translation start site seems to be critical for the induction of *RHOB* transcription (Fritz and Kaina 2001, Wang et al 2003b).

Repression of RhoB by aberrant PI3kinase/PKCiota signaling has been reported to enhance glioma cell motility (Baldwin et al 2008). Moreover, RhoB appears to be critically involved in the development of radiotherapy resistence of glioma cells (Delmas et al 2002, Monferran et al 2008). Integrins have been described to regulate radiation-induced mitotic cell death through RhoB (Monferran et al 2008) and expression of an inducible dominant negative form of RhoB in a radioresistant U87 glioma cell line dramatically reduced cell survival after irradiation (Delmas et al 2002). Another, probably closely related mechanism is the reported RhoB-mediated control of HIF-1alpha stabilization through glycogen synthase kinase-3 in U87 glioblastoma cells, indicating that RhoB is involved in signaling pathways that permit glioma cells to adapt to hypoxia (Skuli et al 2006, Skuli et al 2009).

In human glioma tissue samples, *RHOB* expression was found to decrease with increasing malignancy grade (Forget et al 2002) however, the molecular mechanisms leading to the decreased *RHOB* expression in high-grade gliomas are still unknown. A

study on differently aged mouse tissues described *RHOB* as epigenetically regulated in an age- and tissue-specific manner by histone modifications, but not CpG methylation (Yoon et al 2007). Similarly, recent reports in lung and pancreatic cancer cells pointed to an epigenetic inactivation of *RHOB* by histone modifications (Delarue et al 2007, Mazieres et al 2007, Sato et al 2007). However, the relevance of *RHOB* and its potential inactivation mechanisms in primary human glioma tissue samples *in vivo* had not been investigated.

1.2.3 Ras-like family 11 member A (RASL11A)

This *Ras*-related gene was first described in 2004 and is located on chromosome 13q12 (Louro et al 2004). The *RASL11A* gene belongs to the Ras-subgroup of the Ras superfamily of small GTPase genes (Wennerberg et al 2005). The full-length *RASL11A* transcript is generated from 4 exons with the entire 729 bp coding region from exon 1 to exon 4. A 5'-CpG island includes 103 CpG sites and spans the translation start site (http://genome.ucsc.edu/) (Figure 5). The *RASL11A* gene encodes a small 27 kDa GTPase protein.

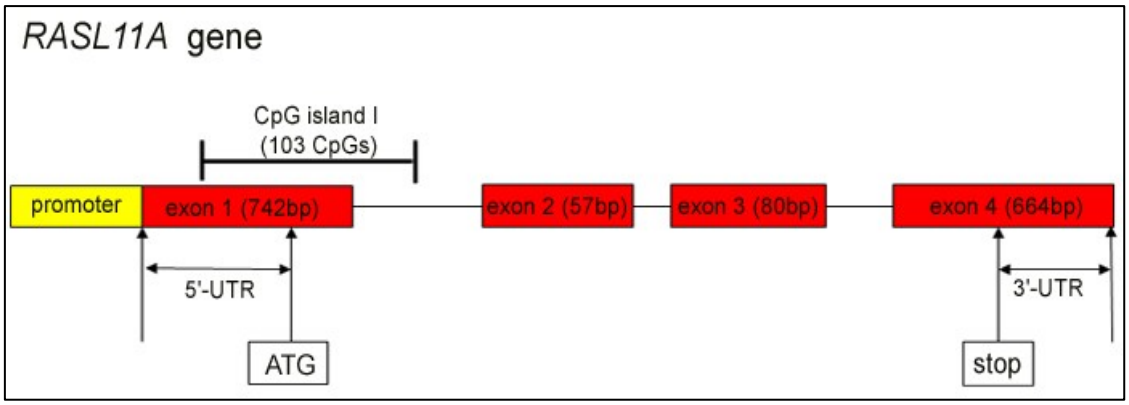

Figure 5: Schematic drawing of the genetic locus of *RASL11A* on chromosome 13q12.2. The *RASL11A* gene consists of 4 exons with a CpG Island spanning exon 1.

RASL11A expression was determined in several human tissues and is down-regulated in prostate tumors, corroborating the hypothesis that the RASL11A protein might have a tumor suppressor role (Louro et al 2004). One study reported RASL11A to regulate rDNA transcription and to be associated and localized with the RNA polymerase I–specific transcription factor UBF in mouse fibroblasts (Pistoni et al 2010). Methylation analysis by MethyLight polymerase chain reaction in prostate carcinomas or

hyperplasias did not display noteworthy results (Bastian et al 2007). Louro et al. reported on two transcript variants with different sizes: 1.6 and 1.2 kb transcript variants (Louro et al 2004). However, the relevance of *RASL11A* and its potential inactivation mechanisms in primary human glioma tissue samples *in vivo* had not been investigated.

1.2.4 Ras-like, estrogen-regulated, growth inhibitor (RERG)

RERG belongs to the Ras-subgroup of the Ras superfamily of small GTPase genes (Wennerberg et al 2005) and can generate two transcript variants. Transcript variant 1 is expressed from 5 exons with the complete 600 bp coding region from exon 2 to exon 5, whereas transcript variant 2 is expressed from 4 exons with the entire 543 bp coding region in exon 2 to exon 4 (http://genome.ucsc.edu/) (Figure 6). One and the same 5'-CpG island, which includes 49 CpG sites and spans the transcription start site (http://genome.ucsc.edu/), may regulate transcription of both *RERG* transcript variants (Figure 6). The *RERG* gene encodes either a small 22.4 kDa GTPase protein (transcript variant 1) or an even smaller 20.1 kDa GTPase protein (transcript variant 2).

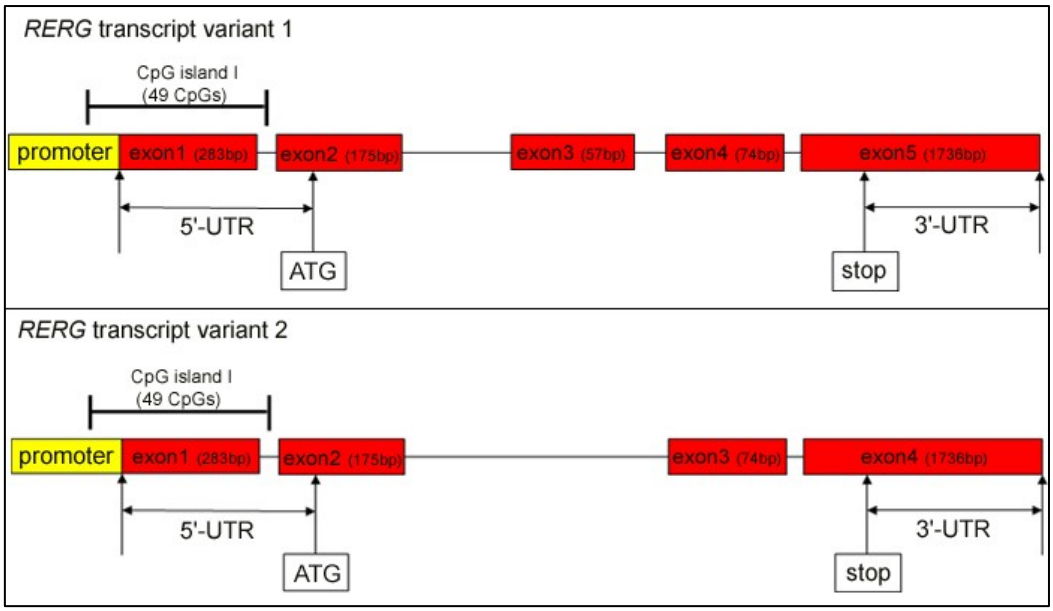

Figure 6: Schematic drawing of the genetic locus of *RERG* on chromosome 12p12.3. The *RERG* gene can generate two different isoforms. Transcript variant 1 consists of 5 exons, whereas transcript variant 2 contains 4 exons. Both transcript variants underly regulation by the same CpG island with 49 CpG sites.

RERG was first described in breast cancer as an estrogen-responsive gene with two potential estrogen receptor binding sites within the promoter region (Finlin et al 2001). Finlin et al. suggested that RERG functions as a negative growth regulator in breast epithelial cells (Finlin et al 2001) and could therefore be a tumor suppressor gene candidate (Key et al 2006). Furthermore, another study reported that RERG has the same growth-inhibiting and gender dependent function in female hepatocarcinogenesis as in breast cancer (Wang et al 2006). Oster et al. reported on *RERG* hypermethylation in colorectal carcinomas, but *RERG* expression did not correlate with promoter hypermethylation (Oster et al 2011). The relevance of *RERG* and its potential inactivation mechanisms in primary human glioma tissue samples *in vivo* had not been investigated.

1.2.5 Aplasia ras homologue member I (ARHI)

The *ARHI* gene was first reported in 1999 (Yu et al 1999) and maps to the chromosomal band 1p31 that often shows allelic losses in oligodendrogliomas (Riemenschneider et al 2008). *ARHI*, with its synonyms *DIRAS3* or *NOEY*, is a maternally imprinted gene (Yu et al 1999) and belongs to the Ras-subgroup of the Ras superfamily (Wennerberg et al 2005). The *ARHI* gene comprises two exons with the second exon containing the 229 bp coding region (http://genome.ucsc.edu/) (Figure 7). The *ARHI* gene is associated with three CpG islands; CpG island I with 51 CpG sites is located about one kb upsteam of the transcription start site. CpG island II consists of 21 CpG sits, spans the transcription start site and seems to be the most relevant for epigenetic inactivation (Yuan et al 2003). The CpG island III with 30 CpG sites is located in exon 2 and spans the translation start (Riemenschneider et al 2008) (Figure 7). The *ARHI* gene encodes a small 26 kDa GTPase protein.

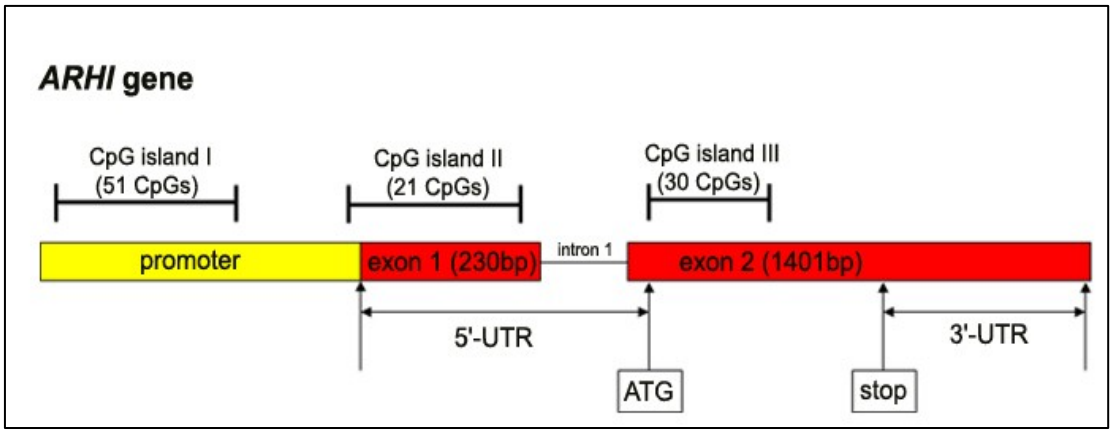

Figure 7: Schematic drawing of the genetic locus of *ARHI* on chromosome 1p31.3. The *ARHI* gene consists of two exons with the 229 bp coding region in exon 2. Three CpG island are spread over the genetic locus of *ARHI* from the promoter region (I) over the transcription start site (II) to the translation start site (III).

In gliomas, epigenetic regulation of the *ARHI* gene is well characterized (Riemenschneider et al 2008). Riemenschneider et al. reported on a decrease of *ARHI* mRNA levels in oligodendrogliomas by frequent biallelic inactivation with allelic losses on 1p and combined CpG island methylation of the retained allele, whereas in astrocytic tumors the biallelic inactivation seems to be a rare event (Riemenschneider et al 2008). The potential tumor suppressor function of ARHI was reported in a broader spectrum of neoplasms including pancreatic, liver, thyroid, ovarian and breast cancer cell lines (Bao et al 2002, Lu et al 2009, Weber et al 2005, Zhao et al 2010). In breast cancer cell lines, the ARHI protein suppresses clonogenic growth, reduces invasiveness and induces apoptosis (Wang et al 2003a). However the functional roles of ARHI in gliomas have not been investigated so far.

1.3 Goals and experimental approach of this study

The aim of this doctoral thesis was to analyze the small Ras-related GTPase genes *RRP22*, *RHOB, RASL11A and RERG* in gliomas for potential genetic or epigenetic inactivation mechanisms and their potential roles as tumor suppressor genes. In addition, the functional roles of another small Ras-related GTPase protein, namely ARHI, should be investigated based on previous molecular studies in our laboratory reporting frequent transcriptional silencing of this gene (Riemenschneider et al 2008).

In a first step, mRNA expression analyses were performed to screen for aberrant expression of *RRP22*, *RHOB*, *RASL11A* and *RERG* in primary human glioma tissues in comparison to non-neoplastic brain tissue. Promoter methylation analyses were additionally carried out for three of the 4 candidate genes. We then selected the most interesting genes, *RHOB* and *RRP22*, for further analysis. Mutations analyses and in case of *RRP22* the analysis of allelic losses involving the *RRP22* gene locus were performed in a panel of 70 glioma tissue samples. Moreover, a chromatin immunoprecipitation assay (ChIP) protocol was established to search for histone modifications as an alternative mechanism for the inactivation of small GTPase genes. Concerning the *ARHI* gene, previous work from our group showed that the gene is frequently silenced by promoter hypermethylation in oligodendrogliomas with allelic losses on chromosome 1p, whereas astrocytic tumors did not reveal biallelic *ARHI* inactivation (Riemenschneider et al 2008). In this doctoral thesis, functional *in vitro* analyses were performed to further characterize the role of ARHI in gliomas.

2 Materials

2.1 Cell lines and patients

2.1.1 Cell lines

Table 1 provides an overview of the six different glioma cell lines used in this study.

Table 1: Glioma cell lines used in this study.

Cell line	Species	Origin	Source
U87MG	human	glioblastoma (WHO grade IV)	ATCC, Manassas, Virginia
T98G	human	glioblastoma (WHO grade IV)	ATCC, Manassas, Virginia
U138MG	human	glioblastoma (WHO grade IV)	ATCC, Manassas, Virginia
A172	human	glioblastoma (WHO grade IV)	ATCC, Manassas, Virginia
U251MG	human	glioblastoma (WHO grade IV)	ATCC, Manassas, Virginia
TP365MG	human	glioblastoma (WHO grade IV)	V.P. Collins, Cambridge, UK

2.1.2 Patients

Primary glioma tissue samples were selected from the tumor tissue collection of the Department of Neuropathology, Heinrich-Heine-University, Düsseldorf, Germany, and investigated according to protocols approved by the institutional review board. All tumors were classified according to the criteria of the World Health Organization (WHO) classification of tumors of the nervous system (Louis et al 2007b). Parts of each tumor were snap-frozen immediately after operation and stored at -80°C. Only tissue samples with an estimated tumor cell content of 80 % or more were used for molecular analyses.

The investigated tumor series comprised 70 human gliomas, including 16 glioblastomas, WHO grade IV (GBM), 6 anaplastic astrocytomas, WHO grade III (AA), 7 diffuse astrocytomas, WHO grade II (A), 11 anaplastic oligoastrocytomas, WHO

grade III (AOA), 10 oligoastrocytomas, WHO grade II (OA), 12 anaplastic oligodendrogliomas, WHO grade III (AO), and 8 oligodendrogliomas, WHO grade II (O). An overview over the whole tumor panel is provided in Figure 22.

For chromatin immunopreciptation (ChIP) analyses we additionally prepared nuclei from seven glioblastoma patients (Figure 34). The respective case numbers correspond to: T1, GB239; T2, GB1060; T3, GB1061; T4, GB1062; T5, GB1063; T6, GB1064; T7, GB1065 (Figure 34, Figure 35, Figure 36).

Non-neoplastic brain tissue samples from different individuals as well as commercially available DNA and RNA extracted from autopsy brain tissue were used as reference and are introduced in the respective subchapters.

2.2 Laboratory equipment

Table 2 summarizes the most important laboratory equipment that was used in this study.

Table 2: Laboratory equipment used in this study.

Equipment	Version	Manufacturer
cell incubator	CB150	Binder GmbH, Tuttlingen
centrifuge	Rotina 46R	Hettich GmbH, Tuttlingen
clean bench	BSB 6 und 4A	Gelaire, Sydney
digital scale	ALC	Sartorius Ag, Göttingen
DNA sequencer	ABI PRISM 377	Applied Biosystem, Foster City
fluorescence microscope	IX 50/ U-RFL-T	Olympus GmbH, Münster
gel chamber (agarose gels)	Sub-Cell	PeqLab GmbH, Erlangen
gel chamber (LOH, mutation)		Welabo, Düsseldorf
gel chamber (protein)	Mini Protean	BioRad GmbH, München
gel documentation system		Bio-Budget GmbH, Krefeld
gel dryer	Model583	BioRad GmbH, München
homogenisator DOUNCE	7 ml	Kleinfeld Labortechnik GmbH, Gehrden

imager	LAS-3000 mini	FUJIFILM, Düsseldorf
Laboratory Automation Workstation, Biomek Fx^P		Beckman Coulter, Brea, CA
PCR thermocycler	T3	Biometra GmbH, Göttingen
pH meter	pH 525	WTW, Weilheim
photometer	nanodrop ND1000	PeqLap GmbH, Erlangen
power supply	PowerPAC 3000	BioRad GmbH, München
reaction tubes (2 ml; 1.5 ml; 0.5 ml)		Sarstedt AG, Nümbrecht
		Eppendorf AG, Hamburg
real time PCR	StepOnePlus™	Applied Biosystem, Foster City
refrigerated centrifuge	EBA 12R	Hettich GmbH, Tuttlingen
shaker	3013	GFL GmbH, Burgwedel
swing out rotor	SW41 TI	Beckman Coulter, Brea, CA
table centrifuge	5417	Eppendorf AG, Hamburg
thermobloc	TD	Falc, Treviglio, Italy
ultracentrifuge	L8-M	Beckman Coulter, Brea, CA
ultrasonic processor	Vibracell 75022	Novodirect GmbH, Kehl/Rhein
ultra turrax	T25	IKA-Werke GmbH, Staufen
vacuum pump		KnF GmbH, Freiburg
vortexer	Zx3	VELP Scientifica, Usmate, Italy
water bath		GFL GmbH, Burgwedel
western blot chamber		BioRad GmbH, München

2.3 Consumables

Table 3 provides an overview of the different types of consumables used in this study.

Table 3: Consumables used in the study.

Consumables	Manufacturer
annexin V, APC-conjugated	ImmunoTools GmbH, Friesoythe
biotinylated protein ladder	Cell Signaling, Danvers, MA
cell dishes/flasks/well plates	Thermo Scientific, Waltham, MA
conical tubes (15 ml; 50 ml)	Greiner AG, Kremsmünster
cryo tubes	Thermo Scientific, Waltham, MA
DEPC treated water	Carl Roth GmbH, Karlsruhe
disposable pipet (1 ml, 5 ml, 10 ml, 25 ml)	Corning Inc., Corning, NY
DPBS	Invitrogen, Carlsbad, CA
DMEM	Invitrogen, Carlsbad, CA
DNA ladder (100 bp)	Bio-Budget GmbH, Krefeld
dNTPs	Bio-Budget GmbH, Krefeld
dithiothreitol (DTT)	Invitrogen, Carlsbad, CA
fetal calf serum	Invitrogen, Carlsbad, CA
filter paper	Whatman GmbH, Dassel
first strand buffer (5x)	Qiagen, Hilden
gloves	Semperit GmbH, Wien
nitrocellulose membrane	Whatman GmbH, Dassel
PCR buffer	Qiagen, Hilden
PCR buffer	Invitrogen, Carlsbad, CA
PCR plates	Applied Biosystem, Foster City
PCR tubes	Bio-Budget GmbH, Krefeld
pd (N_6), random hexamer phosphorylated	GeneLink, Hawthorne, NY

penicillin/ streptavidin	Invitrogen, Carlsbad, CA
pipets	VWR GmbH, Darmstadt
pipet tips (normal, plugged)	StarLab GmbH, Ahrensburg
pipettor	Labbay BV, Geldermalsen, NL
prestained protein ladder	Fermentas GmbH, St. Leon-Rot
propidium iodide	Sigma-Aldrich GmbH, Steinheim
protease inhibitor tablets	Roche GmbH, Grenzach-Wyhlen
Q-solution	Qiagen, Hilden
reaction tubes (2 ml; 1.5 ml; 0.5 ml)	Sarstedt AG, Nümbrecht
	Eppendorf AG, Hamburg
trypsin	PAA GmbH, Pasching
ultracentrifuge polyallomer tubes	Herolab GmbH, Wiesloch
well plates (96, 24, 6)	Thermo Scietific, Waltham, MA

2.4 Chemicals, enzymes and antibodies

The various chemicals, enzymes and antibodies used in this study are listed in the following tables 4 - 6.

Table 4: Chemicals used in this study.

Chemicals	Manufacturer
5-aza-2'-deoxycytidine	Sigma-Aldrich GmbH, Steinheim
acetic acid	Merck KGaA, Darmstadt
acrylamide (40 %)	Merck KGaA, Darmstadt
acrylamide/bisacrylamide (40 %; 19:1)	Merck KGaA, Darmstadt
acrylamide/bisacrylamide (30 %; 37,5:1)	Carl Roth GmbH, Karlsruhe
acrylamide/bisacrylamide (30 %; 29:1)	Carl Roth GmbH, Karlsruhe

agarose	Bio-Budget GmbH, Krefeld
ammonium acetate	Fluka Chemie AG, Buchs, CH
ammonium persulphate	Sigma-Aldrich GmbH, Steinheim
bisacrylamide (2 %)	Merck KGaA, Darmstadt
blasticidin	Invitrogen, Carlsbad, CA
boracic acid	Sigma-Aldrich GmbH, Steinheim
bromophenole blue	Sigma-Aldrich GmbH, Steinheim
bovine serum albumin	Carl Roth GmbH, Karlsruhe
calcium chloride	Merck KGaA, Darmstadt
chlorophorm	Merck KGaA, Darmstadt
deoxycholate	Sigma-Aldrich GmbH, Steinheim
DMSO	Sigma-Aldrich GmbH, Steinheim
EDTA	Sigma-Aldrich GmbH, Steinheim
ethanol	Merck KGaA, Darmstadt
ethidiumbromid	Sigma-Aldrich GmbH, Steinheim
formamid	Merck KGaA, Darmstadt
formaldehyde	Merck KGaA, Darmstadt
glycerol	Merck KGaA, Darmstadt
glycine	Carl Roth GmbH, Karlsruhe
guanidinisothiocyanat	Carl Roth GmbH, Karlsruhe
hepes	Carl Roth GmbH, Karlsruhe
hydrochloric acid	Merck KGaA, Darmstadt
isoamylalcohol	Merck KGaA, Darmstadt
isopropanol	Merck KGaA, Darmstadt
mercaptoethanol	Fluka Chemie AG, Buchs, CH
methanol	Merck KGaA, Darmstadt
magnesium chloride	Carl Roth GmbH, Karlsruhe
milk powder	Carl Roth GmbH, Karlsruhe

nitric acid	Merck KGaA, Darmstadt
NP-40	Fluka Chemie AG, Buchs, CH
phenol	Carl Roth GmbH, Karlsruhe
phenylmethanesulfonyl fluoride	Sigma-Aldrich GmbH, Steinheim
ponceau S	Sigma-Aldrich GmbH, Steinheim
potassium chloride	Merck KGaA, Darmstadt
SDS	Carl Roth GmbH, Karlsruhe
silver nitrate	Merck KGaA, Darmstadt
sodium acetate	Merck KGaA, Darmstadt
sodium carbonate	Merck KGaA, Darmstadt
sodium chloride	Carl Roth GmbH, Karlsruhe
TEMED	Sigma-Aldrich GmbH, Steinheim
trichostatine A	Sigma-Aldrich GmbH, Steinheim
tricin	Sigma-Aldrich GmbH, Steinheim
tris	Merck KGaA, Darmstadt
tritonX-100	Carl Roth GmbH, Karlsruhe
tween-20	Carl Roth GmbH, Karlsruhe

Table 5: Enzymes used in this study.

Enzymes	**Manufacturer**
hot star taq DNA polymerase (#203205)	Qiagen, Hilden
proteinase K (#70633)	Merck KGaA, Darmstadt
protease inhibitor tablets(#11836170001)	Roche GmbH, Grenzach-Wyhlen
RNAse A (#1010914200)	Roche GmbH, Grenzach-Wyhlen
RNAsin (#EO0381)	Fermentas GmbH, St. Leon-Rot
reverse transcriptase (#100004925)	Invitrogen, Carlsbad, CA
taq polymerase (#10342-020)	Invitrogen, Carlsbad, CA

Table 6: Antibodies used in this study.

Antibodies	Manufacturer
goat anti-ARHI (#sc-30321)	Santa Cruz Inc., Santa Cruz, CA
donkey anti-goat (#sc2020)	Santa Cruz Inc., Santa Cruz, CA
mouse anti-tubulin (#T9026)	Sigma-Aldrich GmbH, Steinheim
goat anti-mouse (#31444)	Pierce Technology, Rockford, IL
rabbit anti-Histon H3, C-terminal (#17-10046)	Upstate, Charlottesville, VA
rabbit anti-Histon H3ac (#06-599)	Upstate, Charlottesville, VA
rabbit anti-Histon H4ac (#17-630)	Upstate, Charlottesville, VA
rabbit anti-Histon H3K9me3 (#17625)	Upstate, Charlottesville, VA
goat anti-rabbit (#J6-126203)	Thermo Scietific, Waltham, MA
anti-biotin (#7075)	Cell Signaling, Danvers, MA

2.5 Kits, reagents and assays

The following table 7 provides a list of the different kits, reagents and assays that were employed in this study.

Table 7: Kits, reagents and assays used in this study.

Kits, reagents, assays	Manufacturer
Apo-ONE® caspase 3/7 assay (#TB295)	Promega, Madison, WI
blood and cell culture DNA spin kit (#440250)	GENOMED GmbH, Löhne
BigDye® terminator v1.1 cycle sequencing kit (#4336774)	Applied Biosystem, Foster City
cell proliferation ELISA (#11647229001)	Roche GmbH, Grenzach-Wyhlen
Chromatin Immunoprecipitate (ChIP) Assay Kit (#17-245)	Upstate, Charlottesville, VA

DNA clean up system (#A7280)	Promega, Madison, WI
PCR product purification spin kit (#410250)	GENOMED GmbH, Löhne
RC DC protein assay (#500-0122)	BioRad GmbH, München
Platinum® SYBR® Green (#11733-046)	Invitrogen, Carlsbad, CA
TRIzol®-reagent (#15596-018)	Invitrogen, Carlsbad, CA

2.6 Solutions, buffers and gels

All solutions, buffers and gels used in the own experiments are listed in tables 8 - 10.

Table 8: Solutions used in this study.

Kits, reagents, assays	**Manufacturer**
for apoptosis	
- binding buffer (100x)	0.82 M $CaCl_2$ in sterile water
- RNAse A solution (10 mg/ml)	25 mg RNAse A in 10 mM Tris/HCl (pH: 7.5)
- propidiumiodide solution	50 µg/ml propidiumiodide 200 µg/ml RNAse A
for ChIP analysis	
- swelling buffer (1x)	25 mM HEPES, pH 7.8
-	1.5 mM $MgCl_2$
-	10 mM KCl
-	0.1 % NP-40
-	1 mM DTT + 0.5 mM PMSF
- elution buffer	0.1 M sodium bicarbonate
-	1 % SDS

for separation of nuclei (CHiP analysis)

- nuclei extraction buffer	0.32 M sucrose
	5 mM $CaCl_2$
	3 mM $Mg(Ac)_2$
	0.1 mM EDTA
	10 mM Tris-HCl
	1x protease inhibitor
	0.1 mM PMSF
	0.1 % Triton X-100
	0.1 % NP-40
- sucrose sushion	1.8 M sucrose
	3 mM $Mg(Ac)_2$
	10 mM Tris-HCl (pH: 8)

for silver stain of polyacrylamide gels

- nitric acid (1 %)	100 ml (65 % HNO_3)
	6.4 l distilled water
- silver solution (0.2 %)	4 g $AgNO_3$
	2 l distilled water
- sodium carbonate solution	210 g Na_2CO_3
	3.5 ml formaldehyde (37 %)
	in 7 l distilled water

for bisulfite treatment of DNA

- sodium hydroxide (10 N)	4 g NaOH
	10 ml distilled water
- hydroquinone (10 mM)	0.11 g hydroquinone
	100 ml distilled water
- sodium bisulphite (3 M)	15.6 g sodium bisulphite
	50 ml distilled water

for DNA, RNA and protein extraction by ultracentrifugation

- GITC solution (4 M)	500 g guanidinisothiocyanate
	26.6 ml sodium citrate (1 M, pH 7)
	8.5 ml ß-mercaptoethanol
	1058 ml distilled water
	pH 7 with NaOH
- RNAsin mix	90 µl RNAsin (40 U/µl)
	193.5 µl DTT (0.1 M)
	6916.5 µl DEPC-treated water
- CsCl solution	479.85 g caesium chloride
	4.2 ml sodium acetate (3 M; pH 5)
	in 500 ml DEPC-treated water
- proteinase K buffer:	Tris/HCl (0.01 M)
	EDTA (0.005 M)
	SDS (0.5 %)

for SDS-PAGE and western blot

- cell lysis buffer	50 mM Tris-HCl, pH: 8.0
	150 mM NaCl
	0.5 % TritonX-100
	0.5 % deoxycholate
- blocking buffer	5 % milk in TBS-Tween (0.1 %)
- running buffer for tris-gels (10x)	0.25 M Tris
	2 M glycine
	1 % SDS
- running buffer for tricin-gel (1x)	0.1 M tricin
	0.1 M tris
	1 g SDS
- transfer buffer (1x)	25 mM Tris
	0.2 M glycine
	20 % methanol
- ponceau S (0,1% (w/v))	1 g ponceau S
	50 ml acetic acid
	In 1 l distilled water

- laemmli buffer (4x)	0.1 M Tris pH 6.8 6 % SDS 40 % glycerol 0,04 % bromphenol blue 4 % ß-mercaptoethanol

Table 9: Buffers used in this study.

Buffer	**End concentration**
formamid loading buffer	20 ml formamide 5 ml H_20 a pinch xylen cyanol blue a pinch bromphenol blue
loading buffer for sequencing	76.2 % formamid 19 % 25 mM EDTA-solution pH 8 4.8 % dextran blue
loading buffer for agarose gels	30 % glycerol a pinch xylen cyanol blue a pinch bromphenol blue
TAE buffer (50x)	2 M Tris 1 M acetic acid 50 mM EDTA pH 8.0
TBE buffer (1x)	0.89 M Tris base 0.89 M boracic acid 20 mM EDTA pH 8.0

TE buffer (1x)	10 mM Tris 1 mM EDTA pH 7.5
TBS buffer (10x)	1.37 M NaCl 0.2 M Tris pH 7.6

Table 10: Gels used in this study.

Gels	Compounds
agarose gels (2 %)	2 g agarose 100 ml 1x TAE buffer
gels for LOH analysis (12 %, 19:1; 8 M urea)	135 ml bis-/acrylamide (40%, 19:1) 45 ml 10x TBE 216 g urea 270 ml distilled water 300 µl APS (10 %) 60 µl TEMED
gels for mutation analysis	
- SSCP gel (8 %, 29:1)	38.66 ml acrylamide (40 %) 26.66 ml bisacrylamide (2 %) 20 ml 10x TBE 114.68 ml distilled water 350 µl APS (10 %) 60 µl TEMED
- SSCP gel (10 %, 29:1)	48.34 ml acrylamide (40 %) 33.34 ml bisacrylamide (2 %) 20 ml 10x TBE 98.32 ml distilled water 350 µl APS (10 %) 60 µl TEMED

- SSCP gel (12 %, 29:1)	58 ml acrylamide (40 %) 40 ml bisacrylamide (2 %) 20 ml 10x TBE 82 ml distilled water 350 µl APS (10 %) 60 µl TEMED
gels for sequencing (7 %; 29:1; 10 M urea)	21 g urea 8.4 ml bis-/acrylamide (30 %; 29:1) 6 ml 10x TBE 20 ml distilled water 350 µl APS (10 %) 30 µl TEMED
gels for western blot	
- tris seperating gel (12.5 %)	2.1 ml acrylamide (30 %; 37.5:1) 1.3 ml tris (1.5 M; pH 8.8) 1.6 ml distilled water 0.025 ml SDS (20 %) 0.05 ml APS (10 %) 0.002 ml TEMED
- tris stacking gel (5 %)	0.34 ml acrylamide (30 %; 37.5:1) 0.26 ml tris (1.5 M; pH 8.8) 1.36 ml distilled water 0.01 ml SDS (20 %) 0.02 ml APS (10 %) 0.002 ml TEMED
- tricin separating gel (15 %)	7.5 ml acrylamide (30 %; 37.5:1) 5.18 tris (3 M, pH 8.5) 2.57 distilled water 0.05 ml APS 0.002 ml TEMED

- tricin stacking gel (5 %)
  - 0.7 ml acrylamide (30 %; 37.5:1)
  - 1.27 tris (3 M, pH 8.5)
  - 3.08 distilled water
  - 0.02 ml APS
  - 0.002 ml TEMED

2.7 sh RNAs

The sh-RNAs used for stabile transfection and knock-down of ARHI in glioma cells were ordered from Eurofins MWG GmbH (Ebersberg, Germany). Table 11 shows the individual nucleotide sequences.

Table 11: Sequences of sh-RNAs used for stable transfection of glioma cell lines.

sh RNA	Sequence (sense strand)
sh1_ARHI	TTCAATGGTCGGCAGGTACTC
sh2_ARHI	AACAGCTCCTGCACATTCACA
sh3_ARHI	TTATGCACTTGTCAAGCAGCT

2.8 Oligonucleotides

All primers (Table 12) were ordered from Eurofins MWG GmbH (Ebersberg, Germany).

Table 12: Primers used for mRNA expression and LOH analyses, as well as for mutation, methylation and ChIP analyses.

Gene	Application	Annotation	Primer Sequence	fragment size (bp)
RRP22	Real-time RT-PCR		5'-GTTCCTGTTCGGTGACTACC-3'	184
			5'-CTGCAAGCTCCAGTCCTTAG-3'	
	SSCP analysis	Fragment 1	5'-CCATGAGGCTTTCCAGCG-3'	220
			5'-GTCGCGGATGCTCAAGTC-3'	
		Fragment 2	5'-CTGCTCGACGGCGCC-3'	235
			5'-GGGCTGAAACGCAAGTATCC-3'	
		Fragment 3	5'-GGTTCGAGAGCGGAAGAG-3'	230
			5'-CCAGACCTGTCCTAGCTC-3'	
		Fragment 4	5'-GCGTGTGTATACCCACTGG-3'	228
			5'-CGTGCCAGTTGTACTTGGC-3'	
		Fragment 5	5'-CGCTGCGGCTACCTCG-3'	181
			5'-CCATGGATGGCACTGTCC-3'	
	Microsatellite analysis 22q12	D22S1150	5'-GGAACAGTTTGTGCCCCTG-3'	~168
			5'-CTCAGACCTCATCTCCTGC-3'	
		D22S689	5'-ATGTACAGACCTGCAACTTGCT-3'	~215
			5'-CCTATCTATCTGTCTGTCTGTC-3'	
		D22S1176	5'-CTGTGCCATCTCTAGTGGAC-3'	~89
			5'-GGGGTATGCGTGTACGTG-3'	
		D22S531	5'-AGCCTGGGTGACAGAGTG-3'	~171
			5'-AGCCCTGTGCTATGAGAGG-3'	
	Sodium bisulfite sequencing		5'-ATAGGAATTGGCGGATGATGGT-3'	286
			5'-TCTACCCACTCGACTATCTATC-3'	
	ChIP (Chromatin immunoprecipitation)		5'-CGAGCAGTGTTTGGAAGAG-3'	135
			5'-GTGACTGGGGGACAGAGAT-3'	
RHOB	Real-time RT-PCR		5'-GTTCAGTAAGGACGAGTTCC-3'	172
			5'-GAGAATGACGTCGGTGTCC-3'	
	SSCP analysis	Fragment 1	5'-CACCTGCGCGCAGCC-3'	203
			5'-GGGCACGTACACCTCGG-3'	
		Fragment 2	5'-GCCTGCTGATCGTGTTCAG-3'	215
			5'-CGAGTCCGGGCTGTCC-3'	
		Fragment 3	5'-GGACACCGACGTCATTCTC-3'	208
			5'-GCCGTCATCCGTGCGC-3'	
		Fragment 4	5'-GGCCCGCATGAAGCAGG-3'	208
			5'-GCGCGGCCCTCATAGC-3'	
		Fragment 5	5'-CAGAACGGCTGCATCAACTG-3'	197
			5'-CCACGCCAAGTCCTGGC-3'	
	Sodium bisulfite sequencing		5'-TTTAGATTTTGGAGGTTTTAGATAGTTA-3'	356
			5'-AAACATACAAAACAACAACTCCAAC-3'	
	ChIP (Chromatin immunoprecipitation)		5'-CTGGGCCGTCAATCAAGCT-3'	147
			5'-CCGCTATTTAAAGAGTCCGGC-3'	
RERG	Real-time RT-PCR		5'-TCAACCTACCGACACCAAGC-3'	129
			5'-GACCAGCACAAAGCCTTCC-3'	
	Sodium bisulfite sequencing		5'-TTTGGGTGTAGTACGTTAAAGATTTAAG-3'	349
			5'-TCCTCTACAAATTCGAAATAAATCCC-3'	
RASL11A	Real-time RT-PCR		5'-GACTACCTACTGCCCAAGG-3'	101
			5'-CCAATGAATCTCTTGGTCAGG-3'	
ARHI	Real-time RT-PCR		5'-GTTCAGTAAGGACGAGTTCC-3'	172
			5'-GAGAATGACGTCGGTGTCC-3'	
p21 (WAF1)	Real-time RT-PCR		GCAGACCAGCATGACAGATTT	130
			AAGATGTAGAGCGGGCCTTT	
	positive ChIP control		5'-GTGTCCAGCGCACCAAC-3'	101
			5'-GGCCGAGTTCCAGCAG-3'	
ß-2-MG	cDNA synthesis control by Real-time RT-PCR	3' end	5'-GTTGCTCCACAGGTAGCTCTAG	110
			5'-ACAAGCTTTGAGTGCAAGAGATTG	
		5' end	5'- GTCTCGCTCCGTGGCCTTAG	128
			5'- CATTCTCTGCTGGATGACGTGAG	
ARF	Real-time RT-PCR control		5'-GACCACGATCCTCTACAAGC-3'	111
			5'-TCCCACACAGTGAAGCTGATG-3'	
GAPDH	Real-time RT-PCR control		5'-CATGACAACTTTGGTATCGTG-3'	240
			5'-GTCCACCACTGACACGTTG-3'	
	ChIP control		5'-TACTAGCGGTTTTACGGGCG-3'	166
			5'-TCGAACAGGAGGAGCAGAGAGCGA-3'	

3 Methods

3.1 Molecular biological methods

3.1.1 Extraction of nucleic acids

3.1.1.1 Extraction of nucleic acids from tumor samples

Extraction of DNA and RNA from frozen tumor tissue samples was performed by ultracentrifugation. Tumor samples were homogenized with an Ultra Turrax homogenizer in 6 ml guanidiniumisothiocyanate solution (GITC). The homogenate was centrifuged and the supernatant was layered over 4 ml caesium chloride solution in a SW41.1 polyallomer tube. Ultracentrifugation was done with a swing out rotor for 16 h at 32000 rpm and room temperature to separate RNA, DNA and proteins. The RNA was recovered as a pellet and dissolved in 200 µl RNAsin mix and precipitated with 20 µl 3 M sodium acetate (pH: 5.2) and 500 µl icecold ethanol (95 %) for 30 min at -80 °C. After centrifugation for 20 min at 14000 rpm and 4 °C, the RNA pellet was washed with ethanol (70 %), dried shortly and resuspended in DEPC-treated water. To release the DNA from the caesium chloride solution, the 5 ml mix was precipitated with 350 µl 7.5 M ammonium acetate and incubated 2 h at 37 °C. Next, 2.5 x volume ethanol (95 %) was added and incubated again for 30 min at -80 °C. After centrifugation at 2500 rpm for 20 min at 4 °C and several washing steps with ethanol (70 %), 5 ml proteinase K buffer and 100 µl proteinase K (20 mg/ml) were added and incubated at 55 °C over night. 2.5 ml phenol and 2.5 ml chloroform-isoamylalcohol (24:1) were added the next day and incubated for 20 min at room temperature and centrifuged for 20 min at 2500 rpm and 15 °C. The upper phase was taken and transferred to a new tube. 5 ml of chloroform-isoamylalcohol (24:1) were added, incubated and centrifuged again. Then, the upper phase was transferred to a 50 ml tube and the DNA was precipitated with 4 x volume 5 M sodium chloride and 2.5 x volume ice-cold ethanol (95 %). DNA was centrifuged for 20 min at 2500 rpm and 4 °C and washed with ethanol (70 %) before the DNA pellet was resuspended in 300 µl TE buffer.

3.1.1.2 Extraction of RNA from cultured cells

Total RNA from cultured cells was extracted with TRIzol®-reagent. Cells were washed with PBS and transferred to an Eppendorf tube with 1 ml trizol reagent. After an incubation of 5 min, 200 µl chloroform was added, mixed, incubated for 10 min at room temperature and centrifuged for 10 min at 14000 rpm and 4 °C. The upper phase was transferred to a new Eppendorf tube and combined with 1x volume isopropanol. After the incubation for 15 min at RT and centrifugation for 10 min at 14000 rpm and 4 °C, RNA pellets were washed with ethanol (70 %) and resuspended in 30 µl DEPC-treated water.

3.1.1.3 Extraction of DNA from cultured cells and blood samples

Total DNA extraction from cultured cells and peripheral blood leukocytes was performed with the JetQuick blood and cell culture DNA spin kit (GENOMED GmbH, Löhne) according to the manufactur's protocol.

3.1.2 PCR analysis

The polymerase chain reaction (PCR) is a method to amplify DNA fragments and was first described by Nobel laureate Kari Mullis (Mullis et al 1986, Saiki et al 1985). A DNA polymerase assembles a new single-strand starting from DNA oligonucleotides (primers) that initiate the synthesis. The PCR proceeds in three steps for several cycles: Denaturation (DNA melting to yield single strand DNA), annealing (annealing of the primers to the single-stranded DNA template) and elongation (DNA polymerase synthesises a new, complementary DNA strand). This amplification is an exponential process until one of the reagents becomes limited and the reaction achieves a plateau. PCR products can be separated in agarose gels (e.g. 2 % agarose gels) containing ethidiumbromide for visualization of the amplified DNA.

3.1.2.1 Real-time PCR analysis

Real-time PCR analysis is based on a normal PCR but is performed in the presence of a fluorescence dye (e.g. SybrGreen) to quantify DNA. This dye can intercalate with the DNA and resulting fluorescent PCR products are measured after each cycle. The fluorescence intensity is proportional to the amount of DNA and defined as R_n value (normalized reporter). For that, a constant R_n value is defined, which cuts all curves in

the linear amplification area. The report of the product amplification is diagrammed with the R_n value (ordinate) and the number of cycles (abscissa) (Figure 8).

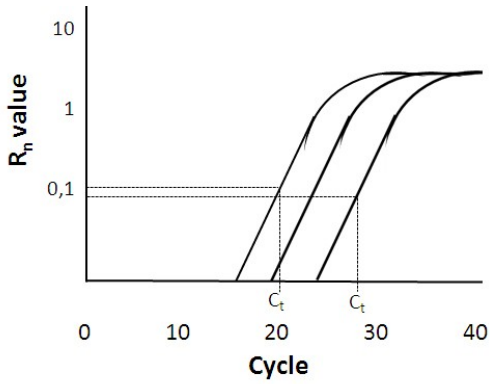

Figure 8: Example of a real-time PCR analysis. Shown are amplification curves with decreasing expression levels from left to right. Higher Ct values indicate lower expression levels that reach the same Rn value at a higher cycle number.

Real-time PCR analyses were run under standard conditions in all experiments with the StepOnePlus™ sequence detection system (Applied Biosystem, Foster City, CA). The program starts with 10 min incubation at 90 °C to activate the HotStar Taq-polymerase through denaturation of an inhibitor protein. Subsequent steps are 40 cycles with 15 s at 95 °C for denaturation of the DNA and 60 s at 60 °C for the annealing and elongation. All samples were run in triplicates.

To optimise the PCR reaction, primer conditions were tested using different concentrations (3 x 3 primer matrix) of the forward and reverse primers (50, 300 and 900 µM). Primers with the lowest C_T-data for the resulting PCR-product and with the right peak for the dissociation curves were used (Table 12).

3.1.2.2 Real time RT-PCR analysis

Gene expression was determined by SybrGreen-based real-time PCR after reverse transcription using the StepOnePlus™ sequence detection system. For reverse transcription, 3 µg RNA in 29.4 µl DEPC-treated water were denatured for 10 min at 70 °C and then incubated on ice for 5 min. After addition of 19.6 µl reaction mix consisting of 0.4 µl DTT (0.1 M), 1 µl RNAsin, 1.7 µl BSA (1 mg/ml), 2.5 µl dNTPs (25 mM), 3 µl pd(N)6 (1,5 µg/µl). 10µl 5x First Strand Buffer and 1µl superscript II reverse transcriptase (200 U/µl), the cDNA synthesis proceeded for 50 min at 42 °C followed by an incubation step for 10 min at 80 °C to inactivate the reverse transcriptase. Before

usage, the cDNA, quality was controlled by PCR with two different ß2-microglobulin primer pairs (Table 12) that cover amplicons in the 5' and 3' parts of this gene, respectively. For analysis by real-time RT-PCR the cDNA was diluted with water and 5 µl of diluted cDNA were added to 20 µl SyprGreen Mix. Fold expression changes relative to the average of 10 non-neoplastic brain tissues (NB) were calculated with the ΔΔCT method (Livak and Schmittgen 2001). ΔC_t was calculated by subtracting the C_t value of the reference gene from the C_t value of the gene of interest. ($C_{t,\ target\ gene}$ - $C_{t,\ reference\ gene}$). The $\Delta\Delta C_t$ value was then calculated as follows: $\Delta C_{t,\ tumor}$ - $\Delta C_{t,\ NB}$. The relative mRNA expression resulted in the reversal of the logarithm $\Delta\Delta C_t$ value ($2^{-\Delta\Delta Ct}$).

ARF1 (ADP-ribosylation factor 1) was used as reference (Table 12) that is expressed at similar levels in glioma tumor samples across tumor grades.

3.1.3 DNA methylation analysis

DNA methylation analyses were performed by direct sequencing of sodium bisulfite-modified DNA (Hayatsu and Shiragami 1979). The method takes advantage of the fact that unmethylated cytosines are converted to uracil by sodium bisulfite treatment, whereas methylated cytosines remain unconverted. The conversion of unmethylated cytosines to uracil occurs by desamination of the cytosine residue to uracil in the presence of sodium bisulfite (Figure 9). These changes can be assessed by sequencing of the sodium bisulfite-treated DNA and can thus be used to investigate the methylation status of CpG dinucleotides in 5'-CpG islands.

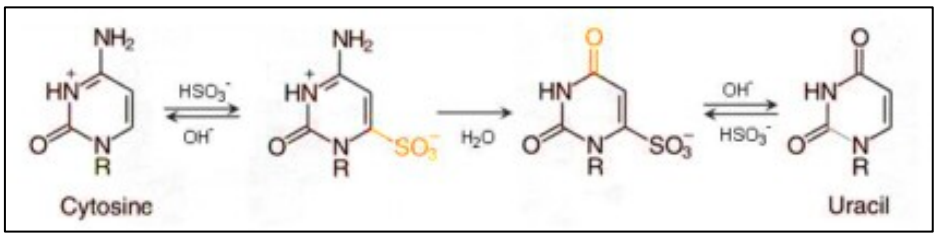

Figure 9: Conversion of unmethylated cytosine to uracil by sodium bisulfite treatment (from: http://www.dkfz.de/funct_genome/epigenetics.html). A cytosine is turned into a sulphonated cytosine intermediate in the presence of bisulfite and then converts into a sulphonated uracil through desamination. The sulpho-group is finally split off under alkaline conditions and uracil is generated.

Sodium bisulfite treatment of 1 µg DNA was performed according to a standard protocol (Herman et al 1996). In brief, DNA was denatured with 0.2 M NaOH for 15 min at 37 °C and bisulphite treatment was done over-night at 55 C° with 0.25 mM hydroquinone and 2.67 M sodium-bisulfite. DNA was then purified with the DNA clean up system (Promega, Madison, WI) and precipitated with sodium acetate and ethanol before resuspension in 15 µl distilled water. Sodium bisulfite-modified DNA was then amplified with specific primers and PCR products were purified with the PCR product purification spin kit (GENOMED GmbH, Löhne).

PCR conditions were used as detailed below and the respective primers are listed in Table 12.

Reaction mix		**Program**	
water	10.9 µl	95 °C	15 min
10 x PCR-buffer	2 µl	95 °C	30 s
dNTPs (2 mM)	2 µl	56 °C	60 s
primer forward (10 pmol)	2 µl	72 °C	120 s
primer reverse (10 pmol)	2 µl	72 °C	10 min
hotstar taq (Qiagen)	0.1 µl	4 °C	stop
bisulfite-modified DNA	1 µl	cycles	x 40

The amplified and purified fragments were then sequenced and the semiquantitative calculation of a promoter methylation score was carried out (Tepel et al 2008). The methylation status at each of the analyzed CpG sites was rated using the following scale: 0, completely unmethylated; 1, a weakly methylated signal detectable in the sequence; 2, methylated signal approximately equal to unmethylated signal; 3, methylated signal markedly stronger than unmethylated signal. Based on this rating scale, a cumulative promoter methylation score was calculated for each tumor (Tepel et al 2008). Tumors with methylation scores exceeding that of three non-neoplastic brain tissue were regarded as hypermethylated. Commercially available hypermethylated DNA (Upstate, Charlottesville, VA) was used as a positive control.

3.1.4 Mutation analysis

Single strand conformation polymorphism (SSCP) heteroduplex analyses (Maxam and Gilbert 1980, Orita et al 1989) were performed to screen for mutations in the genes' coding sequences. This method is based on detecting differences in the secondary structure. Single strands can show altered base pairings dependent on their sequence, which result in different loops and folds. These differences lead to different migration

velocities in non-denaturing polyacrylamide gels. After electrophoresis, the SSCP-bands are visualized by silver staining of the polyacrylamide gels. This allows the differentiation between single strands containing wild type and mutant sequences (Figure 10).

Approximately 150-250 bp long PCR fragments (for primers see Table 12) of the coding sequence are needed for this analysis because shorter fragments do not form secondary structures and sensitivity for mutation detection becomes lower when longer DNA fragments are used.

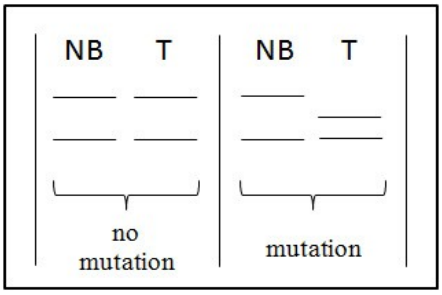

Figure 10: Schematic representation of SSCP band patterns. Note the differences in the single strand pattern (right) in the mutant tumor tissue (T) compared to non-neoplastic brain tissue (NB), while the band pattern of the tumor tissue without a mutation (left) shows no alterations compared to non-neoplastic brain tissue.

PCR settings for the mutation analyses were as detailed below. The respective primers are listed in Table 12.

	Fragment	Reaction mix		Program		Fragment	Reaction mix		Program	
RhoB	**fragment 1** **fragment 3** **fragment 4**	water	10.15 µl	95 °C	5 min	**fragment 2** **fragment 5**	water	15.15 µl	95 °C	5 min
		10 x PCR-buffer	2.5 µl	95 °C	20 s		10 x PCR-buffer	2.5 µl	95 °C	20 s
		dNTPs (2 mM)	2.5 µl	58 °C	20 s		dNTPs (2 mM)	2.5 µl	58 °C	20 s
		primer forward (10 pmol)	1.5 µl	72 °C	20 s		primer forward (10 pmol)	1.5 µl	72 °C	20 s
		primer reverse (10 pmol)	1.5 µl	72 °C	10 min		primer reverse (10 pmol)	1.5 µl	72 °C	10 min
		$MgCl_2$ (50 mM)	0.75 µl	4 °C	stop		$MgCl_2$ (50 mM)	0.75 µl	4 °C	stop
		Q-Solution (20%)	5.0 µl	cycles	x 40		DMSO (100%)	2.5 µl	cycles	x 40
		taq-polymerase (invitrogen)	0.1 µl				taq-polymerase (invitrogen)	0.1 µl		
		DNA (20 ng/µl)	1.0 µl				DNA (20 ng/µl)	1.0 µl		
RRP22	**fragment 1** **fragment 3** **fragment 4** **fragment 5**	water	10.15 µl	95 °C	5 min	**fragment 2**	water	15.15 µl	95 °C	5 min
		10 x PCR-buffer	2.5 µl	95 °C	20 s		10 x PCR-buffer	2.5 µl	95 °C	20 s
		dNTPs (2 mM)	2.5 µl	58 °C	20 s		dNTPs (2 mM)	2.5 µl	58 °C	20 s
		primer forward (10 pmol)	1.5 µl	72 °C	20 s		primer forward (10 pmol)	1.5 µl	72 °C	20 s
		primer reverse (10 pmol)	1.5 µl	72 °C	10 min		primer reverse (10 pmol)	1.5 µl	72 °C	10 min
		$MgCl_2$ (50 mM)	0.75 µl	4 °C	stop		$MgCl_2$ (50 mM)	0.75 µl	4 °C	stop
		Q-Solution (20%)	5.0 µl	cycles	x 40		DMSO (100%)	2.5 µl	cycles	x 40
		taq-polymerase (invitrogen)	0.1 µl				taq-polymerase (invitrogen)	0.1 µl		
		DNA (20 ng/µl)	1.0 µl				DNA (20 ng/µl)	1.0 µl		

PCR products were mixed with 5 µl loading buffer [80 % (v/v) formamide; 20 % (v/v) bromophenolblue/xylencyanol solution] and incubated for 5 min at 95 °C. After cooling down, the samples were separated by electrophoresis on 8 %, 10 % or 12 % nondenaturing polyacrylamide gels (40 % acrylamide/ bisacrylamide; 19:1) at room temperature and 4 °C. After electrophoresis, the SSCP/heteroduplex band patterns were visualized by silver staining of the gels as described for microsatellite analysis (3.1.5). In case of aberrant band patterns, PCR products were sequenced to identify the position and type of the mutation using the BigDye Cycle Sequencing Kit and an ABI PRISM 377 semiautomated DNA sequencer (see methylation analysis 3.1.3).

3.1.5 Microsatellite analyses

Microsatellites (Litt and Luty 1989) are short DNA segments of 2-6 nucleotides that can be repeated 10-100 times. These repeated sequences are distributed over the entire genome with a distance of around 30 kb. Microsatellites show high levels of polymorphism (Weber and May 1989), and can therefore be used as genetic markers. To investigate defined genomic regions for loss of heterozygosity (LOH), microsatellite loci were amplified with primers binding to their 3' and 5' flanking regions. The amplified segments were separated by gel electrophoresis on polyacrylamide gels. Informative markers are microsatellites that show distinct paternally and maternally inherited alleles with typically 4 visible bands on polyacrylamid gels due to distinct migration behaviors of the sense and antisense strands of each allele (heterozygous/informative state). Microsatellites with only two bands on polyacrylamid gels are designated as not informative markers because maternal and paternal alleles have the same number of repeats (homozygous) (Figure 11). Allelic losses in tumor cells can be investigated with this method, when comparing tumor DNA and blood DNA of the same patient but only at loci showing a heterozygous pattern in the constitutional (blood) DNA.

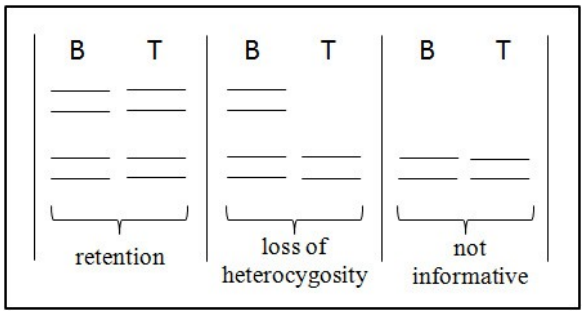

Figure 11: Schematic examples of microsatellite analysis for detection of loss of heterozygosity in tumor DNA. Note retention (left) and loss of heterozygosity (middle) of the polymorphic microsatellite marker in the tumor tissue (T), while in corresponding blood samples (B) of the same patients, both alleles are retained. Not informative (right) microsatellite markers cannot be used for detection of allelic losses.

The PCR settings that were used for microsatellite amplification are detailed below. The respective PCR primers are listed in Table 12.

	Reaction mix		**Program**			**Reaction mix**		**Program**	
D22S531	water	15.9 µl	95 °C	15 min	**D22S689**	water	15.15 µl	95 °C	5 min
	10 x PCR-buffer	2.5 µl	95 °C	15 s		10 x PCR-buffer	2.5 µl	95 °C	20 s
	dNTPs (2 mM)	2.5 µl	58 °C	15 s		dNTPs (2 mM)	2.5 µl	58 °C	20 s
	primer forward (10 pmol)	1.5 µl	72 °C	15 s		primer forward (10 pmol)	1.5 µl	72 °C	20 s
	primer reverse (10 pmol)	1.5 µl	72 °C	10 min		primer reverse (10 pmol)	1.5 µl	72 °C	10 min
	hotstar taq (Quiagen)	0.1 µl	4 °C	stop		$MgCl_2$ (50 mM)	0.75 µl	4 °C	stop
	DNA (20 ng/µl)	1.0 µl	cycles	x 28		taq-polymerase (invitrogen)	0.1 µl	cycles	x 26
						DNA (20 ng/µl)	1.0 µl		
D22S1176	water	9.9 µl	95 °C	5 min	**D22S1150**	water	9.9 µl	95 °C	5 min
	10 x PCR-buffer	2.5 µl	95 °C	20 s		10 x PCR-buffer	2.5 µl	95 °C	20 s
	dNTPs (2 mM)	2.5 µl	58 °C	20 s		dNTPs (2 mM)	2.5 µl	58 °C	20 s
	primer forward (10 pmol)	1.5 µl	72 °C	20 s		primer forward (10 pmol)	1.5 µl	72 °C	20 s
	primer reverse (10 pmol)	1.5 µl	72 °C	10 min		primer reverse (10 pmol)	1.5 µl	72 °C	10 min
	$MgCl_2$ (50 mM)	1.0 µl	4 °C	stop		$MgCl_2$ (50 mM)	1.0 µl	4 °C	stop
	Q-Solution (20%)	5.0 µl	cycles	x 32		Q-Solution (20%)	5.0 µl	cycles	x 26
	taq-polymerase (invitrogen)	0.1 µl				taq-polymerase (invitrogen)	0.1 µl		
	DNA (20 ng/µl)	1.0 µl				DNA (20 ng/µl)	1.0 µl		

After amplification of microsatellite loci, 4-6 µl PCR products were mixed together with 5 µl loading buffer [80 % (v/v) formamide; 20 % (v/v) bromophenolblue/xylencyanol solution] and incubated for 10 min at 95 °C. After cooling down, the samples were loaded on 12 % polyacrylamide gels (40 % acrylamide; 2 % bisacrylamide; 8 M urea) and run in warm 0.5 x TBE at 45 W for 45 min – 2 h dependent on PCR product size. The last step was to visualise the amplicons by silver staining of the gels (Budowle et al 1991). Gels were fixed with 10 % ethanol for 10 min followed by a sensitization step with 1 % nitric acid for 1-3 min. After washing, the gels were stained with 2 % silver-

solution for 20 min (exclude from light). Next, gels were washed three times before they were developed with 3 % sodium carbonate. Reaction was stopped by adding 10 % acetic acid for 5 min and washed again with water.

3.1.6 Chromatin immunoprecipitation assay

Chromatin immunoprecipitation is a method to investigate protein-DNA interactions. Proteins can be isolated with specific antibodies by immunopreciptation and the DNA bound to these specific proteins can be used for further investigations. The ChIP method was independently established and optimized for the own project. The experimental procedure is schematically shown in Figure 12.

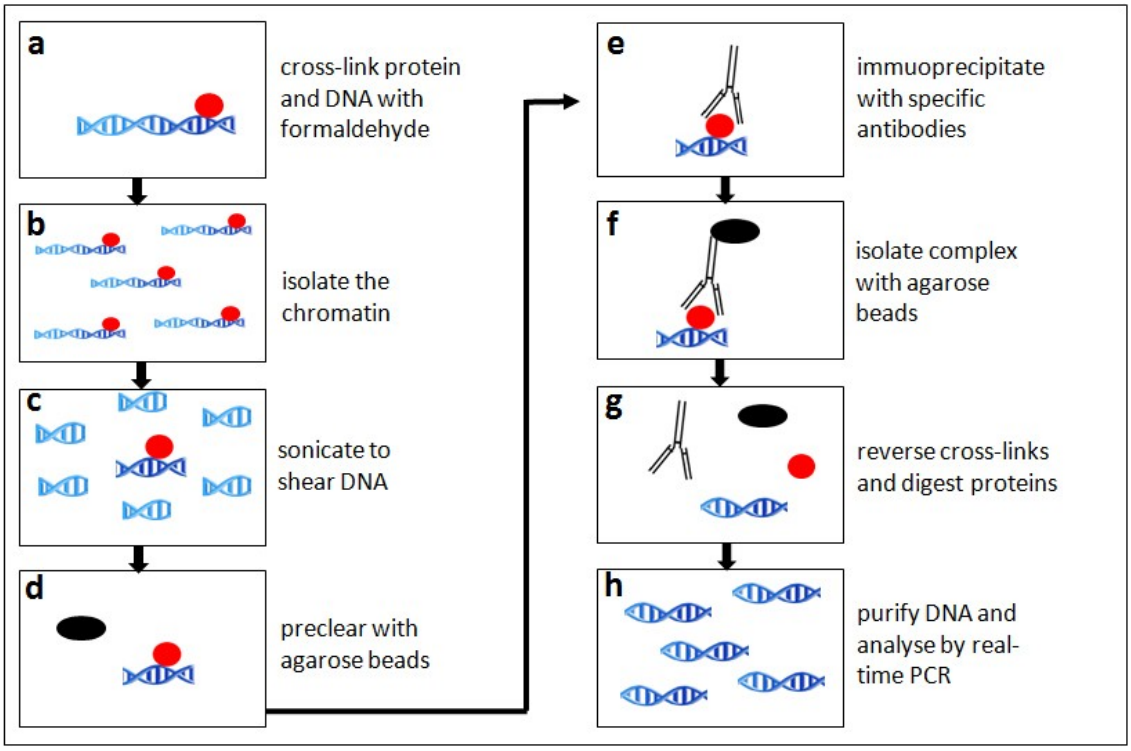

Figure 12: Overview of the ChIP assay protocol. Protein (red) and DNA (blue) were cross-linked with formaldehyde (a). The chromatin was isolated (b) and DNA was sheared by sonification (c). Agarose beads were used for preclearing to reduce unspecific binding (d). Next step was the immunoprecipitation with specific antibodies (e) followed by the isolation of the complex with agarose beads (f). After reversing the cross-link and the digestion of the proteins (g), the DNA was purified and analyzed by real-time PCR (h).

Chromatin immunoprecipitation was performed from trichostatin A-treated and untreated glioblastoma cells as well as from fresh frozen glioblastoma tissues. DNA and proteins from 1 x 10^6 glioblastoma cells were crosslinked with 1 % formaldehyde for 10 minutes and then resuspended in swelling buffer to isolate nuclei. Purification of nuclei from fresh frozen tissues was accomplished via sucrose gradient ultracentrifugation (Jiang et al 2008). Frozen tissues were homogenized by douncing in nuclear extraction buffer, nuclei were then fixed by adding 1 % formaldehyde for 10 min, the tissue homogenates were transferred on top of a sucrose cushion and ultracentrifuged at 25000 rpm for 3 hours at 4 °C.

Nuclei prepared from cells or tumor tissues were further processed using a commercial ChIP assay kit (Upstate, Charlottesville, VA) according to the manufacturer's recommendations. After resuspension in SDS-lysis buffer, genomic DNA was sheared to 200–800 bp fragments by sonication 9 x 9 sec on ice with an ultrasonic processor. Sonicated samples were then precleared with protein A agarose/salmon sperm DNA for 30 min at 4 °C to reduce non-specific binding of the beads to DNA. A 5 % sample volume was saved as input control while the rest was used for immunoprecipitation with specific antibodies at 4 °C overnight. In case of cell lines, immunoprecipitation was performed with anti-H3ac (acetylated histone H3) and anti-H4ac (acetylated histone H4) antibodies. In the tumors, we employed antibodies against H3ac and H3K9me3 (trimethylated on the 9^{th} lysine of histone H3) for immunoprecipitation. In both assays rabbit anti-human IgG fraction served as a negative isotype control. Antibody/histone/DNA complexes were collected using protein A agarose/salmon sperm DNA (1 h at 4 °C) and the histone/DNA complexes were then eluted from the antibodies (2 x 15 min incubation at room temperature in freshly prepared elution buffer). After reversing the histone-DNA crosslink with NaCl for 4-6 hours at 65 °C the DNA was extracted by standard proteinase K digest and subsequent phenol/chloroform extraction.

Immunoprecipitated DNA was assessed by using real-time PCR analysis with primers targeting the promoter sequences of interest and normalized to the respective input fraction as a reference. For the *in vitro* experiments, *GAPDH* was used as a negative control gene associated with euchromatin and not regulated by histone modifications. The *CDKN1A/p21* served as a positive control gene previously shown to be regulated by histone modifications in human glioblastoma cells (Yin et al 2007) (for primers compare Table 12). Results obtained from glioblastoma cells were reproduced in three

independent biological experiments. The results from fresh frozen glioblastoma tissues were based on the measurement of three technical replicates due to the restriced amounts of available fresh frozen glioblastoma tissues. Three normal brain tissues were used to determine the histone pattern under normal (non-neoplastic) conditions. Tricin-SDS-PAGE (Schagger 2006) was performed to control for the efficiency of trichostatin A treatment and the specificity of ChIP-antibody reactions.

3.2 Protein based methods

3.2.1 Extraction of proteins from cultured cells

Cells were washed with PBS once and lysed in 500 µl lysis buffer with proteinase inhibitors by scraping the cells from 10 cm dishes with a cell scraper. Protein extracts were then incubated on ice for 15 min before centrifuging them for 20 min and 13000 rpm at 4 °C to remove cell debris. Supernatant was then used to quantify total protein concentration and for further experiments.

3.2.2 Protein quantification

The colorimetric protein determination assay is based on the Lowry protocol (Lowry et al 1951) and proceeds in two steps. At first, a blue violet complex is generated through the binding oft peptides to copper (II) ions in an alkaline solution. The second step consists of the reduction of copper (II) to copper (I), which reduces the yellow folin-ciocalteu reagent to molybdenum-blue. This color conversion is used to quantify the protein amount by photometry with 750 nm. RC DC protein assay (BioRad GmbH, München) was used to determine the amount of proteins. 10 µl protein extract and 50 µl reagent A' (reagent A : reagent S; 50:1) were mixed together. Afterwards, 400 µl reagent B were added to the mixture and incubated for 20 min. To determine the protein amount, the absorbance was measured at 750 nm against a blank sample relative to a BSA standard curve.

3.2.3 Sodium Dodecyl Sulfate - Polyacrylamide Gel Electrophoresis (SDS-PAGE)

SDS-PAGE is a method to separate proteins according to their molecular weight and is based on the Laemmli protocol (Laemmli 1970). The polyacrylamide gels consist of a mixture of acrylamide and bisacrylamide and the polymers are cross-linked by APS and TEMED. According to the amount of polyacrylamide, the matrix is getting more or less dense with a different pore size. The SDS is acting as a detergent that binds and denatures the proteins. These proteins also get a negative charge because of the sulfate groups of the SDS so that the separation only depends on the molecular weight of the proteins. Small proteins migrate faster through the matrix than big proteins.

The stacking gel above the separating gel was used to get a better separating effect. Because of the lower pH and bigger pores, the proteins migrate very fast without separation. So the proteins are collected and concentrated before separation.

At first, the separating gel was poured in an appropriate gel chamber and covered with isopropanol to avoid dehydration and the reaction with oxygen. After polymerization, the isopropanol was rinse thoroughly before pouring the stacking gel and inserting the gel comb to generate the gel slots.

20 µg of protein was mixed with loading buffer including SDS + ß-mercaptoethanol and boiled for 5 min at 95 °C. Thereby, the proteins get denatured, lose their native conformation and surface charge.

The gels were run at 180 V for about 90 min and used for western blotting afterwards.

3.2.4 Western blot analysis

Western blotting is used to transfer proteins from gels onto a membrane (Burnette 1981, Towbin et al 1979). The proteins bind to the nitrocellulose membrane because of the hydrophobic interaction.

The membrane was laid on top of the gel followed by filter paper. This system was set in transfer cassettes and placed in a standard tank system filled with transfer buffer (Figure 13). The transfer proceeded at 250 mA and 4 °C for 60 min. After a short washing step the proteins can be visualized in specific or unspecific manner.

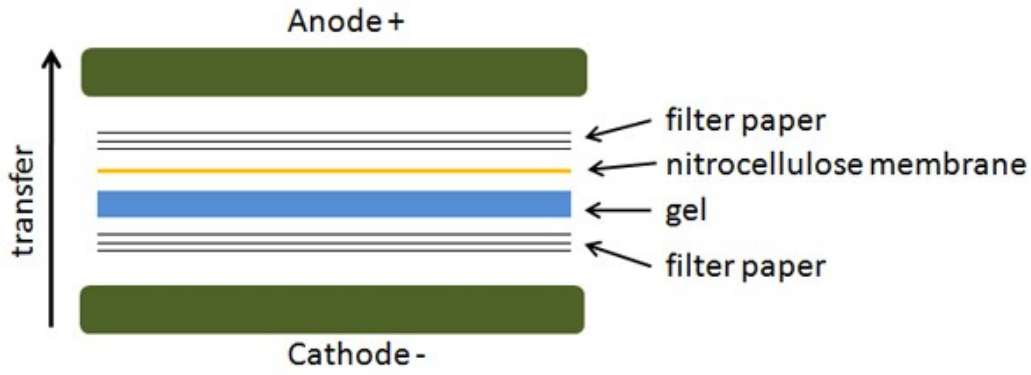

Figure 13: Schematic represetation of a western blot transfer. Gel and nitrocellulose membrane are surrounded with filter papers. The transfer proceeds from the cathode to the anode, so that the proteins are transferred from the gel onto the membrane.

3.2.4.1 Non specific staining of proteins with Ponceau S

All proteins are stained with Ponceau S. With this method the transfer of the proteins to the membrane was controlled. The membrane was incubated with Ponceau S for a few minutes at room temperature and could be destained with water.

3.2.4.2 Specific antigen – antibody reaction

The principle to visualize specific proteins on the nitrocellulose membrane is based on an antigen – antibody reaction. After blocking the membrane with 5 % dry milk powder in TBS-tween-20 to reduce unspecific background binding, the primary antibody binds to its antigen (the target protein) and the secondary labeled antibodies recognize the primary antibody. This secondary antibody is labeled with horseradish peroxidase (HRP), an enzyme catalyzing the oxidation of luminol using peroxide as an oxidizing agent (Figure 14). This chemiluminescent reaction is detectable by photometric methods using the chemiluminescent HRP substrate from Millipore (Charlottesville, VA).

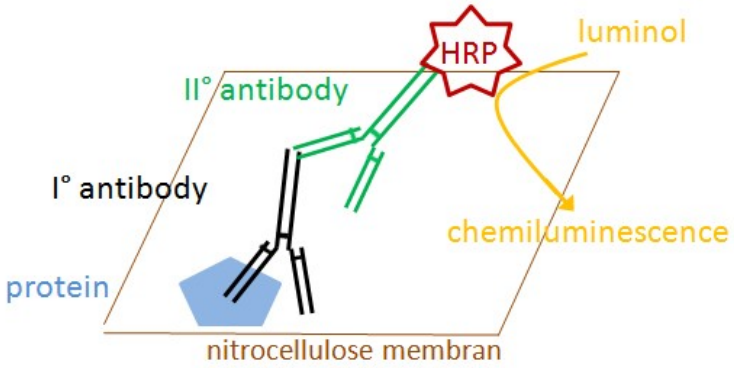

Figure 14: Schematic representation of an antigen-antibody reaction. The primary antibody binds to its antigen, whereas the secondary antibody recognizes the primary antibody because of its different specificity. The enzyme (HRP) linked to the second antibody catalyzes the chemiluminescence reaction.

3.3 Cell based methods

3.3.1 Cultivation of glioma cells

All glioblastoma cell lines were grown under standard condition. Dulbecco´s modified Eagle´s medium (DMEM) was used as basal medium. 10 % (v/v) heat-inactivated fetal bovine serum (FCS) and 1 % (v/v) penicillin G/streptomycin were added to the medium and cells were incubated at 37 °C in a humidified atmosphere containing 5 % CO_2.

Liquid nitrogen was used to store cultured cells. To minimize the effect of freezing, the cells were stored in FCS containing 10 % DMSO. Cells were slowly cooled before freezing and warmed quickly when thawed.

3.3.2 Treatment of glioma cells with 5-aza-2'-deoxycytidine or histone deacetylase inhibitor trichostatin A

Two glioblastoma cell lines (A172 and U87MG) were grown under standard or under two different treatment conditions with either the demethylating agent 5-aza-2'-deoxycytidine (1 µM for 72 h) or the histone deacetylase inhibitor trichostatin A (1 µM for 36 h). After harvesting the cells and extracting the mRNA, expression analyses of cells under the different treatment conditions compared to the untreated controls were performed by real-time reverse transcription PCR analysis as described above. Results obtained were reproduced in at least three independent biological experiments.

3.3.3 Generation of stably ARHI-depleted glioblastoma cell lines

Transfection describes the process of introducing external nucleic acids into cells. Two different ways of transfection are known: transient and stable transfection. The transiently transfected nucleic acids are only temporarily expressed in the cell and get lost after cell division whereas stably transfected nucleic acids are permanently integrated in the genome of the host cells.

To obtain stably transfected glioblastoma cell lines the pcDNA^{TM} 6.2-GW/EmGFP-miR vector (Invitrogen, Carlsbad, CA) was used (Figure 15). Three different pre-designed shRNA oligonucleotides targeting the *ARHI* gene (Qiagen, Hilden, Germany) were utilized to control for potential off-target effects (Table 11). Cells were also transfected with the pcDNA^{TM} 6.2-GW/EmGFP-miR-negative control plasmid containing an insert that can form a hairpin structure that is processed into mature miRNA, but is predicted not to target any known vertebrate gene. This plasmid served as a negative control for the RNAi experiments.

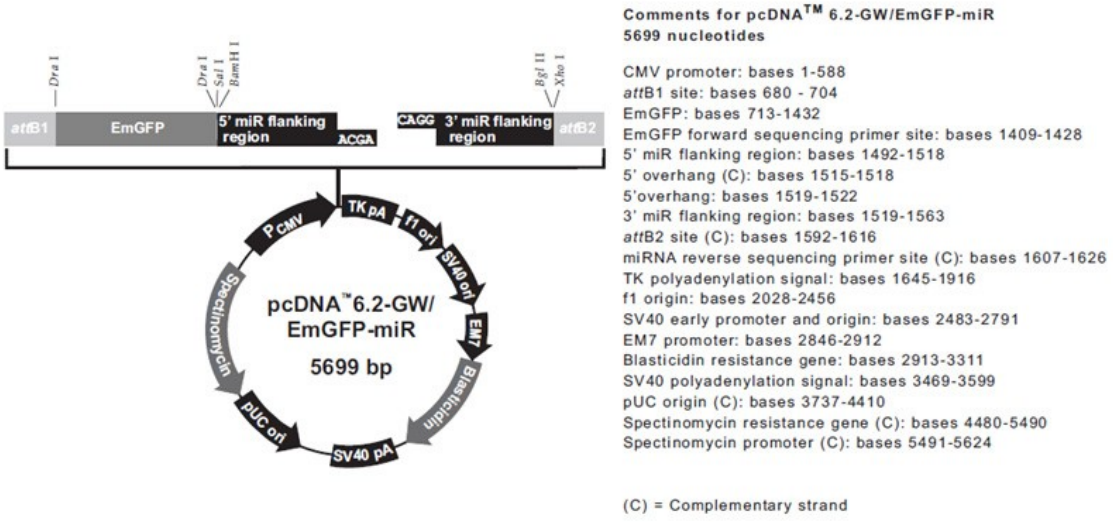

Figure 15: The pcDNA^{TM} 6.2-GW/EmGFP-miR vector (Invitrogen, Carlsbad, CA) used for stable transfection of glioblastoma cell lines. This vector includes the green fluorescence protein gene, a blasticidin and spectinomycin resistant gene.

To only select stably transfected cells a “death curve” experiment was done to determine the minimum concentration of blasticidin required to kill untransfected mammalian cell.

Stable transfection was performed using a commercial BLOCK-iT™ Pol II miR RNAi Expression Vector kit (Invitrogen,) according to the manufacturer's recommendations. In brief, cells were plated at a density of 320000 cells/ 24-well (A172) or 200000 cells/ 24-well (U251) one day before transfection. Cells were then transfected with the pcDNA™ 6.2-GW/EmGFP-miR vectors containing sequence-verified shRNA oligonucleotids using GeneJuice transfection reagent (Merck, Darmstadt, Germany) according to the manufacturer's recommendations. The following day, cells were placed to a larger-sized tissue culture format in fresh medium containing the appropriate concentrations of blasticidin (2 µg/ml). Medium was changed every two days and resistant colonies with GFP (green fluorescence protein) were picked with sterile pipet tips and transferred into wells of a 96-well plate. These colonies were expanded and subsequently used for real-time RT-PCR and Western blot to control for the efficiency of ARHI-silencing. The colonies with GFP and the highest ARHI-silencing efficiency were used in functional assays.

3.3.4 Functional assays

3.3.4.1 Proliferation assay

To determine the effect of shRNA-mediated *ARHI* knock-down on cell proliferation, the stably transfected cell lines were investigated using a commercially available colorimetric cell proliferation ELISA (Roche, Mannheim, Germany). The proliferation assay was first described by Prostmann et al. (Porstmann et al 1985) and is based on the measurement of BrdU incorporation during DNA synthesis in proliferating cells.

1000 cells (U251) and 2000 cells (A172) per well were seeded and incubated with BrdU labeling reagent over night at 37 °C in a humidified atmosphere containing 5 % CO_2. Cells were then fixed and incubated with anti-BrdU antibody conjugated with peroxidase (POD) according to the manufacturer's recommendations. After a few washing steps, the BrdU-containing complexes were detected by the substrate reaction. The absorbance correlates with the amount of DNA synthesis and thereby with cell proliferation. Results were reproduced in at least three independent biological experiments.

3.3.4.2 Apoptosis assay

Apoptosis is a programmed cell death and is involved in many biological events (Wyllie et al 1980). An endogenous signal cascade leads to the characteristics of apoptosis: cell membrane changes, cell shrinkage, nuclear fragmentation, chromatin condensation, activation of caspases and chromosomal DNA fragmentation. To determine the effect of shRNA-mediated *ARHI* knock-down on apoptosis, the stably transfected cell lines were investigated using a commercially available Apo-ONE homogeneous caspase-3/7 assay (Promega, Madison, WI) and by flow cytometry (fluorescence activated cell sorting = FACS).

Apo-ONE homogeneous caspase 3/7 assay:

Caspase 3/7 activity is an indicator of apoptosis. During apoptosis, these proteases can cleave proteins at the C-terminal side with the amino acid sequence DEVD (asp-glu-val-asp). In this assay, rhodamine 110 is used as a profluorescent substrate that is linked to DEVD (Z-DEVD-R110). After sequential cleavage of the DEVD peptide from the substrate (Z-DEVD-R110) by caspase 3 and/or 7, rhodamine 110 becomes intensely fluorescent and can be measured with an excitation at 499 nm and an emission maximum of 521 nm.

5000 cells (A172) and 4000 cells (U251) were seeded over-night at 37 °C in a humidified atmosphere containing 5 % CO_2. Cells were then incubated with the Apo-ONE reagent, incubated in the dark by shacking at 300 – 500 rpm and measured after 30 min and then every hour up to 18 h. Results were reproduced in at least three independent biological experiments.

FACS analysis:

Apoptosis detection by FACS analysis (Nicoletti et al 1991, van Engeland et al 1996) is based on the following principle:

The phosphoglycerid phosphatidylserine is normally located at the cytoplasmic side of the cell membrane and switches to the cell surface during apoptosis. This rearrangement can be detected with annexin V. Annexin V labeled with a fluorescence dye (allophycocyanin = APC) binds strongly to phosphatidylserine and can therefore be measured by FACS analysis. To differentiate between apoptosis and necrosis (acute

traumatic cell death), we additionally used the fluorescence dye propidiumiodide that only can diffuse into necrotic cells with permeable cell membranes (Figure 16).

1 x 10^6 cells in 70 µl binding buffer were incubated with 50 µg/ml propidium iodide solution and 5 µl annexin V conjugated with APC for 15 min at room temperature. Cells were placed on ice and washed once with binding buffer before measured by FACS analysis with the CyFlow 'space' (Partec GmbH, Görlitz).

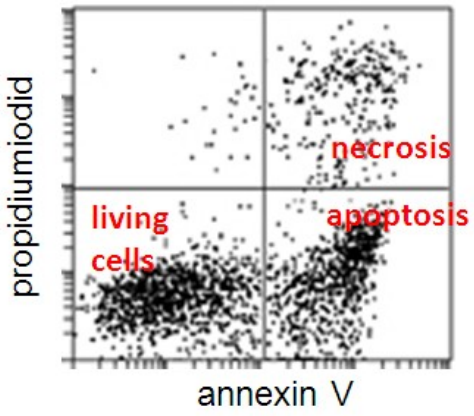

Figure 16: Example for the detection of apoptosis using FACS analysis. Note that apoptotic and necrotic cells are annexin V positive whereas only necrotic cells are propidiumiodid positive. Living cells are double negative (changed from: http://media.wiley.com/ CurrentProtocols/TX/tx0210/tx0210-fig-0001-1-full.gif).

3.4 Statistical methods

Two-sided student's t-test analyses were employed to compare *RRP22* and *RHOB* mRNA expression levels between the different WHO grades, to compare *RRP22* mRNA expression levels between tumors with and without *RRP22* 5'-CpG island hypermethylation (relative to non-neoplastic brain tissue) and to analyze cell proliferation and apoptosis after stable knock-down of the *ARHI* gene. One-sided student's t-test analyses were used to evaluate the increase in *RRP22* and *RHOB* expression levels in glioblastoma cell lines after treatment with 5-aza-2'-deoxycytidine and trichostatin A. One-sided student's t-test analyses were also used to assess the increase of *RRP22* and *RHOB* immunoprecipitated DNA bound to acetylated histones after trichostatin A treatment. P-values of <0.05 (*), <0.01 (**) and <0.001 (***) were considered as significant.

4 Results

4.1 Molecular characterization of small GTPase genes

RRP22, *RHOB*, *RASL11A* and *RERG* were suggested as candidate tumor suppressors in human cancer in various studies (Du and Prendergast 1999, Finlin et al 2001, Forget et al 2002, Louro et al 2004, Zucman-Rossi et al 1996). RHOB has been described to enhance glioma cell motility (Baldwin et al 2008), to regulate radiation-induced mitotic cell death (Monferran et al 2008), to reduce cell survival after irradiation (Delmas et al 2002) and to initiate apoptosis in transformed cells (Prendergast 2001). A study on different mouse tissues reported *RHOB* as epigenetically regulated in an age- and tissue-specific manner by histone modifications, but not CpG methylation (Yoon et al 2007). Similarly, recent reports in lung and pancreatic cancer cells pointed to an epigenetic inactivation of *RHOB* by histone modifications (Delarue et al 2007, Mazieres et al 2007, Sato et al 2007). Two studies in gliomas reported that RRP22 may suppress tumor cell growth, promote caspase-independent cell death, decrease invasiveness, inhibit glioma cell growth in soft agar and that DNA hypermethylation may be a potential cause for inactivation of *RRP22* in glioblastoma cell lines (Chen et al 2011, Elam et al 2005). The functional roles of RASL11A and RERG proteins in tumorigenesis are not so well characterized. Two studies reported that RERG may inhibit tumor growth in breast cancer (Finlin et al 2001) and that *RERG* may be regulated by histone deacetyltransferases in hepatocellular carcinomas (Wang et al 2006). Only a single study reported *RASL11A* to be downregulated in human prostate cancer (Louro et al 2004).

In this doctoral thesis, human glioma tissue samples were examined for their expression level of these four genes. Three of the genes were additionally analyzed for their DNA methylation pattern. The two most interesting candidates (*RRP22*, *RHOB*) were selected for further analysis. Mutation analyses for *RRP22* and *RHOB* as well as microsatellite analysis for *RRP22* on chromosome 22q12 were performed. Furthermore, the chromatin immunoprecipitation (ChIP) protocol was established in the lab and carried out to analyze the role of histone modifications for the regulation of the *RHOB* and *RRP22* promoters in primary tumor tissues and glioma cells cultured *in vitro*.

4.1.1 mRNA expression analysis in human gliomas and glioblastoma cell lines

4.1.1.1 *RRP22* mRNA expression analysis

Investigation of a series of 70 glioma patients by means of real-time reverse transcription PCR analysis revealed decreased *RRP22* mRNA levels (<0.7-fold relative to non-neoplastic brain tissue) in 47 out of 70 gliomas (67 %, Figure 22). Interestingly, when comparing *RRP22* expression levels between the different WHO grades, *RRP22* expression decreased with higher malignancy grade (Figure 17). Highest *RRP22* expression levels were observed in WHO grade II lesions (mean: 1.7; standard deviation, SD: 1.7), intermediate expression levels in WHO grade III gliomas (mean: 0.8; SD: 1.4) and lowest expression levels in glioblastomas of WHO grade IV (mean: 0.3; SD: 0.8). The expression differences between the different WHO grades were statistically significant, particularly when comparing high-grade (malignant) gliomas (WHO grade III and IV) to low-grade gliomas of WHO grade II (student's t-test WHO grade II versus WHO grade III, p = 0.034; WHO grade II versus WHO grade IV, p = 0.003). All five glioblastoma cell lines (A172, U138MG, T98G, TP365MG and U87MG) exhibited a nearly complete loss of *RRP22* mRNA expression (<0.1, Figure 22).

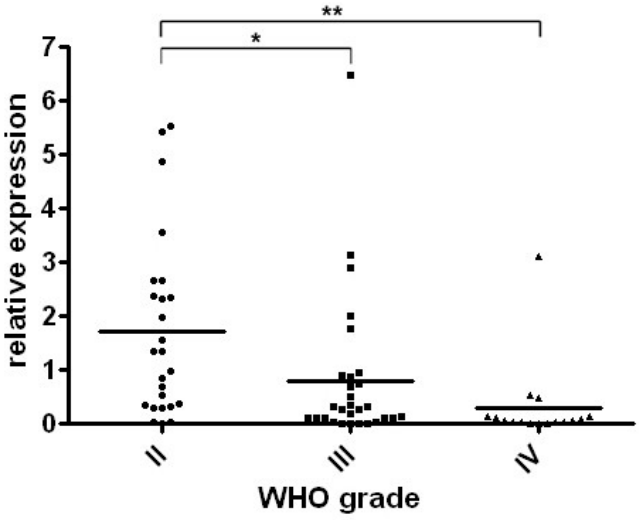

Figure 17: *RRP22* mRNA expression in human gliomas stratified for WHO grade. Note that *RRP22* mRNA expression is significantly decreased with increasing WHO malignancy grade. Abscissa, WHO grades; ordinate, mRNA expression relative to non-neoplastic brain tissue.

4.1.1.2 *RHOB* mRNA expression analysis

The overall transcript levels for *RHOB* were also reduced (<0.7-fold relative to non-neoplastic brain tissue) in the majority of the investigated tumors in 53 out of 70 cases (76 %, Figure 22). Highest *RHOB* expression levels were observed in WHO grade II lesions (mean: 0.51; standard deviation, SD: 0.5), intermediate expression levels in WHO grade III gliomas (mean: 0.4; SD: 0.33) and lowest expression levels in glioblastomas of WHO grade IV (mean: 0.38; SD: 0.2). However, no statistically significant association of *RHOB* expression levels with WHO grade was observed (Figure 18). All five glioblastoma cell lines (A172, U138MG, T98G, TP365MG and U87MG) exhibited a nearly complete loss of *RHOB* expression (<0.1, Figure 22).

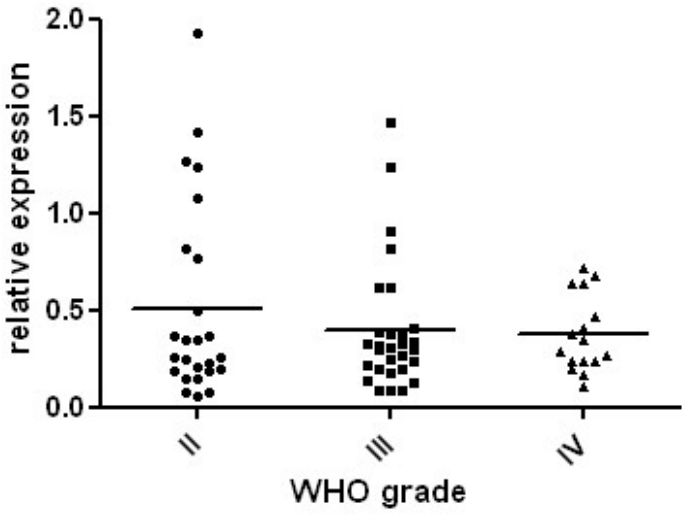

Figure 18: *RHOB* mRNA expression in human gliomas stratified for WHO grade. Note that *RHOB* mRNA expression is only slightly decreased with increasing malignancy. Abscissa, WHO grades; ordinate: mRNA expression relative to non-neoplastic brain tissue.

4.1.1.3 *RRP22* and *RHOB* expression analyses in glioblastoma cell lines after treatment with 5'-aza-2'-deoxycytidine and trichostatin A

In vitro treatment with the demethylating agent 5'-aza-2'-deoxycytidine (AZA) and the histone deacetylase inhibitor trichostatin A (TSA) was performed to search for potential mechanisms that might be involved in the transcriptional downregulation of these two genes (Figure 19).

Treatment with 5-aza-2'-deoxycytidine induced a significant increase of *RRP22* transcripts in two selected glioblastoma cell lines (A172: 4-fold, p = 0.027; U87MG: 11-fold, p = 0.0051) relative to the untreated control cells (CTRL), thus suggesting a regulation of *RRP22* mRNA expression by *RRP22* 5'-CpG island methylation. For *RHOB*, only a slight but significant increase was found in the two selected glioblastoma cell lines (A172: 1.5-fold, p = 0.016; U87MG: 2-fold, p = 0.033) in relation to the untreated control cells (Figure 19a).

Treatment of the two glioblastoma cell lines (A172 and U87MG) with trichostatin A revealed significant increases of the mRNA expression levels of both genes relative to the untreated control cells in A172 (*RRP22*: 6-fold, p = 0.009; *RHOB*: 20-fold, p = 0.0014) and U87MG (*RRP22*: 9-fold, p = 0.026; *RHOB*: 26-fold, p = 0.005) glioblastoma cell lines, which suggests a role of histone modification in the transcriptional downregulation of the investigated genes (Figure 19b).

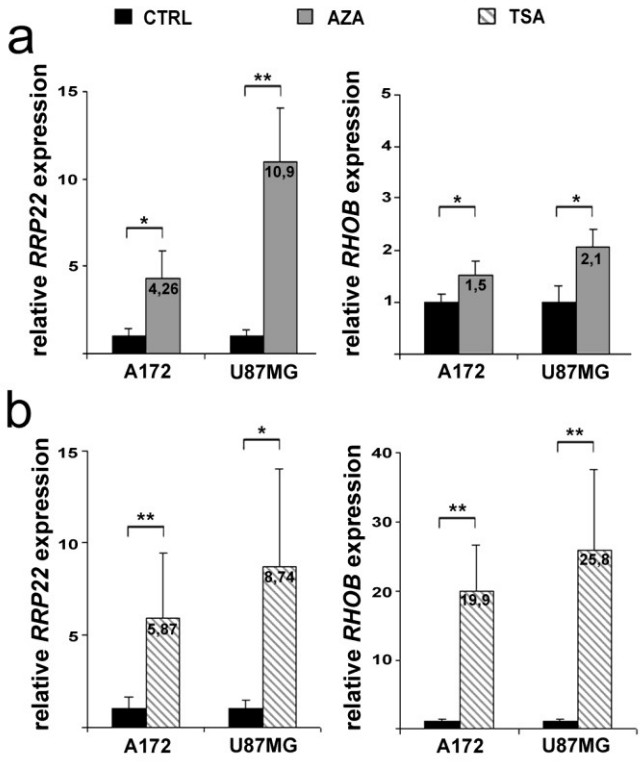

Figure 19: mRNA expression levels of *RRP22* and *RHOB* in human glioblastoma cell lines (A172, U87) after treatment with 5-aza-2′-deoxycytidine (AZA, a) or trichostatin A (TSA, b) relative to untreated control cells (CTRL=1). Note the strong increase of mRNA expression after treatment with TSA for both genes. Treatment with AZA also caused a strong increase in the mRNA expression of *RRP22* and a moderate but also significant increase in *RHOB* mRNA expression. Abscissa, cell lines; ordinate, relative mRNA expression.

4.1.1.4 *RASL11A* mRNA expression analysis

Investigation of a smaller series of 45 glioma patients by means of real-time reverse transcription PCR analysis revealed reduced *RASL11A* transcript levels (<0.7-fold relative to non-neoplastic brain tissue) in the majority of the investigated tumors (40 out of 45 cases, 89 %). Highest *RASL11A* expression levels were observed in WHO grade IV lesions (mean: 0.50; SD: 0.37) and in WHO grade II gliomas (mean: 0.50; SD: 0.43). Lowest expression levels were detected in anaplastic gliomas of WHO grade III (mean: 0.29; SD: 0.16). Statistically significant association of *RASL11A* expression levels with WHO grade was observed when comparing anaplastic gliomas of WHO grade III to low-grade gliomas of WHO grade II (student's t-test, p = 0.037) as well as when comparing WHO grade III lesions to WHO grade IV tumors (student's t-test, p = 0.049). However, a clear progression-associated down-regulation of *RASL11A* was not observed (Figure 20). *RASL11A* was thus not further investigated for genetic and epigenetic inactivation mechanisms.

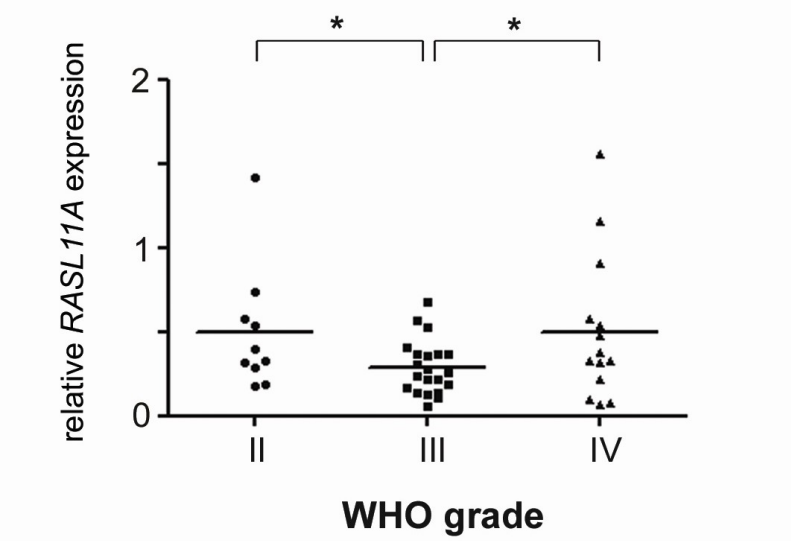

Figure 20: *RASL11A* mRNA expression in human gliomas stratified for WHO grade. Note that *RASL11A* mRNA expression is lowest in WHO grade III tumors compared to WHO grade II and IV tumors. Abscissa, WHO grades; ordinate: mRNA expression relative to non-neoplastic tissue.

4.1.1.5 *RERG* mRNA expression analysis

The overall transcript levels in a series of 46 glioma patients were reduced (<0.7-fold relative to non-neoplastic brain tissue) in the majority of the investigated tumors (43 out of 46 cases, 93 %). The *RERG* mRNA expression was downregulated to a similar extend in WHO grade II tumors (mean: 0.23; SD: 0.12), WHO grade III gliomas (mean: 0.27; SD: 0.37) and WHO grade IV tumors (mean: 0.29; SD: 0.27) (Figure 21). *RERG* was investigated for promoter hypermethylation, however, was found to show methylation in both gliomas and in normal brain tissue samples (see below).

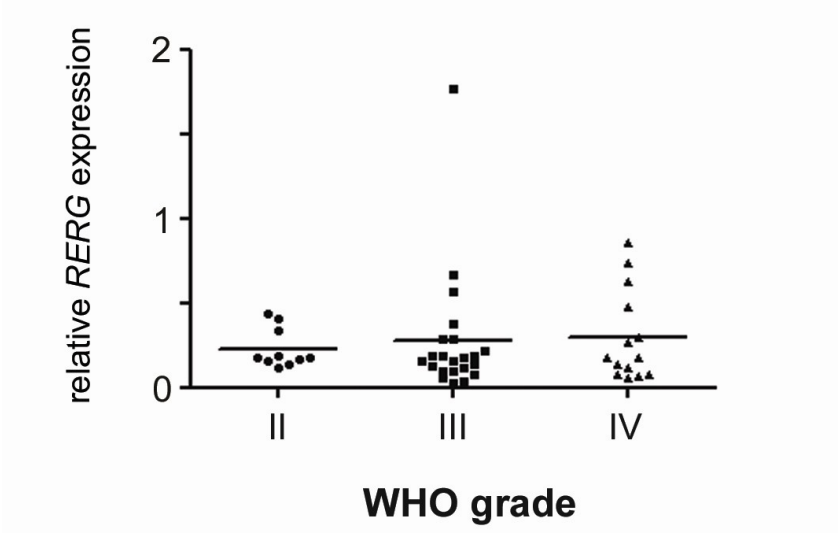

Figure 21: *RERG* mRNA expression in human gliomas stratified for WHO grade. Note that *RERG* mRNA expression is similarly downregulated relative to normal brain tissue in tumors of different WHO grades. Abscissa, WHO grades; ordinate: mRNA expression relative to non-neoplastic tissue.

4.1.2 DNA methylation analysis

The following paragraphs detail the results obtained 5'-CpG island methylation analyses of *RRP22* and *RHOB* in primary glioma tissue samples. Figure 22 provides a schematic overview of the data in relation to mRNA expression of these genes as well as allelic losses on 22q.

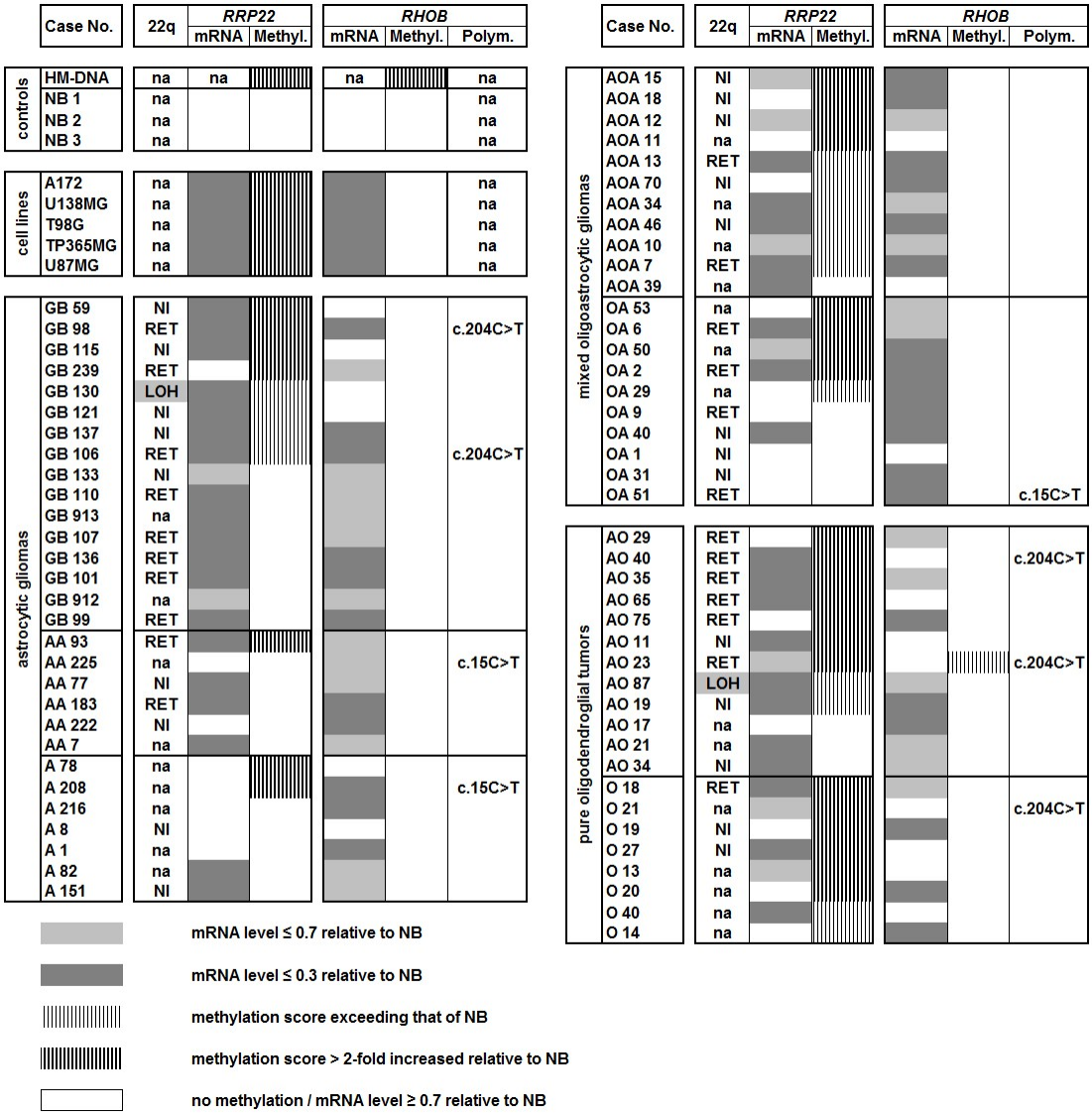

Figure 22: Molecular genetic aberrations of the most interesting candidate genes (*RRP22* and *RHOB)* in human gliomas. Note that the mRNA expression levels for both genes are decreased in the majority of the investigated tumors. Aberrant DNA methylation was detected in the 5'-CpG island of *RRP22* but not in the promoter region of *RHOB*. mRNA, expression level of the investigated genes; Methyl., methylation of the 5'-CpG island; NB1-3, 3 different samples of non-neoplastic brain tissue; HM-DNA, *in vitro* hypermethylated DNA control; Polym., polymorphisms detected for *RHOB*; LOH, loss of heterozygosity on 22q12; RET, retention on 22q12; NI, not informative; na, not analyzed.

4.1.2.1 DNA hypermethylation of the *RRP22* 5'-CpG island partially accounts for the transcriptional downregulation of *RRP22* in human gliomas

The amplified fragment of the *RRP22* 5'-CpG island covered in total 36 CpG sites (nt 29,711,182-29,711,416 according to UCSC, CpGs +53 to +88 relative to the transcription start site) and 24 of these CpG sites overlap with a region that had been shown to be methylated in glioblastoma cell lines before (Elam et al 2005).

Direct sequencing of sodium bisulfite-modified DNA revealed *RRP22* 5'-CpG island hypermethylation in 43 out of 70 glioma patients (61 %) and in all five investigated glioblastoma cell lines, whereas three non-neoplastic brain tissues showed an unmethylated 5'-CpG island (Figure 22, Figure 23). *In vitro* treatment with the demethylating agent 5'-aza-2'-deoxycytidine (AZA) induced a significant increase of *RRP22* transcripts in two selected glioblastoma cell lines (Figure 19), thus providing further evidence for a relationship between *RRP22* 5'-CpG island methylation and mRNA expression in glioma cells.

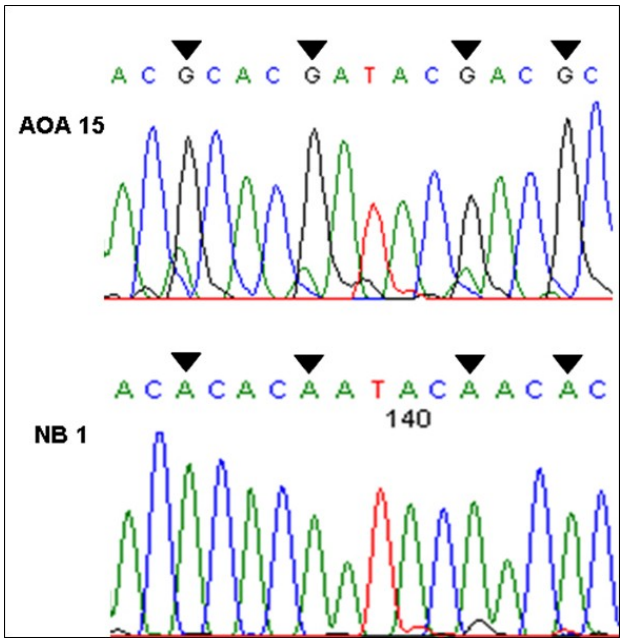

Figure 23: *RRP22* 5'-CpG-island methylation analysis by direct sequencing of sodium bisulfite-modified DNA (CpG sites are marked with arrows). Note that G nucleotides are retained after bisulfite treatment in the methylated sample AOA15. In contrast, the non-neoplastic brain tissue sample (NB) lacks *RRP22* 5'-CpG-island methylation in the identical genomic region with the guanine being replaced by an adenine in the sequence.

Indeed, lower mean *RRP22* mRNA expression levels were found in the primary gliomas with increased *RRP22* methylation (mean: 0.82; SD: 1.16) compared to tumors with low or absent *RRP22* methylation (mean: 1.33; SD: 0.38). However, these expression differences did not reach statistical significance (student's t-test, p = 0.15; Figure 24).

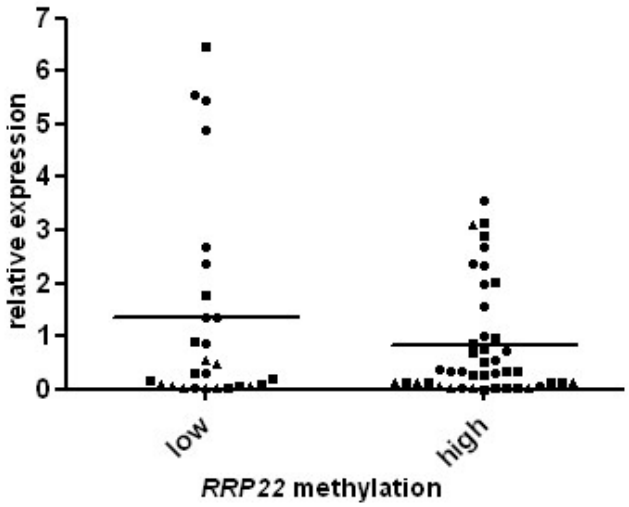

Figure 24: *RRP22* mRNA expression analysis in human gliomas in relation to the *RRP22* promoter methylation status. Tumors with increased *RRP22* methylation scores (relative to that of non-neoplastic brain tissue) had lower mean *RRP22* mRNA expression levels when compared to tumors with absent or low *RRP22* methylation. However, due to large variations in each group, the difference in mean expression did not reach statistical significance (student's t-test, p = 0.15). Abscissa, methylation status; ordinate, relative mRNA expression

Only 30 out of the 47 gliomas with decreased *RRP22* expression demonstrated aberrant 5'-CpG island methylation, suggesting that additional mechanisms might contribute to the reduced expression of *RRP22* in a subgroup of human gliomas. Data on the methylation pattern of the *RRP22* 5'-CpG island in the investigated glioma samples and the calculated methylation scores are provided in Figure 25.

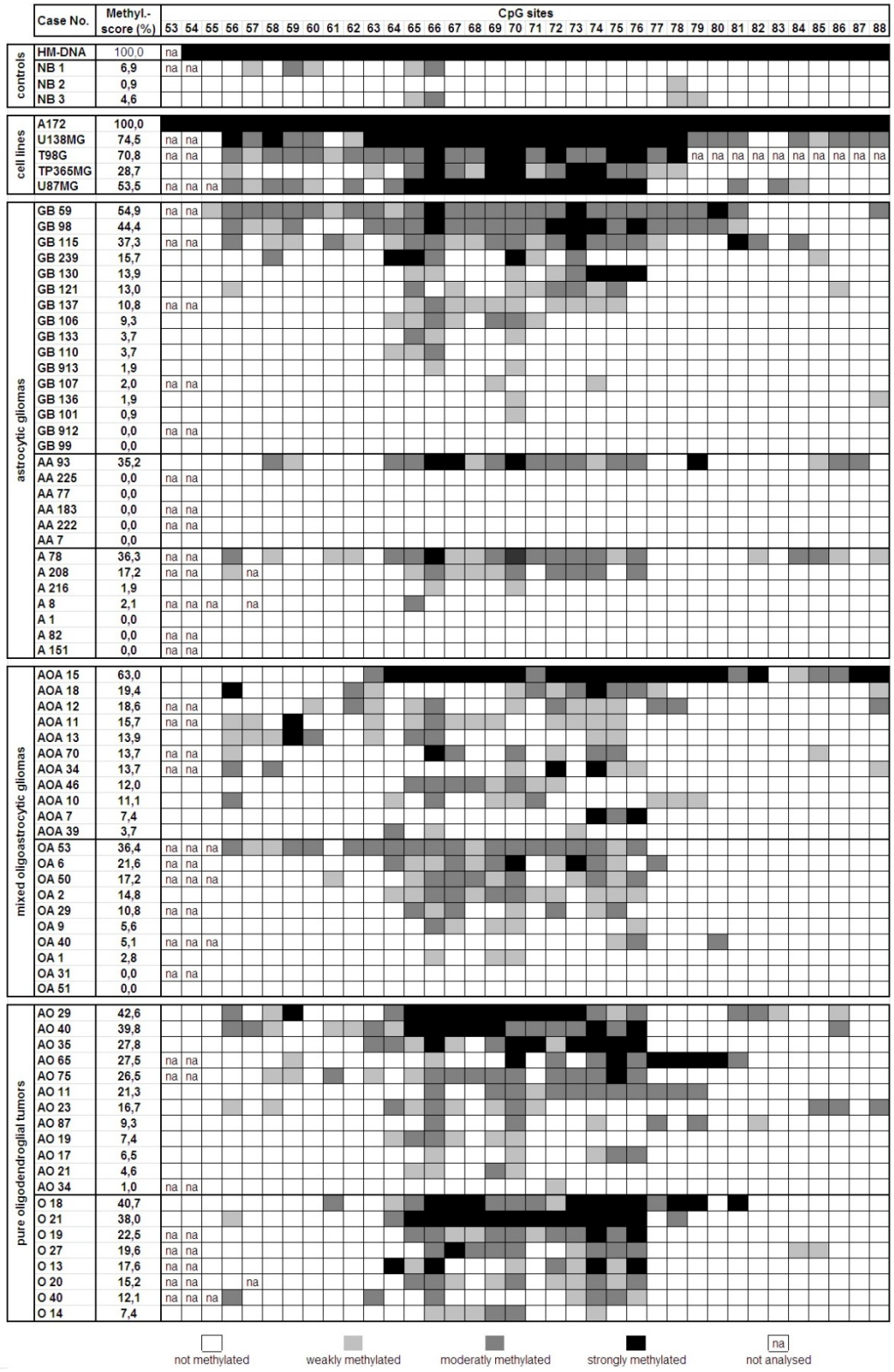

Figure 25: Methylation scores (me-score) and methylation patterns of the 5´-CpG island of *RRP22* (CG sites +53 to +88 relative to the transcription start site) in the investigated human gliomas. Tumors with a cumulative methylation score (described in 3.1.3) of higher than 7 were regarded as being hypermethylated in comparison to non-neoplastic brain tissue (NB).

4.1.2.2 DNA hypermethylation is absent in the *RHOB* promoter

A fragment spanning 29 CpG sites (nt 20,646,555-20,646,827 according to UCSC), including the CpG sites -29 to -1 relative to the transcription start site of *RHOB*, was investigated for aberrant methylation in gliomas. This area was chosen as a crucial region within the *RHOB* promoter containing regulatory elements like an inverted CCAAT box, a TATA box and a number of putative Sp1 transcription factor binding sites (Wang et al 2003b) (Figure 4).

Promoter hypermethylation that could explain the downregulation of *RHOB* transcripts was not detected. Only a single tumor (AO23, Figure 22, Figure 26) had a slightly increased *RHOB* methylation score, which, however, did not associate with decreased mRNA expression. The absence of *RHOB* promoter hypermethylation in the five investigated glioblastoma cell lines (Figure 22, Figure 26) and the only slight increase of the *RHOB* transcript levels after treatment with 5-aza-2'-deoxycytidine (AZA) (Figure 19) matched with the findings in the primary glioma samples. Data on the methylation scores and methylation patterns detected for the *RHOB* promoter in gliomas are provided in Figure 26.

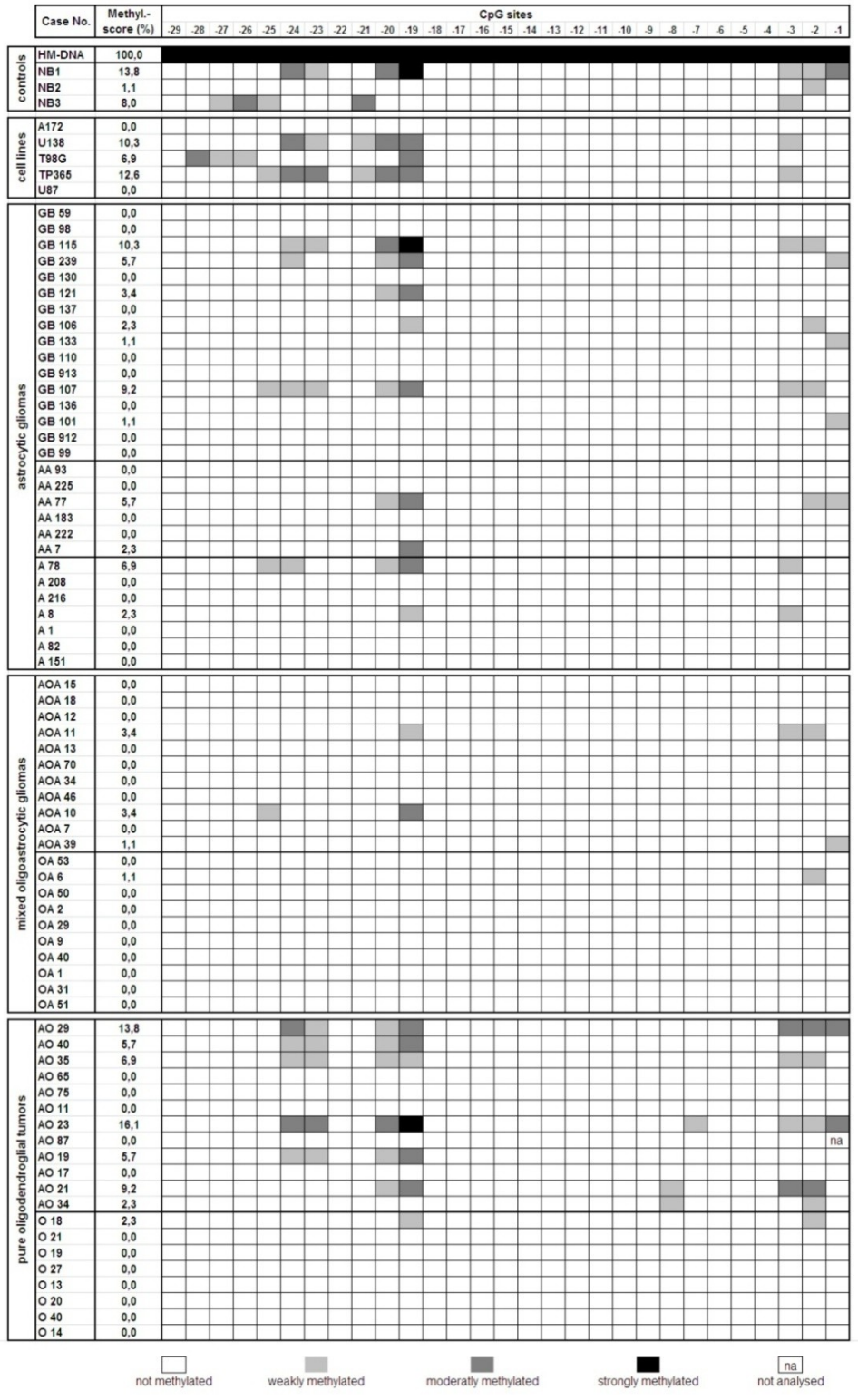

Figure 26: Methylation scores and methylation patterns determined in the 5'-CpG island associated with the *RHOB* promoter region (CG sites -29 to -1 relative to the transcription start site) in human gliomas. Tumors with a cumulative methylation score (described in 3.1.5) higher than 14 were regarded as being hypermethylated in comparison to non-neoplastic brain tissue (NB).

4.1.2.3 DNA hypermethylation of the *RERG* promoter was observed in glioma patients as well as in non-neoplastic brain tissue

A DNA fragment spanning 34 CpG sites (nt 15,374,498-15,374,158 according to UCSC), covering CpG sites -8 to 26 relative to the transcription start site of *RERG*, was investigated for CpG methylation. Aberrant methylation was detected in the majority of the investigated glioma patients, as well as in 5 non-neoplastic brain tissues arguing for a tissue-, but not tumor-specific methylation of *RERG* in the central nervous system. Only 7 patients (GB59, A78, AOA10, AOA11, OA6, AO35, AO40) exhibited a methylation score exceeding that of non-neoplastic brain tissue (Figure 27). However, the expression levels of these tumors revealed no differences when compared to those in tumors with lower methylation scores. The methylation scores and methylation patterns of the *RERG* promoter in the investigated glioma and normal brain tissue samples is provided in Figure 27.

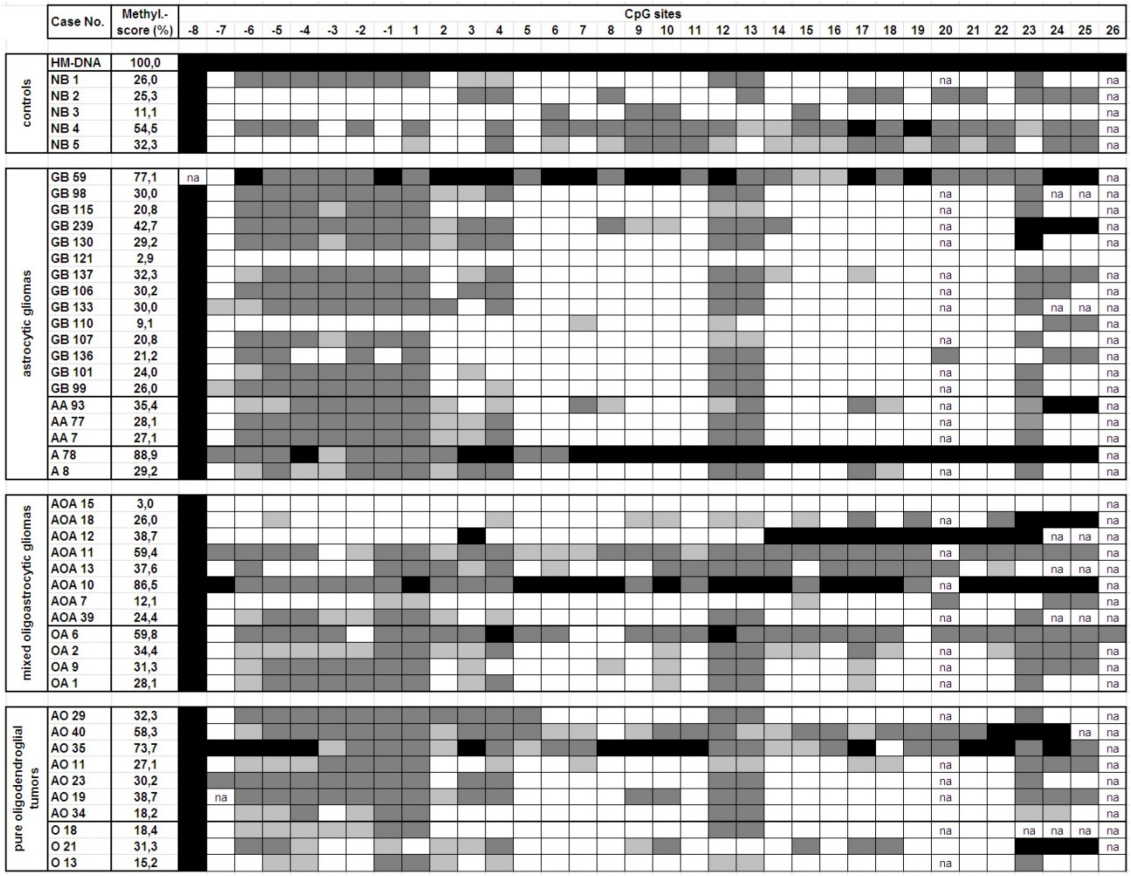

Figure 27: Methylation scores and methylation patterns of the *RERG* promoter (CpG sites -8 to 26 relative to the transcription start site) in human gliomas. Tumors did not exhibit obvious hypermethylation as compared to non-neoplastic brain tissue samples.

4.1.3 Results of mutational analyses

Single strand conformation polymorphism (SSCP)/heteroduplex analyses were performed to screen for mutations in the *RRP22* and *RHOB* coding sequences. For both genes, primer pairs were used to cover the entire coding sequence of each gene. Mutation analyses of *RRP22* and *RHOB* did not detect somatic mutations in any of the 70 gliomas. For *RHOB*, however, two different DNA sequence polymorphisms were found: five patients (GB98, GB106, AO40, AO23, O21) harbored the c.204C>T (p.Arg68Arg) polymorphism and three patients (AA225, A208, OA51) the c.15C>T (p.Arg5Arg) polymorphism (Figure 22, Figure 28). Both alterations represent single nucleotide exchanges that do not result in a change of the amino acid sequence of the RHOB protein.

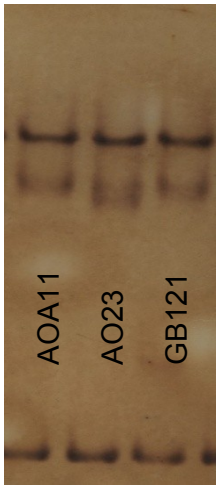

Figure 28: Example of the SSCP analysis of the *RHOB* coding sequence. Note the shift in the band pattern of patient AO23 (middle lane) in comparison to the two other samples AOA11 (left lane) and GB121 (right lane). This fragment was then sequenced and was found to correspond to a known single nucleotide polymorphism not translating into an amino acid exchange or any other protein modification.

4.1.4 Microsatellite analyses for allelic losses on chromosome 22q12

As *RRP22* is located in a chromosomal region that is often affected by allelic losses in human tumors, including gliomas (Ino et al 1999), a set of microsatellite markers spanning the *RRP22* locus on 22q12 was analyzed to determine the presence of allelic losses in the gliomas of the own patient series. Peripheral blood samples were available from 47 of the 70 patients. To investigate for allelic losses spanning the *RRP22* locus on 22q12, loss of heterozygosity (LOH) analysis at the following four microsatellite markers was employed [nucleotide (nt) numbering according to the UCSC genome browser at http://www.genome.ucsc.edu, primers supplied in Table 12]: *D22S1176* (nt 32,226,567-32,226,714) and *D22S531* (nt 30,699,219-30,699,650) located telomerically as well as *D22S1150* (nt 29,501,326-29,501,658) and *D22S689* (nt 28,856,340-28,856,833) located centromerically to *RRP22* (nt 29,708,923-29,711,748). Only two patients (GB130, AO87) with allelic losses in the tumor tissue were identified (Figure 22,

Figure 29). Both patients with *RRP22* allelic deletions exhibited 5'-CpG island hypermethylation of the second allele (3.1.3) resulting in strongly decreased *RRP22* mRNA expression levels of 0.1 relative to non-neoplastic brain tissue.

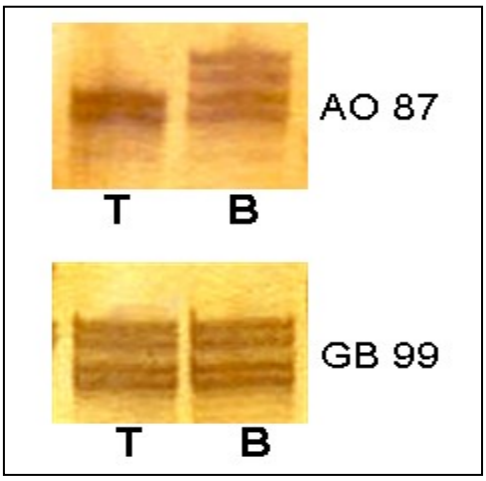

Figure 29: Examples of microsatellite analyses for the detection of allelic losses on 22q12 in gliomas. Note loss of heterozygosity of the polymorphic microsatellite marker D22S689 in AO87 and retention of D22S689 in GB99 in the tumor tissue (*T*), while in corresponding blood samples (*B*) of the same patients both alleles are present.

4.1.5 Chromatin immunoprecipitation (ChIP) analysis in glioblastoma cell lines

Because of the lack of detectable promoter methylation of *RHOB* and the non-significant association between DNA hypermethylation and decreased expression of *RRP22,* both genes were additionally investigated for histone modifications by performing chromatin immunoprecipitation (ChIP) analyses. *In vitro* treatment of glioblastoma cell lines with the histone deacetylase inhibitor trichostatin A (TSA) suggested that histone modifications contribute to *RRP22* and *RHOB* downregulation in cultured glioma cells. A significant increase in the mRNA expression levels for both genes was found relative to the untreated controls (Figure 19). For ChIP analysis, *GAPDH* was used as a control gene associated with euchromatin and not regulated by histone modifications, while *CDKN1A*/*p21* served as a control gene previously shown to be inactivated by histone modifications in human glioblastoma cells (Yin et al 2007). To confirm these findings on *GAPDH* and *CDKN1A*/*p21*, the expression levels of these genes before and after trichostatin A treatment were analyzed by real-time RT-PCR (Figure 30). In fact, no significant increase was found for *GAPDH* mRNA expression level (1.7-fold for U87MG, $p = 0.063$; and 1.4-fold for A172, $p = 0.067$,) whereas the transcript level was significantly increased for *CDKN1A*/*p21* (5.6-fold for U87MG, $p = 0.004$; and 5.0-fold for A172, $p = 0.02$).

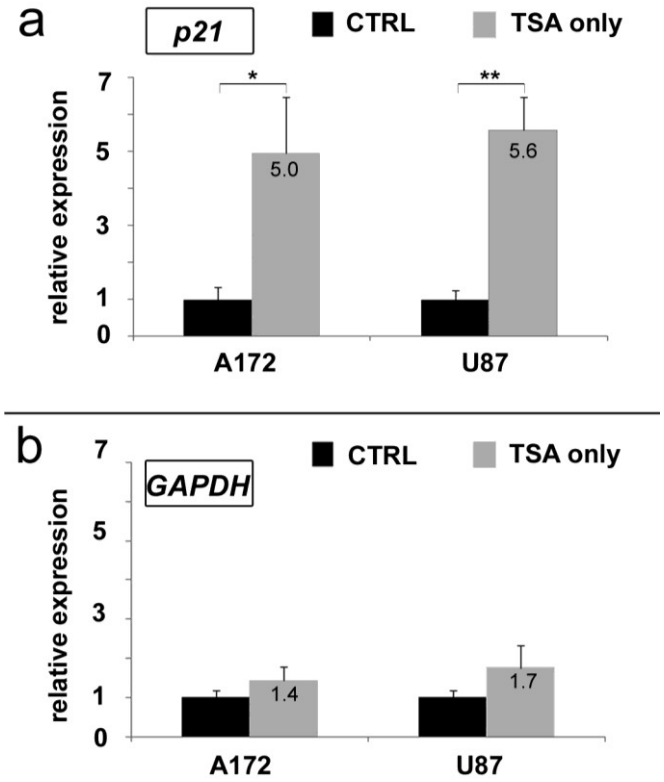

Figure 30: mRNA expression analysis of *CDKN1A*/*p21* (a) and *GAPDH* (b) in glioblastoma cell lines after treatment with trichostatin A (TSA only) relative to untreated control cells (CTRL). Note the significant increase of *CDKN1A*/*p21* expression in both cell lines, while the *GAPDH* expression levels remain unaffected after treatment. Abscissa, cell lines; ordinate, relative mRNA expression.

Consequently, chromatin immunoprecipitation (ChIP) analyses were employed with the same two cell lines to assess a potential euchromatinization of the *RRP22* and *RHOB* promoter after trichostatin A treatment. Tricin-SDS-PAGE was used to confirm the euchromatinizing effect of trichostatin A (TSA) treatment in the glioblastoma cell lines. TSA treatment lead to an increase of acetylated histone H3 and H4 in the unbound protein fraction compared to the non-treated control cells (Co) (Figure 31). Furthermore, Tricin-SDS-PAGE was carried out to control for specificity of the antibodies used. A strong signal in the bound fraction of the ChIP assay was detected, while this is not the case with the negative control antibody IgG (Figure 31).

Figure 31: Western Blots following tricin-SDS-PAGE with the antibodies anti-H3ac (left) and anti-H4ac (right) after immunoprecipitation. Note the specificity of the used antibodies in the bound fraction and the increase of the acetylated histones in the unbound fraction after treatment with trichostatin A (TSA) compared to control cells (Co).

Quantitative real-time PCR analyses following chromatin immunoprecipitation were done with primers targeting the respective promoter regions of *RRP22* and *RHOB* (Table 12). Primers for the *GAPDH* promoter were used as stated in the ChIP assay (-118 to -48 relative to the transcription start side). Primers for the *CDKN1A*/*p21* gene were utilized (-259 to -165 relative to the transcription start side) close to the area reported in the study from Yin et al. (Yin et al 2007). A fragment (-169 to -41 relative to the transcription start site) spanning the reported transcription binding sites namely an inverted CCAAT box, a TATA box and a number of putative Sp1 transcription factor binding sites were analyzed for *RHOB* (Wang et al 2003b) (Figure 4). The promoter of *RRP22* is less well characterized. Here, primers for the promoter region were used that were located closely to the transcription start site (-195 to -78 relative to the transcription start site).

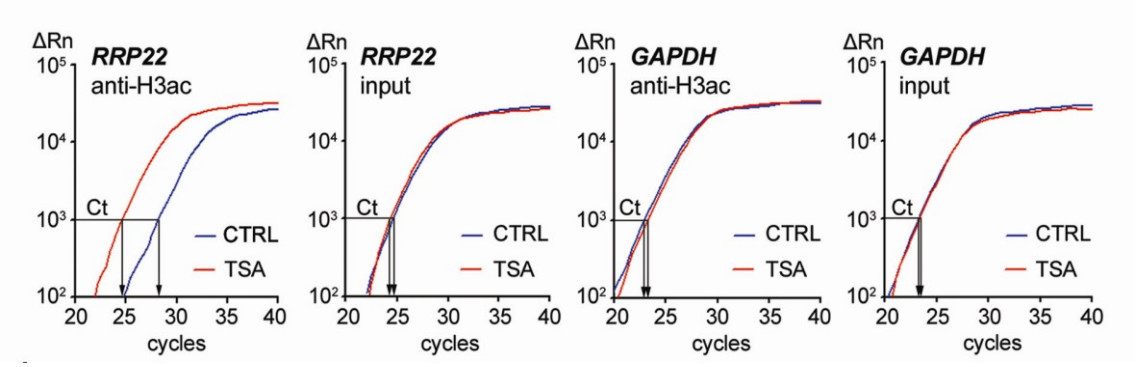

Figure 32: Quantitative real-time PCR analysis of *RRP22* promoter DNA after euchromatinizing treatment with trichostatin A (TSA). Note that in the glioblastoma cell line A172 the TSA (red) curve for anti-H3ac-bound *RRP22* is shifted to the left relative to the CTRL (blue) curve, while the reference curves (input) for TSA and CTRL pass the threshold (Ct) at an approximately equal cycle number. This corresponds to markedly increased *RRP22* promoter DNA levels bound to H3ac after treatment with trichostatin A. *GAPDH* is the control gene not affected by euchromatizing treatment with trichostatin A. Abscissa, cycle number; ordinate, relative amount of PCR product.

Real-time RT-PCR revealed a significant increase of *RRP22* promoter DNA bound to acetylated histone H3 and histone H4 in two selected cell lines (Figure 32, Figure 33). A 23-fold increase ($p = 0.002$) was detected for U87MG and a 13-fold increase ($p = 0.0007$) for A172 of *RRP22* promoter DNA bound to acetylated histone H3 after treatment with trichostatin A. A 16-fold increase ($p = 0.002$) for U87 and a 10-fold increase ($p = 0.0003$) for A172 were detected for *RRP22* promoter DNA bound to acetylated histone H4. No euchromatinization could be detected for the *RHOB* promoter when comparing trichostatin A-treated (TSA) to untreated cells (CTRL). The *CDKN1A/p21* gene was used as a positive control and exhibited a significant increase of promoter DNA bound to acetylated histone H3 and H4. A 5-fold increase ($p = 0.0003$) was detected for U87MG and a 2.4-fold increase ($p = 0.002$) for A172 of *CDKN1A/p21* DNA bound to acetylated histone H3 after treatment with trichostatin A. A 4-fold increase ($p = 0.0014$) for U87 and a 2.3-fold increase ($p = 0.002$) for A172 was analyzed for *CDKN1A/p21* promoter DNA bound to acetylated histone H4.

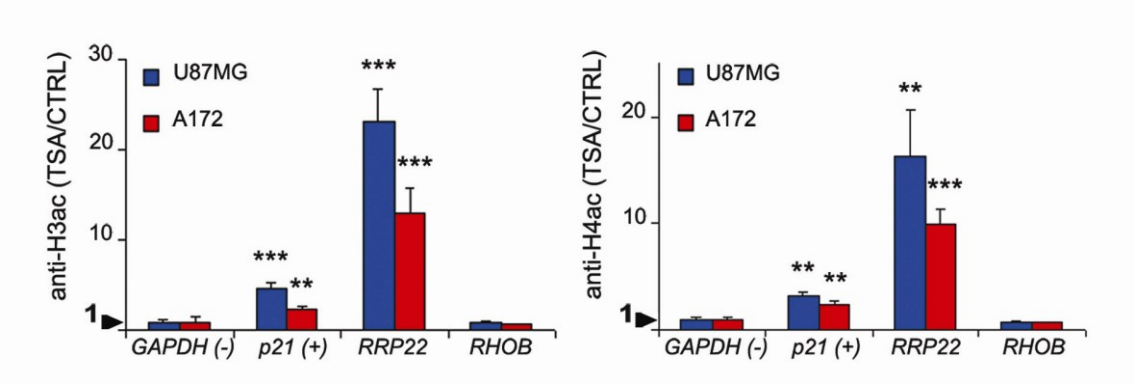

Figure 33: Quantitative real-time PCR analyses of *RRP22* and *RHOB* promoter DNA binding to anti-H3ac and anti-H4ac after euchromatinizing treatment with trichostatin A (TSA). Note that after TSA treatment an increase of promoter DNA binding to H3ac (left) and H4ac (right) is observed in both cell lines for *RRP22* (ratio TSA/CTRL >1) but not for *RHOB*. *CDKN1A/p21*, positive control gene known to be inactivated by histone modifications in gliomas; *GAPDH*, negative control gene not regulated by histone modifications. Abscissa, genes; ordinate, DNA amount bound to the histones (TSA/CTRL).

Taken together, *in vitro* treatment with the histone deactylase inhibitor trichostatin A caused euchromatinization of the *RRP22* but not the *RHOB* promoter in the glioblastoma cell lines U87MG and A172.

4.1.5.1 Histone modification status of *RRP22* and *RHOB* in human glioma tissues

The chromatin immunoprecipitation assay confirmed the hypotheses of the heterochromatinization of the *RRP22* but not the *RHOB* promoter in human glioma cell lines. To further address the relevance of histone modifications for the regulation of *RRP22* and *RHOB* in primary tissue, the ChIP protocol was optimized for application to the analysis of human glioma tissue samples. Chromatin of three non-neoplastic brain tissues (*NB1, -4 and -5*) and 7 glioblastomas (*T1-T7*) was isolated and prepared for the ChIP assay. Antibodies against acetylated histone H3 (associated with euchromatin) and histone H3 trimethylated at lysine residue 9 (H3K9me3, associated with heterochromatin) were used for the analyses. For the negative control gene *GAPDH*, the three non-neoplastic brain tissues and seven tumor tissues were found to demonstrate a ratio of H3ac- to H3K9me3-bound DNA invariably exceeding 1 (Figure

34). This histone modification pattern indicates a prevailing euchromatic stage of the H3-bound promoters.

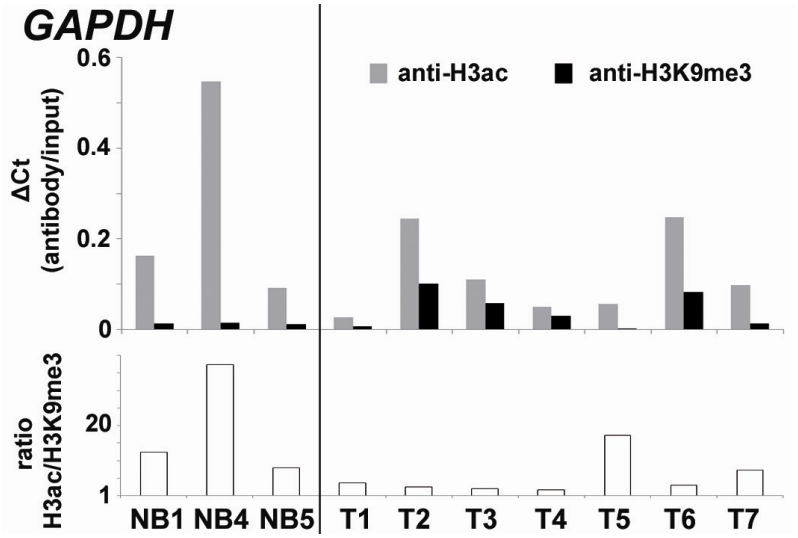

Figure 34: Chromatin immunoprecipitation assay of the control gene promoter *GAPDH* in human glioma tissues. Shown are ΔCt values (antibody/input) for chromatin immunoprecipation with antibodies against H3ac and H3K9me3 as well as the H3ac/H3K9me3 ratios for three different non-neoplastic brain tissues (NB) and 7 glioblastomas (T1-7). Note that in non-neoplastic brain tissues and also in the tumors the ratio between anti-H3ac and anti-H3K9me3 is invariably exceeding 1 indicating a prevailing euchromatic stage of the H3-bound promoters.

The same non-neoplastic tissues and tumor samples were used to investigate the promoter DNA of *RHOB* and *RRP22* bound to the euchromatic acetylated histone H3 (H3ac) or the heterochromatic methylated histone H3 (H3K9me3) (Figure 35, Figure 36). Like *GAPDH*, a similar euchromatic pattern was observed for the *RHOB* promoter (Figure 35) in the non-neoplastic tissue samples as well as in all investigated tumors.

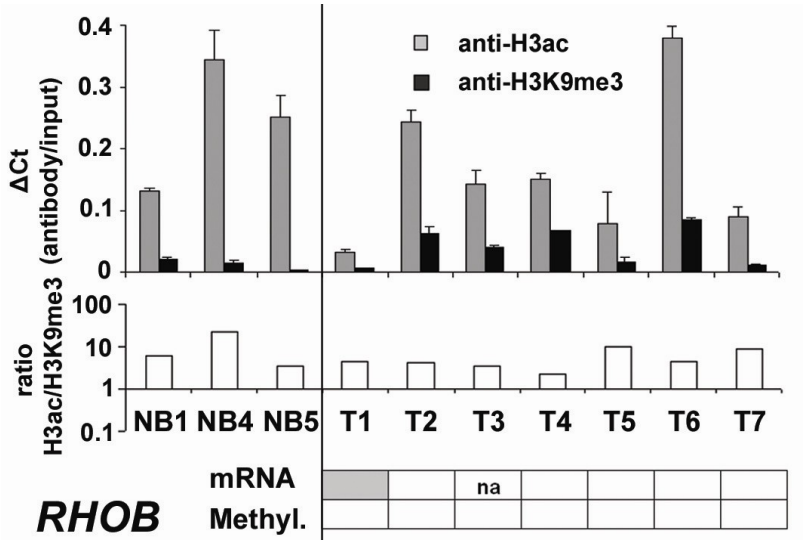

Figure 35: Chromatin immunoprecipitation is not indicative of a heterochromatinization of the *RHOB* promoter in human glioma tissues. Shown are ΔCt values (antibody/input) for chromatin immunoprecipation with antibodies against H3ac and H3K9me3 as well as the H3ac/H3K9me3 ratios for three different non-neoplastic brain tissues (NB) and 7 glioblastomas. Note that in non-neoplastic brain and tumor tissue the ratio between anti-H3ac and anti-H3K9me3 is invariably exceeding 1 indicating a prevailing euchromatic stage of the H3-bound promoters. In line with these findings the tumors do not exhibit downregulation at the mRNA level, except for slightly reduced mRNA expression levels in T1 (color-code for visualization of mRNA expression (mRNA) and methylation status (Methyl.) is the same as introduced in Figure 22).

For *RRP22*, in striking contrast, three out of the seven investigated glioblastomas (*T2*, *T3* and *T4*) exhibited a shift towards heterochromatinization of the H3-bound *RRP22* promoter (ratio H3ac/H3K9me3 <1, Figure 36, ▼) in comparison to non-neoplastic brain tissue, thus suggesting an involvement of histone modification in promoter inactivation. Notably, heterochromatinization of the *RRP22* promoter was observed alone (two out of three patients) as well as in conjunction with *RRP22* DNA hypermethylation (one out of three patients), while *RRP22* mRNA expression was strongly decreased in both of these settings.

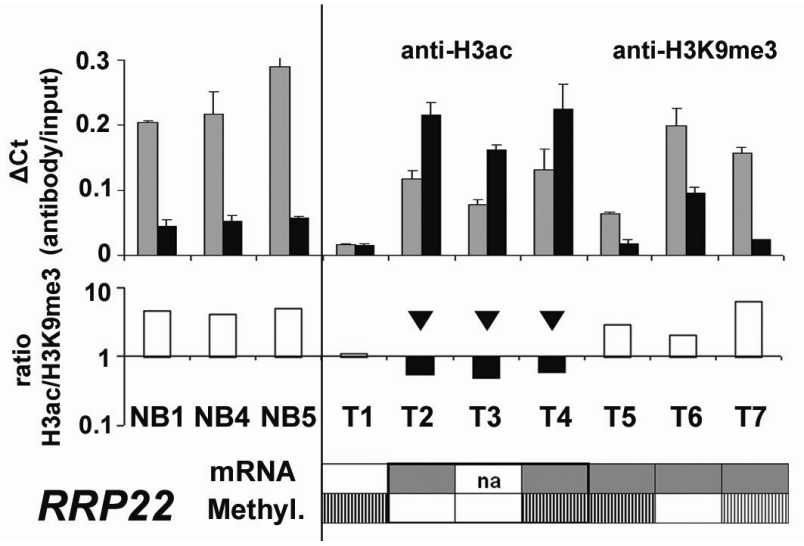

Figure 36: Chromatin immunoprecipitation assay confirmed heterochromatinization of the *RRP22* promoter in human glioma tissues. Shown are ΔCt values (antibody/input) for chromatin immunoprecipation with antibodies against H3ac and H3K9me3 as well as the H3ac/H3K9me3 ratios for three different non-neoplastic brain tissues (NB) and 7 glioblastomas (T1-7). Three glioblastomas (T2, T3 and T4) show a shift towards a heterochromatinization of the H3-bound *RRP22* promoter (ratio H3ac/H3K9me3 <1, ▼). One of these three patients has a concomitant *RRP22* hypermethylation, while the other two patients lack *RRP22* methylation. Note that also in T2 histone heterochromatinization alone is sufficient to effectively reduce *RRP22* mRNA expression levels (color-code for visualization of mRNA expression and methylation status is the same as introduced in Figure 22).

4.2 Functional analyses of ARHI in glioblastoma cell lines

The small Ras-related GTPase gene *ARHI* was molecularly characterized in previous work of our group (Riemenschneider et al 2008). Riemenschneider et al. reported on *ARHI* silencing by frequent biallelic inactivation in oligodendroglial tumors with 1p deletion and promoter hypermethylation of the retained allel. *ARHI* expression in astrocytic gliomas turned out to be normal or rather increased. In breast cancer cell lines the expression of *ARHI* suppresses clonogenic growth, reduces invasiveness and induces apoptosis (Wang et al 2003a). Other studies reported about a potential tumor suppressor function of ARHI in the pathogenesis of different human neoplasms, including pancreatic, liver, thyroid, ovarian and breast cancer cell lines (Bao et al 2002, Lu et al 2009, Weber et al 2005, Zhao et al 2010). However, the functional role of ARHI in glioblastoma cell lines had not yet been investigated.

In this doctoral thesis, further analyses were performed to investigate the functional roles of ARHI in gliomas by generating *ARHI* depleted glioblastoma cell lines. For these experiments, two glioblastoma cell lines with the highest *ARHI* mRNA transcript levels were chosen (A172, U251) to 'knock-down' the *ARHI* gene (3.3.3) by using shRNA-based RNAi experiments and stable transfection with the pcDNA^{TM} 6.2-GW/EmGFP-miR vector (Invitrogen, Carlsbad, CA). Cell-based assays were performed with these transfected cell lines to investigate the effect of ARHI depletion on cell proliferation and apoptosis.

4.2.1 Generation of ARHI-depleted glioblastoma cell lines

To analyze the impact of ARHI in glioblastoma cell lines, vector-based shRNA-mediated RNAi was used to generate glioblastoma cell lines with a stable knock-down of the *ARHI* gene. Experiments were performed in two distinct cell lines to avoid cell specific alterations. Two different hairpins (sh1, sh2) were used to avoid off-target effects of the relevant shRNAs and two different subclones of each hairpin (shX-1 and shX-2) were utilized to exclude insertion-site specific side effects (3.3.3). Before starting with the functional assays, the *ARHI* knock-down was first controlled by real-time RT-PCR (3.1.2.2). Subclones with a sufficient *ARHI* knock-down (< 25 %) were validated in a second step by western blot analysis (3.2.4) (Figure 37). Only subclones with an *ARHI* mRNA level decreased to < 25 %, and similar ARHI knock-down at the protein level were used for further experiments.

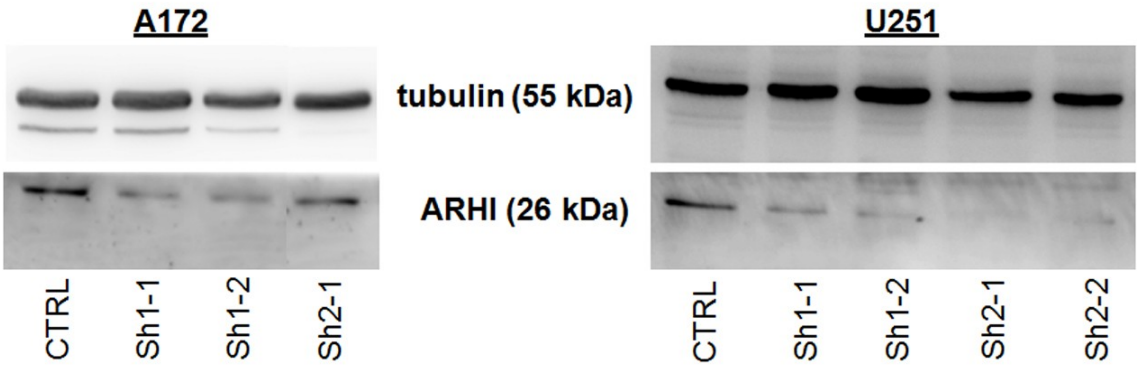

Figure 37: Western blot analysis of ARHI depleted and control cell lines A172 (left) and U251 (right). Note the reduced protein expression level in the anti-ARHI sh-RNA-treated cells as compared to the control-transfected cells. CTRL, cells transfected with a negative control vector; shX-Y (X, small hairpin; Y, subclone), ARHI-depleted cell lines; tubulin, control for equal protein loading.

.

4.3 Results of functional assays

4.3.1 Influence of ARHI knock-down on glioma cell proliferation

A commercially available colorimetric cell proliferation ELISA (Roche, Mannheim, Germany) was used to investigate the effect of ARHI on cell proliferation as described in 3.3.4.1. Three different subclones for the cell line A172 and 4 different sublones for the cell line U251 with two different hairpins in each case were analyzed relative to the control cells. The assay was reproduced in at least three independent biological experiments with 4 technical replicates each.

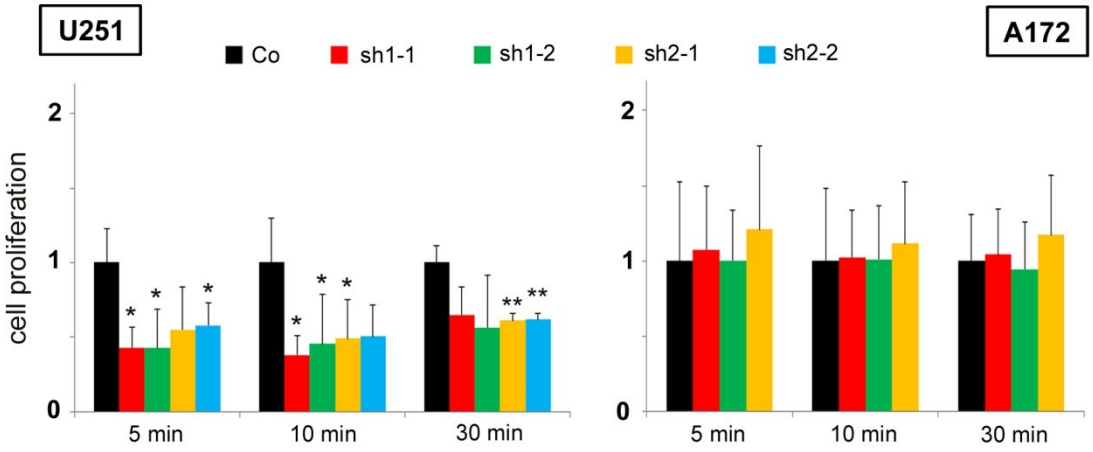

Figure 38: Results of proliferation assays in ARHI-depleted cells compared to control-transfected cells in two different cell lines (left: U251; right: A172). Proliferation was measured after 5 min, 10 min and 30 min. Data are means of three biological replicates for each subclone at each time point. Note the decreased cell proliferation in the cell line U251 for all ARHI-depleted subclones compared to control cells at each time point, while the cell line A172 appears not to be impacted by ARHI depletion. Abscissa, time points; ordinate, relative cell proliferation.

All subclones (sh1-1, sh1-2, sh2-1) of the cell line A172 exhibited no alterations in cell proliferation in the ARHI-depleted cells relative to the control cells, measured after different time points (5 min, 10 min, 30 min). In contrast, all subclones (sh1-1, sh1-2, sh2-1, sh2-2) of the cell line U251 revealed a decrease in cell proliferation in the ARHI-depleted cell lines in comparison to the control cells, even when the assay was evaluated over different time points (5 min, 10 min, 30 min). Decreased proliferation rates ranging from 100 % down to 38 % (U251, 10 min, sh1-1) were measured. For

most of the subclones these findings reached significance: subclone sh1-1 after 5 min ($p = 0.012$) and 10 min ($p = 0.022$); subclone sh1-2 after 5 min ($p = 0.030$) and 10 min ($p = 0.049$); subclone sh2-1 after 10 min ($p = 0.043$) and 30 min ($p = 0.004$); subclone sh2-2 after 5 min ($p = 0.035$) and 30 min ($p = 0.004$), whereas a few subclones showed a tendency towards decreased proliferation that did not reach the significance threshold (Figure 38). Taken together, ARHI-depletion led to a decrease in cell proliferation in one of the two selected glioma cell lines.

4.3.2 Influence of ARHI knock-down on apoptotic activity

To examine the consequence of *ARHI* knock-down on apoptosis in glioma cells, the commercially available apo-ONE® homogeneous caspase-3/7 assay (Promega, Madison, WI) and FACS-analysis were used as described in 3.3.4.2. Three ARHI-depleted subclones of the cell line A172 and 4 ARHI-depleted subclones of the cell line U251 with two different hairpins in each case were analyzed in comparison to control-transfected cells (3.3.3). The assays were reproduced in at least three independent biological experiments. In case of the caspase-3/7 assay, the biological experiments were done with three technical replicates.

Figure 39 illustrates the caspase 3/7 activity. All three subclones of the cell line A172 exhibited no alterations in the caspase 3/7 activity over a defined time period. For cell line U251, three of four subclones revealed also no changes in caspase 3/7 activity, whereas one subclone (sh1-2) indicated an increase in the caspase 3/7 activity over time; 1.23 fold change after one hour ($p = 0.043$); 1.41 fold change after one and a half hours ($p = 0.012$); 1.55 fold change after two hours ($p = 0.008$). The same subclone sh1-2 (U251) exhibited also an increase in the caspase 3/7 activity after three hours (2.68 fold change) but this latter finding was not significant due to a high standard deviation.

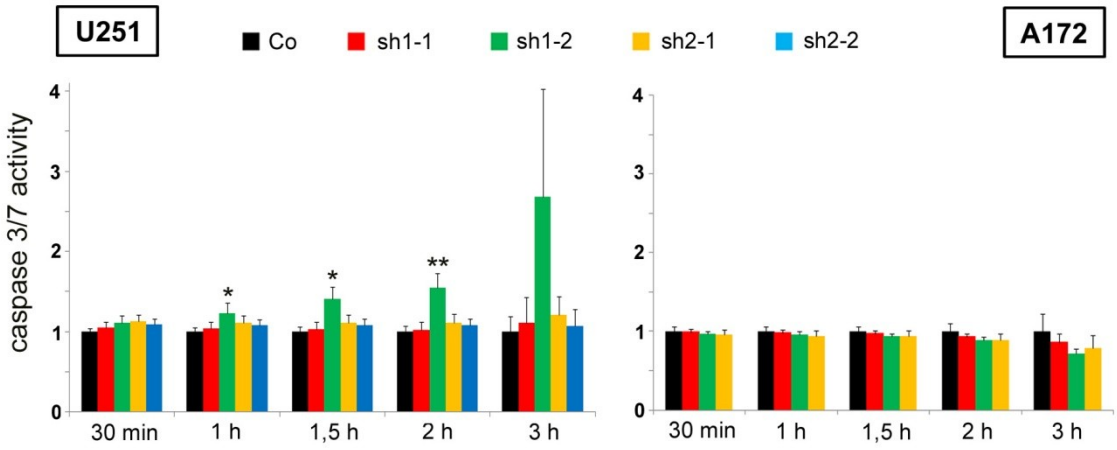

Figure 39: Caspase 3/7 assay of ARHI-depleted cells in two different cell lines (left: U251; right: A172). Caspase 3/7 activity was measured after 30 min, 1 h, 1.5 h, 2 h and 3 h. Data are means of three biological replicates for each subclone at each time point. Note the increased caspase activity in subclone sh1-2 for the cell line U251, while the other subclones and all subclones in A172 reveal no alterations. Abscissa, time points; ordinate, caspase 3/7 activity.

Bao et. al. (Bao et al 2002) reported *ARHI* as a potential tumor suppressor gene that induces apoptosis in ovarian and breast cancer cells through a caspase-independent pathway. Given the largely negative findings in the caspase 3/7-assay, the effect of *ARHI* knock-down was also investigated by FACS analysis. FACS analysis can measure cell apoptosis through a caspase-independent analysis. When measuring apoptosis by FACS analysis, mitomycin c (MMC) was used to reveal apoptotic effects. Mitomycin c binds to the DNA, inhibits DNA synthesis and therefore can initiate apoptosis (Kim et al 2003, Pirnia et al 2002).

Figure 40 shows the dot plot results of each subclone for the cell line A172 (A) and U251 (B) measured by FACS analysis. As described in 3.3.4.2, annexin V coupled to APC (allophycocyanin) was used to detect apoptotic cells. Additionally, propidium iodide, which only can permeate through damaged membranes, was used to distinguish between apoptotic and necrotic cells. In Figure 40, cells treated with mitomycin c (MMC) exhibited an increase in the annexin V staining and therefore indicate an apoptotic process (A172 Co + MMC = 3.67 %; U251 Co + MMC = 4.75 %). All subclones of the cell line A172 and three out of 4 subclones of the cell line U251 revealed no alterations. Only the subclone sh1-2 of the cell line U251 indicated a

tendency towards increased apoptosis (2.7 %). The same subclone also exhibited an increase in the caspase 3/7 activity as described above.

Taken together, ARHI-depleted cell lines did not show a consistent change in spontaneous apoptotic activity. Only a single subclone of the cell line U251 (sh1-2) exhibited a tendency towards increased apoptosis as measured by both FACS analysis and the caspase 3/7 assay.

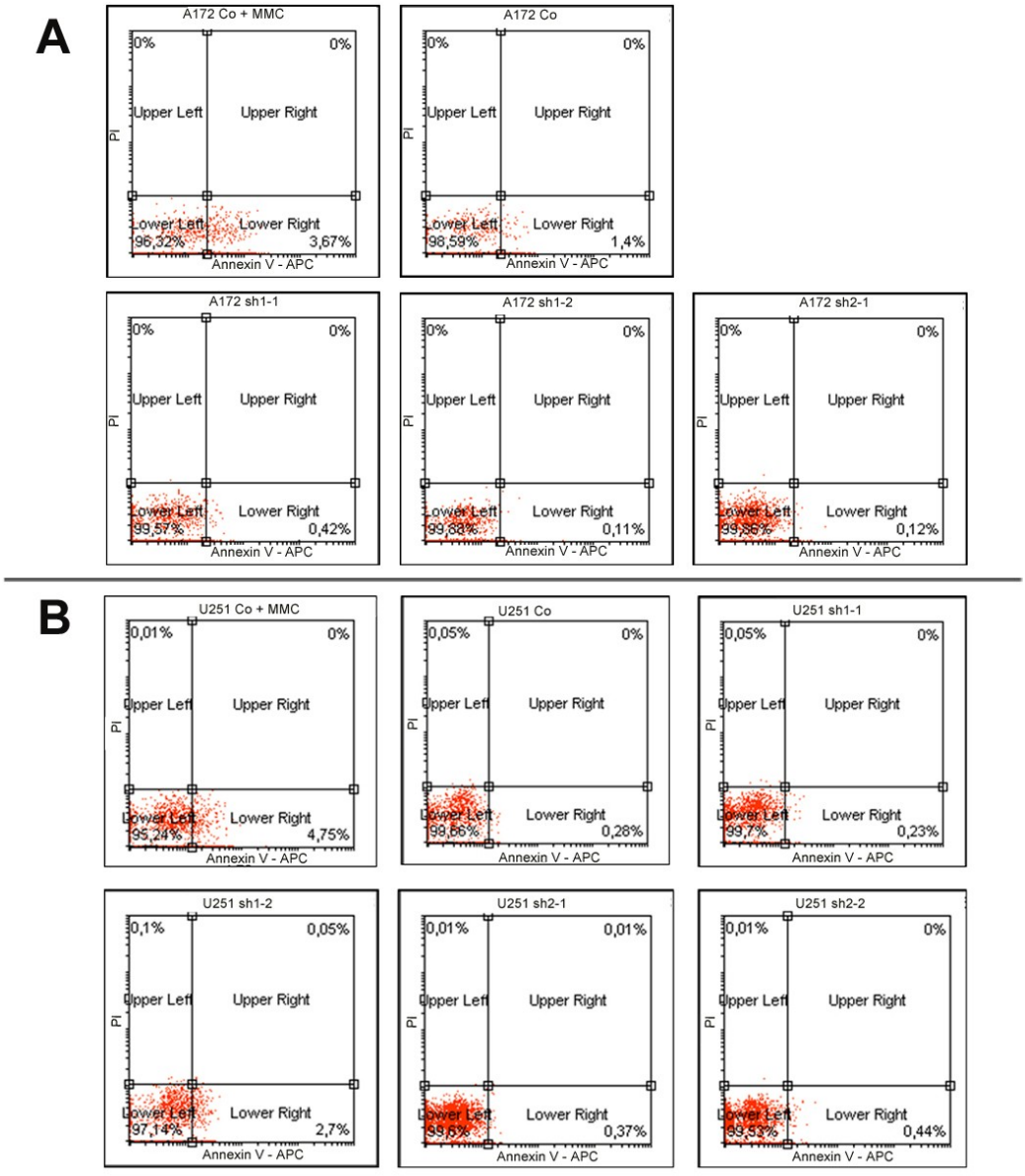

Figure 40: FACS analysis of *ARHI* knock-down cells in two different cell lines (A: A172; B: U251). Note the slight increase in apoptosis for the subclone sh1-2 of the cell line U251, while the other subclones reveal no alterations. Abcissa: Annexin – APC (allophycocyanin) stained cells; ordinate: propidium iodide (PI) stained cells. MMC (mitomycin c): positive control.

5 Discussion

Gliomas are the most common primary tumors and account for about 40 % of all tumors in the central nervous system (Louis et al 2007b). Despite surgical intervention, most glioma patients suffer from recurrences. Moreover, initially low grade diffuse gliomas are characterized by an inherent tendency for spontaneous malignant progression over time. This feature is of considerable clinical importance for the patients' prognosis. Many molecular mechanisms underlying malignant progression were identified over the last decades (Louis et al 2007b, Riemenschneider and Reifenberger 2009a). The *RAS*-oncogene is one of the most commonly mutated genes in human tumors with mutation rates ranging up to 90 % in certain tumor types such as pancreatic carcinoma (Rajalingam et al 2007). Ras belongs to the Ras superfamily, a group of small GTPases that regulate a wide spectrum of cellular processes and share pronounced sequence homologies (Bos 1989, Hall 1990, Newton 2003). While most of the Ras family members possess oncogenic properties, other members of this group were reported as tumor suppressor genes (Elam et al 2005, Finlin et al 2001, Forget et al 2002, Louro et al 2004, Riemenschneider et al 2008). The research work summarized in this doctoral thesis mainly aimed at a better understanding of the molecular pathogenesis of human gliomas, in particular concerning the involvement of small GTPase genes with potential tumor suppressor function. Therefore, a series of glioma patients was investigated for expression of four selected genes, namely *RRP22*, *RHOB*, *RASL11A* and *RERG*. The two most interesting GTPase genes (*RRP22*, *RHOB*) were selected for further analysis. In case of *RRP22,* a decreasing mRNA expression with increasing glioma malignancy was detected and the *RRP22* gene was found to be hypermethylated in glioblastoma cell lines (Elam et al 2005). The *RHOB* gene was chosen because of its good characterization in other tumor entities outside the nervous system (Delarue et al 2007, Mazieres et al 2007, Sato et al 2007) and the decreased expression found in our glioma panel compared to non-neoplastic brain tissue. Methylation analyses by sequencing of sodium bisulfite-modified DNA and mutation analyses by SSCP were utilized to characterize genetic and epigenetic mechanisms possibly accounting for the transcriptional downregulation of these genes in gliomas. In case of *RRP22*, microsatellite analysis for allelic losses were additionally performed as *RRP22* is known to be located in a chromosomal region that is often affected by allelic losses in human tumors, including gliomas (Ino et al 1999). Moreover, chromatin immunoprecipitation assays were established and carried out to

investigate the role of histone modifications as an alternative or additional cause for the observed transcriptional downregulation. Histone modifications were investigated *in vitro* in glioblastoma cell lines before and after treatment with histone deacetylase inhibitors, as well as in primary human tumor samples. Different antibodies, either detecting histone modifications associated with euchromatin (H3ac/H4ac) or with heterochromatin (H3K9me3) were used to examine the histone modification pattern in glioblastoma patients.

In addition, ARHI-depleted glioblastoma cell lines were generated to investigate the functional role of another small GTPase protein in gliomas, namely ARHI. RNAi experiments were performed with different pre-designed shRNA oligonucleotides targeting the *ARHI* gene, followed by proliferation and apoptosis assays comparing ARHI-depleted glioma cell clones with control-transfected glioma cell clones derived from two distinct established glioma cell lines.

5.1 Molecular analyses of *RRP22* in human gliomas

The Ras-related gene *RRP22* has been suggested as a tumor suppressor in glioma cells (Chen et al 2011, Elam et al 2005) but its relevance and inactivating mechanisms in glioma patient samples had not been assessed so far. As such, a comprehensive molecular analysis of *RRP22* was performed in a panel of 70 human gliomas and a reduction of *RRP22* transcript levels was found in two thirds of the investigated tumors. Interestingly, *RRP22* mRNA expression levels were significantly lower in high-grade (WHO grade III and IV) when compared to low-grade (WHO-grade II) gliomas. These findings are in accordance with a recently published study reporting on *RRP22* transcriptional down-regulation with increasing WHO grade in astrocytomas (Chen et al 2011). Taken together, the data suggest a potential role of *RRP22* inactivation in glioma progression.

RRP22 methylation analysis revealed hypermethylation of the *RRP22* 5'-CpG island in a subset of gliomas with decreased *RRP22* mRNA expression levels as well as in all glioblastoma cell lines. This finding is in line with a previous report on hypermethylation of *RRP22* in selected glioblastoma cell lines (Elam et al 2005). Furthermore, when treating A172 and U87 glioblastoma cell lines with the demetyhylating agent 5-aza-2'-deoxycytidine *in vitro,* a significant increase in *RRP22* transcript levels was found, arguing for a causal relationship between *RRP22* 5'-CpG island methylation and

decreased expression. Nevertheless, there was only a limited correlation of the *RRP22* methylation status to *RRP22* mRNA expression levels in the tumor panel. In fact, a number of *RRP22*-hypermethylated gliomas did not exhibit reduced *RRP22* transcript levels, which might be explained by the often marked degree of cellular and molecular heterogeneity of these tumors. Given that *RRP22* hypermethylation in such cases may be restricted to a subset of tumor cells, expression might still be sustained from unmethylated tumor cell subpopulations or contaminating non-neoplastic cell populations, such as microglial or lymphocytic cells. Similar pitfalls in the correlation of methylation and expression data when using lysate-base approaches have been described for other hypermethylated genes, such as *MGMT* (Felsberg et al 2009).

More importantly, however, *RRP22* hypermethylation could only explain reduced mRNA expression in a subset of tumor samples (30 out of 47 patients), suggesting that mechanisms in addition to methylation might contribute to the frequent downregulation of *RRP22* expression in human gliomas. The search for tumor-associated structural genetic alterations yielded only low frequencies of allelic losses at the *RRP22* locus on chromosome 22q12.2 and tumor-associated mutations were not detectable.

As histone modifications may serve as an important alternative mechanism of epigenetic gene inactivation (Kouzarides 2007, Schones and Zhao 2008), glioblastoma cell lines were treated *in vitro* with the histone deactylase inhibitor trichostatin A, leading to an euchromatinization of gene promoters. Indeed, trichostatin A treatment significantly increased the mRNA expression levels of *RRP22,* suggesting that histone modifications contribute to downregulation of this gene in gliomas. Chromatin immunoprecipitation after trichostatin A treatment corroborated a significant increase of *RRP22* promoter DNA bound to acetylated histones H3 (H3ac) and H4 (H4ac). The finding of a regulation of *RRP22* promoter by histone modifications was confirmed by chromatin immunoprecipitation in a separate subset of glioblastoma tissue samples. Three out of seven glioblastoma tissue samples showed a shift towards heterochromatinization of the *RRP22* promoter relative to non-neoplastic brain tissue. This heterochromatinization of *RRP22* was found alone or in coincidence with *RRP22* DNA methylation and in both settings resulted in a marked downregulation of *RRP22* transcripts. Thus, histone modifications might serve as an additional cause of *RRP22* inactivation, and either alone or in conjunction with *RRP22* 5'-CpG island hypermethylation account for the gene's frequent transcriptional downregulation in human gliomas.

Taken together, this study systematically assessed the molecular aberrations and inactivation mechanisms of *RRP22* in primary human tumors. Histone modifications either alone or together with *RRP22* 5'-CpG island hypermethylation are capable of conveying transcriptional downregulation of the *RRP22* gene in human gliomas.

5.2 Molecular analyses of *RHOB* in human gliomas

The Ras-related gene *RHOB* has also been suggested as a tumor suppressor gene candidate in human glioma cells (Baldwin et al 2008, Delmas et al 2002, Forget et al 2002, Monferran et al 2008), but its inactivation mechanism in glioma patients has not been clarified so far. Here, a panel of 70 human gliomas was used to analyze the molecular inactivation mechanisms of *RHOB*. A frequent reduction of *RHOB* transcript levels (76 %) was found in comparison to non-neoplastic brain tissue. Contrary to a recent publication (Forget et al 2002), however, a decrease of *RHOB* expression with brain tumor progression could not be corroborated. This discrepancy might be due to the fact that *RHOB* expression was investigated at the mRNA level by real-time RT-PCR, while in the cited study RHOB expression was analyzed at the protein level by Western blot analysis (Forget et al 2002).

Only a single tumor (AO23) exhibited a slightly elevated *RHOB* promoter methylation score relative to non-neoplastic brain tissue that yet did not result in decreased *RHOB* expression. Tumor-associated mutations were not detectable. Just two different *RHOB* polymorphisms were found in some patients [c.204C>T (p.Arg68Arg), c.15C>T (p.Arg5Arg)]. Both alterations represent single nucleotide exchanges that do not result in a change of the amino acid sequence of the RHOB protein.

As described above, histone modifications may serve as an important alternative mechanism of gene inactivation (Kouzarides 2007, Schones and Zhao 2008). However, the histone modification pattern for *RHOB* was neither changed in glioblastoma cell lines after trichostatin A treatment nor did it differ in primary tissue when comparing the histone pattern of tumors and non-neoplastic controls. Thus, there was no evidence for a direct effect of histone modifications on the regulation and the transcriptional silencing of the *RHOB* promoter in gliomas, as this had been reported in lung or pancreatic cancer cells (Delarue et al 2007, Mazieres et al 2007, Sato et al 2007). Nevertheless, only certain types of histone modifications, which were investigated, can be excluded. Other histone modifications or promoter sites may well convey an impact on the activation status of the *RHOB* promoter in human gliomas and

need to be assessed in subsequent studies. The fact that increased *RHOB* expression was observed after treatment with both the demethylating agent 5-aza-2'-deoxycytidine (even when only moderate) as well as the histone deactylase inhibitor trichostatin A may indicate that *RHOB* is transcriptionally repressed by other factors that themselves underlie regulation by methylation or histone modifications. In this context, it should be denoted that *RHOB* just recently has been suggested as being transcriptionally regulated by TGF-beta/Smad signaling (Vasilaki et al 2010), which appear to govern a complex intracellular transcriptional network through modulation of histones and target gene methylation (Kesari et al 2007, van Grunsven et al 2005). Moreover, *RHOB* expression has been found to be influenced by a number of additional crucial signaling molecules, such as ErbB2, Ras, EGFR, integrins and FAK, with all of them being expressed in human gliomas (Jiang et al 2004, Monferran et al 2008, Riemenschneider et al 2006, Skuli et al 2009). Further research is needed to pinpoint the most relevant molecular aberrations accounting for the frequent transcriptional downregulation of *RHOB* in glial neoplasms.

Taken together*, RHOB* seems unaffected by direct epigenetic regulatory mechanism in gliomas but appears to be transcriptional repressed by yet unidentified upstream regulators.

5.3 Molecular analyses of *RASL11A* and *RERG* in human gliomas

The Ras-related genes *RASL11A* and *RERG* have been suggested as tumor suppressors (Finlin et al 2001, Key et al 2006, Louro et al 2004) but their relevance and inactivating mechanisms in glioma patient samples had not been assessed so far. In a first step, these genes were analyzed for their mRNA expression levels in a panel of 45 human glioma tissues. Both genes were downregulated in the tumor samples compared to non-neoplastic brain tissue samples. *RASL11A* and *RERG* have not been investigated extensively in human gliomas but studies in other tumor identities outside the nervous system reported both genes to be transcriptionally downregulated (Finlin et al 2001, Louro et al 2004). However, a decreased expression level with increasing malignancy could not be detected as detected for *RRP22* or *RHOB*. Methylation analysis for *RERG* exhibited a frequent DNA hypermethylation in gliomas as well as in non-neoplastic brain tissues. This finding indicates a tissue-, and not tumor-specific methylation of *RERG* in the central nervous system. Only seven patients carried tumors with methylation scores exceeding that of non-neoplastic brain tissue but these

tumors did not exhibit reduced expression levels compared to low methylated tumor samples. One study reported on *RERG* to be hypermethylated in colorectal carcinomas, however, the degree of DNA methylation was not correlated with the respective *RERG* mRNA expression levels (Oster et al 2011). In contrast, the gene promoter of *RASL11A* was found to be unmethylated in human prostate cancer (Bastian et al 2007). Moreover, the own expression data did not reveal a clear-cut progression-associated loss of *RASL11A* expression. Thus, this gene was not further investigated for epigenetic inactivation mechanisms in human gliomas.

5.4 Functional analysis of ARHI in human glioblastoma cell lines

ARHI is one of approximately 40 known imprinted genes. The small GTPase is expressed from the paternal allele, while the maternal copy is silenced early in embryonal development (Yu et al 1999). *ARHI* belongs to the Ras superfamily. Despite strong homology (54-59 %) with the *RAS*-oncogene, *ARHI* has characteristics of a tumor suppressor gene (Yu et al 1999). As an imprinted gene, loss of ARHI function can be achieved with a “single hit” on the second active allele during carcinogenesis (Zou et al 2011). *ARHI* is located on chromosome band 1p31, a chromosomal region that is often affected by allelic losses in human oligodendrogliomas (Reifenberger et al 1994). Riemenschneider et al. found a decrease of *ARHI* mRNA transcription levels in oligodendrogliomas by frequent biallelic inactivation through allelic losses on 1p and CpG island methylation of the other allele. In contrast, biallelic inactivation of *ARHI* seems to be a rare event in astrocytic tumors including glioblastomas (Riemenschneider et al 2008). A tumor suppressor function of ARHI was reported in a broader spectrum of neoplasms including pancreatic, ovarian, breast, liver and thyroid cell lines (Bao et al 2002, Lu et al 2009, Weber et al 2005, Zhao et al 2010). In breast cancer cell lines, the ARHI protein suppresses clonogenic growth, reduces invasiveness and induces apoptosis (Wang et al 2003a). Also in other tumor entities, ARHI was found to induce cell cycle arrest and to inhibit tumor growth and angiogenesis (Bao et al 2002, Lu et al 2009, Zhao et al 2010). However, the functional roles of ARHI in gliomas had not been addressed so far.

Therefore, ARHI protein expression was knocked down in two glioblastoma cell lines using stable transfection of shRNA oligonucleotides targeting this gene or control vectors with scrambled shRNA constructs. To explore the biological relevance of ARHI for glioma cell proliferation, the commercially available colorimetric cell proliferation

ELISA was used. A decreased proliferation rate was detected in one of the two investigated glioblastoma cell lines after depletion of the ARHI protein. Interestingly, this finding was in contrary other studies suggesting ARHI as a tumor suppressor. This discrepancy might be due to cell line specific differences as no significant effect of ARHI knockdown on proliferation was observed in a second glioblastoma cell line. However, these findings may also indicate that the ARHI protein exerts different functions in distinct type of gliomas. Biallelic inactivation of *ARHI* has been shown to associate with better prognosis of patients with oligodendroglial tumors (Riemenschneider et al 2008), similar to allelic losses on chromosome 1p, which are a marker for response to radio- and chemotherapy as well as longer survival in these tumors (Cairncross et al 1998, van den Bent et al 2006). It remains to be investigate whether ARHI is a candidate gene that contributes to chemo- and radiosensitivity of 1p/19q-deleted gliomas, e.g. by studying our stably transfected cell lines for differential responses to radio- or alkylating chemotherapy *in vitro*. On the other hand, ARHI lacks promoter methylation and is even overexpressed in glioblastomas, suggesting that it may serve tumor promoting rather than tumor suppressive functions in these highly malignant gliomas.

The influence of ARHI knockdown on apoptotic activity in glioblastoma cells was examined by using the commercially available Apo-ONE homogeneous caspase-3/7 assay. Here, only a single subclone (U251 sh1-2) exhibited an increase of caspase 3/7 activity in one of the two generated ARHI depleted cell lines. This is also contrary to the suggestion of ARHI having tumor suppressor functions in glioblastoma cells. However, the positive result in just one single subclone may be due to an insertion-site specific side effect of this particular subclone. Furthermore, the impact of the detected caspase 3/7 activity and its biological relevance on apoptosis in the specific case of ARHI are unclear. One group reported that ARHI inhibits cell growth and decreases cell invasiveness through a caspase-independent mechanism in ovarian and breast cancer cells (Bao et al 2002). Therefore, additional analyses for potential effects on apoptosis were performed by FACS analysis. In line with the prior findings, this method also revealed no apoptotic effects except for the same single subclone (U251 sh1-2). This subclone (U251 sh1-2) showed a slight increase in the apoptotic marker annexin V. Again, this may argue for an insertion-site specific side effect of this particular subclone. On the other hand, the lack of significant effects on apoptosis could be also due to the fact that subclones with increased apoptotic effects were sorted out during the selection phase of generating stable cell lines. Moreover, as stated above, the

negative findings for apoptosis and proliferation may also relate to the fact that only astrocytic (glioblastoma) cell lines were used for the functional characterization of ARHI. Astrocytic tumors exhibited neither promoter hypermethylation nor loss of expression in a previous study (Riemenschneider et al 2008). Therefore, oligodendroglial cell lines could be a better *in vitro* model and should be assessed in subsequent studies. However, oligodendroglial tumor cell lines carrying the characteristic 1p/19q deletion and *IDH1* mutation are not generally available.

Taken together, the knock-down of the ARHI protein does not significantly influence glioblastoma cell apoptosis or proliferation. But interestingly, a contrary tendency could be detected, which may suggest ARHI not to be a tumor suppressor in gliomas but perhaps to be involved in chemo- and radiotherapy resistance or in oncogenic processes. Further analysis like cytotoxicity assays after treatment with chemotherapeutics and other functional assays would be of interest to better characterise the role of ARHI in gliomas.

6 Abstract

Gliomas are the most common primary tumors of the central nervous system. The oncogenic Ras genes encoding small GTPases are among the most frequently mutated protooncogenes in human cancers. Other members of this family were identified that exhibit tumor suppressive functions in different types of cancers. This doctoral thesis focuses on the molecular and functional characterization of small GTPases with potential tumor suppressor function in primary human gliomas.

Own molecular analyses of primary human glioma tissues revealed a frequent decrease in the mRNA expression levels of *RRP22*, *RHOB*, *RERG* and *RASL11A* relative to normal brain tissue. The two most interesting candidates (*RRP22, RHOB*) were selected for further analyses to characterize the molecular mechanism underlying their reduced expression in gliomas. Treatment of cultured glioblastoma cells with 5'-aza-2'-deoxycytidine or trichostatin A increased *RRP22* expression. These finding are in line with a frequent 5'-CpG island hypermethylation and heterochromatinization of the *RRP22* promoter detected in primary glioma tissue samples. Thus, DNA hypermethylation and histone modification both contribute to the frequent transcriptional downregulation of the *RRP22* gene in human gliomas. In contrast, the *RHOB* gene did not show these epigenetic alterations, suggesting that *RHOB* is transcriptionally repressed in gliomas by other, yet unknown molecular mechanisms.

Another part of this doctoral thesis addressed the functional characterization of the Ras-related gene *ARHI*, for which previous studies reported on frequent biallelic inactivation in oligodendroglial but not in astrocytic tumors including glioblastomas. To further investigate the functional role of ARHI in glioma cells, stable ARHI-depleted glioblastoma cell lines were generated and subjected to proliferation and apoptosis assays to assess functional consequences of *ARHI* downregulation. While there was no change in apoptotic activity in ARHI-depleted cells, one of two ARHI-depleted glioblastoma cell lines showed reduced proliferative activity. Additional experiments are necessary to fully understand the functional role of ARHI in gliomas.

Taken together, the results summarized in this thesis reveal new insights into the role of small GTPase genes in gliomas and the involvement of epigenetic alterations leading to transcriptional downregulation of *RRP22* in these tumors.

7 Zusammenfassung

Gliome sind die häufigsten primären Tumoren des zentralen Nervensystems. Onkogene Mutationen in Ras GTPasen stellen eine der häufigsten Veränderungen in Tumoren des Menschen dar. Kürzlich wurden neue Mitglieder dieser Proteinfamilie identifiziert, die Tumorsuppressorfunktionen aufweisen. In dieser Doktorarbeit wurden kleine GTPasen mit möglicher Tumorsupressorfunktion molekular und funktionell in humanen Gliomen untersucht.

Hierbei fand sich eine verminderte Expression der Gene *RRP22*, *RHOB*, *RERG* und *RASL11A* in einem großen Teil primärer Gliome. Die beiden Gene *RRP22* und *RHOB* wurden weitergehend hinsichtlich der ihrer verminderten Expression in Gliomen zugrundeliegenden genetischen oder epigenetischen Mechanismen hin analysiert. Für *RRP22* ergab sich in primären Gliomen und Gliomzelllinien eine aberrante DNA methylierung und eine Heterochromatinisierung des Promotobereichs. Der Nachweis einer verstärkten *RRP22* Expression in Glioblastom-Zelllinien nach Behandlung mit 5‘-aza-2‘-deoxycytidine oder Trichostatin A unterstützt diese Ergebnisse. Zusammenfassend sprechen die eigenen Resultate dafür, dass sowohl eine DNA Hypermethylierung als auch Histonmodifikationen zu einer transkriptionellen Herrunterregulation von *RRP22* in Gliomen führen. Für *RHOB* ließen sich diese Veränderungen nicht nachweisen, so dass die in Gliomen verminderte *RHOB* Expression durch andere, noch unbekannte Mechanismen bedingt sein muss.

Zusätzlich wurde ein weiteres Ras-verwandtes Gen, das *ARHI* Gen, funktionell untersucht. Dieses Gen ist in Oligodendrogliomen, aber nicht in Astrozytomen und Glioblastomen, häufig biallelisch inaktiviert und mit einer verminderten Expression detektierbar. Zunächst wurden Glioblastom-Zelllinien mit einem stabilen ARHI ‚knock-down‘ generiert, um die funktionellen Untersuchungen durchzuführen. Anschließend wurden Apoptose- und Proliferationstests durchgeführt. Während sich kein konsistenter Effekt einer verminderten *ARHI*-Expression auf die Apoptose zeigte, ergab sich in einer von zwei untersuchten Gliomzelllinien eine verminderte Proliferationsrate. Weitere Untersuchungen sind nötig, um die vollständige Funktion des ARHI-Proteins in Gliomen zu verstehen.

Insgesamt unterstreichen die Ergebnisse dieser Arbeit die Bedeutung von kleinen GTPase-Genen in Gliomen und belegen epigenetische Veränderungen als einen molekularen Mechanismus der Inaktivierung des *RRP22* Gens in Gliomen.

8 References

Baldwin RM, Parolin DA, Lorimer IA (2008). Regulation of glioblastoma cell invasion by PKC iota and RhoB. *Oncogene* **27:** 3587-3595.

Balss J, Meyer J, Mueller W, Korshunov A, Hartmann C, von Deimling A (2008). Analysis of the IDH1 codon 132 mutation in brain tumors. *Acta Neuropathol* **116:** 597-602.

Bao JJ, Le XF, Wang RY, Yuan J, Wang L, Atkinson EN *et al* (2002). Reexpression of the tumor suppressor gene ARHI induces apoptosis in ovarian and breast cancer cells through a caspase-independent calpain-dependent pathway. *Cancer Res* **62:** 7264-7272.

Bastian PJ, Ellinger J, Heukamp LC, Kahl P, Muller SC, von Rucker A (2007). Prognostic value of CpG island hypermethylation at PTGS2, RAR-beta, EDNRB, and other gene loci in patients undergoing radical prostatectomy. *Eur Urol* **51:** 665-674; discussion 674.

Bernards A, Settleman J (2004). GAP control: regulating the regulators of small GTPases. *Trends Cell Biol* **14:** 377-385.

Bigner SH, Vogelstein B (1990). Cytogenetics and molecular genetics of malignant gliomas and medulloblastoma. *Brain Pathol* **1:** 12-18.

Bos JL (1989). ras oncogenes in human cancer: a review. *Cancer Res* **49:** 4682-4689.

Budowle B, Chakraborty R, Giusti AM, Eisenberg AJ, Allen RC (1991). Analysis of the VNTR locus D1S80 by the PCR followed by high-resolution PAGE. *Am J Hum Genet* **48:** 137-144.

Burnette WN (1981). "Western blotting": electrophoretic transfer of proteins from sodium dodecyl sulfate--polyacrylamide gels to unmodified nitrocellulose and radiographic detection with antibody and radioiodinated protein A. *Anal Biochem* **112:** 195-203.

Cairncross G, Berkey B, Shaw E, Jenkins R, Scheithauer B, Brachman D *et al* (2006). Phase III trial of chemotherapy plus radiotherapy compared with radiotherapy alone for pure and mixed anaplastic oligodendroglioma: Intergroup Radiation Therapy Oncology Group Trial 9402. *J Clin Oncol* **24:** 2707-2714.

Cairncross JG, Ueki K, Zlatescu MC, Lisle DK, Finkelstein DM, Hammond RR *et al* (1998). Specific genetic predictors of chemotherapeutic response and survival in patients with anaplastic oligodendrogliomas. *J Natl Cancer Inst* **90:** 1473-1479.

Chen R, Yang L, Fang J, Huo L, Zhang M, Chen F *et al* (2011). RRP22: a novel neural tumor suppressor for astrocytoma. *Med Oncol*.

Cox AD, Der CJ (2002). Ras family signaling: therapeutic targeting. *Cancer Biol Ther* **1:** 599-606.

Delarue FL, Adnane J, Joshi B, Blaskovich MA, Wang DA, Hawker J *et al* (2007). Farnesyltransferase and geranylgeranyltransferase I inhibitors upregulate RhoB expression by HDAC1 dissociation, HAT association and histone acetylation of the RhoB promoter. *Oncogene* **26:** 633-640.

Delmas C, Heliez C, Cohen-Jonathan E, End D, Bonnet J, Favre G *et al* (2002). Farnesyltransferase inhibitor, R115777, reverses the resistance of human glioma cell lines to ionizing radiation. *Int J Cancer* **100:** 43-48.

Di Rocco F, Carroll RS, Zhang J, Black PM (1998). Platelet-derived growth factor and its receptor expression in human oligodendrogliomas. *Neurosurgery* **42:** 341-346.

Du W, Prendergast GC (1999). Geranylgeranylated RhoB mediates suppression of human tumor cell growth by farnesyltransferase inhibitors. *Cancer Res* **59:** 5492-5496.

Elam C, Hesson L, Vos MD, Eckfeld K, Ellis CA, Bell A *et al* (2005). RRP22 is a farnesylated, nucleolar, Ras-related protein with tumor suppressor potential. *Cancer Res* **65:** 3117-3125.

Fallon KB, Palmer CA, Roth KA, Nabors LB, Wang W, Carpenter M *et al* (2004). Prognostic value of 1p, 19q, 9p, 10q, and EGFR-FISH analyses in recurrent oligodendrogliomas. *J Neuropathol Exp Neurol* **63:** 314-322.

Felsberg J, Rapp M, Loeser S, Fimmers R, Stummer W, Goeppert M *et al* (2009). Prognostic significance of molecular markers and extent of resection in primary glioblastoma patients. *Clin Cancer Res* **15:** 6683-6693.

Finlin BS, Gau CL, Murphy GA, Shao H, Kimel T, Seitz RS *et al* (2001). RERG is a novel ras-related, estrogen-regulated and growth-inhibitory gene in breast cancer. *J Biol Chem* **276:** 42259-42267.

Forget MA, Desrosiers RR, Del M, Moumdjian R, Shedid D, Berthelet F *et al* (2002). The expression of rho proteins decreases with human brain tumor progression: potential tumor markers. *Clin Exp Metastasis* **19:** 9-15.

Fritz G, Kaina B (2001). Transcriptional activation of the small GTPase gene rhoB by genotoxic stress is regulated via a CCAAT element. *Nucleic Acids Res* **29:** 792-798.

Griffin CA, Burger P, Morsberger L, Yonescu R, Swierczynski S, Weingart JD *et al* (2006). Identification of der(1;19)(q10;p10) in five oligodendrogliomas suggests mechanism of concurrent 1p and 19q loss. *J Neuropathol Exp Neurol* **65:** 988-994.

Grossman SA, Batara JF (2004). Current management of glioblastoma multiforme. *Semin Oncol* **31:** 635-644.

Hall A (1990). The cellular functions of small GTP-binding proteins. *Science* **249:** 635-640.

Hayatsu H, Shiragami M (1979). Reaction of bisulfite with the 5-hydroxymethyl group in pyrimidines and in phage DNAs. *Biochemistry* **18:** 632-637.

Hegi ME, Diserens AC, Gorlia T, Hamou MF, de Tribolet N, Weller M *et al* (2005). MGMT gene silencing and benefit from temozolomide in glioblastoma. *N Engl J Med* **352:** 997-1003.

Henson JW (2006). Treatment of glioblastoma multiforme: a new standard. *Arch Neurol* **63:** 337-341.

Herman JG, Graff JR, Myohanen S, Nelkin BD, Baylin SB (1996). Methylation-specific PCR: a novel PCR assay for methylation status of CpG islands. *Proc Natl Acad Sci U S A* **93:** 9821-9826.

Hermanson M, Funa K, Hartman M, Claesson-Welsh L, Heldin CH, Westermark B *et al* (1992). Platelet-derived growth factor and its receptors in human glioma tissue: expression of messenger RNA and protein suggests the presence of autocrine and paracrine loops. *Cancer Res* **52:** 3213-3219.

Ino Y, Silver JS, Blazejewski L, Nishikawa R, Matsutani M, von Deimling A *et al* (1999). Common regions of deletion on chromosome 22q12.3-q13.1 and 22q13.2 in human astrocytomas appear related to malignancy grade. *J Neuropathol Exp Neurol* **58:** 881-885.

Jenkins RB, Blair H, Ballman KV, Giannini C, Arusell RM, Law M *et al* (2006). A t(1;19)(q10;p10) mediates the combined deletions of 1p and 19q and predicts a better prognosis of patients with oligodendroglioma. *Cancer Res* **66:** 9852-9861.

Jeuken JW, von Deimling A, Wesseling P (2004). Molecular pathogenesis of oligodendroglial tumors. *J Neurooncol* **70:** 161-181.

Jiang K, Delarue FL, Sebti SM (2004). EGFR, ErbB2 and Ras but not Src suppress RhoB expression while ectopic expression of RhoB antagonizes oncogene-mediated transformation. *Oncogene* **23:** 1136-1145.

Jiang Y, Matevossian A, Huang HS, Straubhaar J, Akbarian S (2008). Isolation of neuronal chromatin from brain tissue. *BMC Neurosci* **9:** 42.

Kanai M, Crowe MS, Zheng Y, Vande Woude GF, Fukasawa K (2010). RhoA and RhoC are both required for the ROCK II-dependent promotion of centrosome duplication. *Oncogene* **29:** 6040-6050.

Karlsson R, Pedersen ED, Wang Z, Brakebusch C (2009). Rho GTPase function in tumorigenesis. *Biochim Biophys Acta* **1796:** 91-98.

Kesari S, Jackson-Grusby L, Stiles CD (2007). "Smad"eningly erratic: target gene methylation determines whether TGFbeta promotes or suppresses malignant glioma. *Dev Cell* **12:** 324-325.

Key MD, Andres DA, Der CJ, Repasky GA (2006). Characterization of RERG: an estrogen-regulated tumor suppressor gene. *Methods Enzymol* **407:** 513-527.

Kim TI, Tchah H, Lee SA, Sung K, Cho BJ, Kook MS (2003). Apoptosis in keratocytes caused by mitomycin C. *Invest Ophthalmol Vis Sci* **44:** 1912-1917.

Kouzarides T (2007). Chromatin modifications and their function. *Cell* **128:** 693-705.

Laemmli UK (1970). Cleavage of structural proteins during the assembly of the head of bacteriophage T4. *Nature* **227:** 680-685.

Litt M, Luty JA (1989). A hypervariable microsatellite revealed by in vitro amplification of a dinucleotide repeat within the cardiac muscle actin gene. *Am J Hum Genet* **44:** 397-401.

Livak KJ, Schmittgen TD (2001). Analysis of relative gene expression data using real-time quantitative PCR and the 2(-Delta Delta C(T)) Method. *Methods* **25:** 402-408.

Louis DN, Ohgaki H, Wiestler OD, Cavenee WK (2007a). WHO Classification of Tumours of the Central Nervous System, 4th edn. IARC Press: Lyon.

Louis DN, Ohgaki H, Wiestler OD, Cavenee WK, Burger PC, Jouvet A *et al* (2007b). The 2007 WHO classification of tumours of the central nervous system. *Acta Neuropathol* **114:** 97-109.

Louro R, Nakaya HI, Paquola AC, Martins EA, da Silva AM, Verjovski-Almeida S *et al* (2004). RASL11A, member of a novel small monomeric GTPase gene family, is down-regulated in prostate tumors. *Biochem Biophys Res Commun* **316:** 618-627.

Lowry OH, Rosebrough NJ, Farr AL, Randall RJ (1951). Protein measurement with the Folin phenol reagent. *J Biol Chem* **193:** 265-275.

Lu X, Qian J, Yu Y, Yang H, Li J (2009). Expression of the tumor suppressor ARHI inhibits the growth of pancreatic cancer cells by inducing G1 cell cycle arrest. *Oncol Rep* **22:** 635-640.

Malumbres M, Barbacid M (2003). RAS oncogenes: the first 30 years. *Nat Rev Cancer* **3:** 459-465.

Maxam AM, Gilbert W (1980). Sequencing end-labeled DNA with base-specific chemical cleavages. *Methods Enzymol* **65:** 499-560.

Mazieres J, Tovar D, He B, Nieto-Acosta J, Marty-Detraves C, Clanet C *et al* (2007). Epigenetic regulation of RhoB loss of expression in lung cancer. *BMC Cancer* **7:** 220.

Mitchell P, Ellison DW, Mendelow AD (2005). Surgery for malignant gliomas: mechanistic reasoning and slippery statistics. *Lancet Neurol* **4:** 413-422.

Mollemann M, Wolter M, Felsberg J, Collins VP, Reifenberger G (2005). Frequent promoter hypermethylation and low expression of the MGMT gene in oligodendroglial tumors. *Int J Cancer* **113:** 379-385.

Monferran S, Skuli N, Delmas C, Favre G, Bonnet J, Cohen-Jonathan-Moyal E *et al* (2008). Alphavbeta3 and alphavbeta5 integrins control glioma cell response to ionising radiation through ILK and RhoB. *Int J Cancer* **123:** 357-364.

Mullis K, Faloona F, Scharf S, Saiki R, Horn G, Erlich H (1986). Specific enzymatic amplification of DNA in vitro: the polymerase chain reaction. *Cold Spring Harb Symp Quant Biol* **51 Pt 1:** 263-273.

Newton HB (2003). Molecular neuro-oncology and development of targeted therapeutic strategies for brain tumors. Part 1: Growth factor and Ras signaling pathways. *Expert Rev Anticancer Ther* **3:** 595-614.

Nicoletti I, Migliorati G, Pagliacci MC, Grignani F, Riccardi C (1991). A rapid and simple method for measuring thymocyte apoptosis by propidium iodide staining and flow cytometry. *J Immunol Methods* **139:** 271-279.

Nielsen E, Cheung AY, Ueda T (2008). The regulatory RAB and ARF GTPases for vesicular trafficking. *Plant Physiol* **147:** 1516-1526.

Norden AD, Wen PY (2006). Glioma therapy in adults. *Neurologist* **12:** 279-292.

Ohgaki H, Kleihues P (2005). Population-based studies on incidence, survival rates, and genetic alterations in astrocytic and oligodendroglial gliomas. *J Neuropathol Exp Neurol* **64:** 479-489.

Ohgaki H, Kleihues P (2007). Genetic pathways to primary and secondary glioblastoma. *Am J Pathol* **170:** 1445-1453.

Orita M, Iwahana H, Kanazawa H, Hayashi K, Sekiya T (1989). Detection of polymorphisms of human DNA by gel electrophoresis as single-strand conformation polymorphisms. *Proc Natl Acad Sci U S A* **86:** 2766-2770.

Oster B, Thorsen K, Lamy P, Wojdacz TK, Hansen LL, Birkenkamp-Demtroder K *et al* (2011). Identification and validation of highly frequent CpG island hypermethylation in colorectal adenomas and carcinomas. *Int J Cancer*.

Perry A, Tonk V, McIntire DD, White CL, 3rd (1997). Interphase cytogenetic (in situ hybridization) analysis of astrocytomas using archival, formalin-fixed, paraffin-embedded tissue and nonfluorescent light microscopy. *Am J Clin Pathol* **108:** 166-174.

Pirnia F, Schneider E, Betticher DC, Borner MM (2002). Mitomycin C induces apoptosis and caspase-8 and -9 processing through a caspase-3 and Fas-independent pathway. *Cell Death Differ* **9:** 905-914.

Pistoni M, Verrecchia A, Doni M, Guccione E, Amati B (2010). Chromatin association and regulation of rDNA transcription by the Ras-family protein RasL11a. *EMBO J* **29:** 1215-1224.

Porstmann T, Ternynck T, Avrameas S (1985). Quantitation of 5-bromo-2-deoxyuridine incorporation into DNA: an enzyme immunoassay for the assessment of the lymphoid cell proliferative response. *J Immunol Methods* **82:** 169-179.

Prendergast GC (2001). Actin' up: RhoB in cancer and apoptosis. *Nat Rev Cancer* **1:** 162-168.

Rajalingam K, Schreck R, Rapp UR, Albert S (2007). Ras oncogenes and their downstream targets. *Biochim Biophys Acta* **1773:** 1177-1195.

Reifenberger G, Louis DN (2003). Oligodendroglioma: toward molecular definitions in diagnostic neuro-oncology. *J Neuropathol Exp Neurol* **62:** 111-126.

Reifenberger G, Collins VP (2004). Pathology and molecular genetics of astrocytic gliomas. *J Mol Med* **82:** 656-670.

Reifenberger J, Reifenberger G, Liu L, James CD, Wechsler W, Collins VP (1994). Molecular genetic analysis of oligodendroglial tumors shows preferential allelic deletions on 19q and 1p. *Am J Pathol* **145:** 1175-1190.

Riemenschneider MJ, Betensky RA, Pasedag SM, Louis DN (2006). AKT activation in human glioblastomas enhances proliferation via TSC2 and S6 kinase signaling. *Cancer Res* **66:** 5618-5623.

Riemenschneider MJ, Reifenberger J, Reifenberger G (2008). Frequent biallelic inactivation and transcriptional silencing of the DIRAS3 gene at 1p31 in oligodendroglial tumors with 1p loss. *Int J Cancer* **122:** 2503-2510.

Riemenschneider MJ, Reifenberger G (2009a). Molecular neuropathology of gliomas. *Int J Mol Sci* **10:** 184-212.

Riemenschneider MJ, Reifenberger G (2009b). Novel insights into the pathogenesis of gliomas based on large-scale molecular profiling approaches. *Curr Opin Neurol* **22:** 619-624.

Riemenschneider MJ, Jeuken JW, Wesseling P, Reifenberger G (2010). Molecular diagnostics of gliomas: state of the art. *Acta Neuropathol* **120:** 567-584.

Saiki RK, Scharf S, Faloona F, Mullis KB, Horn GT, Erlich HA *et al* (1985). Enzymatic amplification of beta-globin genomic sequences and restriction site analysis for diagnosis of sickle cell anemia. *Science* **230:** 1350-1354.

Sanson M, Marie Y, Paris S, Idbaih A, Laffaire J, Ducray F *et al* (2009). Isocitrate dehydrogenase 1 codon 132 mutation is an important prognostic biomarker in gliomas. *J Clin Oncol* **27:** 4150-4154.

Sato N, Fukui T, Taniguchi T, Yokoyama T, Kondo M, Nagasaka T *et al* (2007). RhoB is frequently downregulated in non-small-cell lung cancer and resides in the 2p24 homozygous deletion region of a lung cancer cell line. *International Journal of Cancer* **120:** 543-551.

Sayagues JM, Tabernero MD, Maillo A (2007). [Cytogenetic alterations in meningioma tumors and their impact on disease outcome]. *Med Clin (Barc)* **128:** 226-232.

Schagger H (2006). Tricine-SDS-PAGE. *Nat Protoc* **1:** 16-22.

Schmidt A, Hall A (2002). Guanine nucleotide exchange factors for Rho GTPases: turning on the switch. *Genes Dev* **16:** 1587-1609.

Schones DE, Zhao K (2008). Genome-wide approaches to studying chromatin modifications. *Nat Rev Genet* **9:** 179-191.

Schrock E, Blume C, Meffert MC, du Manoir S, Bersch W, Kiessling M *et al* (1996). Recurrent gain of chromosome arm 7q in low-grade astrocytic tumors studied by comparative genomic hybridization. *Genes Chromosomes Cancer* **15:** 199-205.

Schwartzbaum JA, Fisher JL, Aldape KD, Wrensch M (2006). Epidemiology and molecular pathology of glioma. *Nat Clin Pract Neurol* **2:** 494-503; quiz 491 p following 516.

Skuli N, Monferran S, Delmas C, Lajoie-Mazenc I, Favre G, Toulas C *et al* (2006). Activation of RhoB by hypoxia controls hypoxia-inducible factor-1alpha stabilization through glycogen synthase kinase-3 in U87 glioblastoma cells. *Cancer Res* **66:** 482-489.

Skuli N, Monferran S, Delmas C, Favre G, Bonnet J, Toulas C *et al* (2009). Alphavbeta3/alphavbeta5 integrins-FAK-RhoB: a novel pathway for hypoxia regulation in glioblastoma. *Cancer Res* **69:** 3308-3316.

Stupp R, Mason WP, van den Bent MJ, Weller M, Fisher B, Taphoorn MJ *et al* (2005). Radiotherapy plus concomitant and adjuvant temozolomide for glioblastoma. *N Engl J Med* **352:** 987-996.

Tepel M, Roerig P, Wolter M, Gutmann DH, Perry A, Reifenberger G *et al* (2008). Frequent promoter hypermethylation and transcriptional downregulation of the NDRG2 gene at 14q11.2 in primary glioblastoma. *Int J Cancer* **123:** 2080-2086.

Towbin H, Staehelin T, Gordon J (1979). Electrophoretic transfer of proteins from polyacrylamide gels to nitrocellulose sheets: procedure and some applications. *Proc Natl Acad Sci U S A* **76:** 4350-4354.

van den Bent MJ, Carpentier AF, Brandes AA, Sanson M, Taphoorn MJ, Bernsen HJ *et al* (2006). Adjuvant procarbazine, lomustine, and vincristine improves progression-free survival but not overall survival in newly diagnosed anaplastic oligodendrogliomas and oligoastrocytomas: a randomized European Organisation for Research and Treatment of Cancer phase III trial. *J Clin Oncol* **24:** 2715-2722.

van den Bent MJ, Dubbink HJ, Marie Y, Brandes AA, Taphoorn MJ, Wesseling P *et al* (2010). IDH1 and IDH2 mutations are prognostic but not predictive for outcome in anaplastic oligodendroglial tumors: a report of the European Organization for Research and Treatment of Cancer Brain Tumor Group. *Clin Cancer Res* **16:** 1597-1604.

van Engeland M, Ramaekers FC, Schutte B, Reutelingsperger CP (1996). A novel assay to measure loss of plasma membrane asymmetry during apoptosis of adherent cells in culture. *Cytometry* **24:** 131-139.

van Grunsven LA, Verstappen G, Huylebroeck D, Verschueren K (2005). Smads and chromatin modulation. *Cytokine Growth Factor Rev* **16:** 495-512.

Vasilaki E, Papadimitriou E, Tajadura V, Ridley AJ, Stournaras C, Kardassis D (2010). Transcriptional regulation of the small GTPase RhoB gene by TGF{beta}-induced signaling pathways. *FASEB J* **24:** 891-905.

Wang AG, Fang W, Han YH, Cho SM, Choi JY, Lee KH *et al* (2006). Expression of the RERG gene is gender-dependent in hepatocellular carcinoma and regulated by histone deacetyltransferases. *J Korean Med Sci* **21:** 891-896.

Wang L, Hoque A, Luo RZ, Yuan J, Lu Z, Nishimoto A *et al* (2003a). Loss of the expression of the tumor suppressor gene ARHI is associated with progression of breast cancer. *Clin Cancer Res* **9:** 3660-3666.

Wang S, Yan-Neale Y, Fischer D, Zeremski M, Cai R, Zhu J *et al* (2003b). Histone deacetylase 1 represses the small GTPase RhoB expression in human nonsmall lung carcinoma cell line. *Oncogene* **22:** 6204-6213.

Watanabe T, Katayama Y, Yoshino A, Yachi K, Ohta T, Ogino A *et al* (2007). Aberrant hypermethylation of p14ARF and O6-methylguanine-DNA methyltransferase genes in astrocytoma progression. *Brain Pathol* **17:** 5-10.

Weber F, Aldred MA, Morrison CD, Plass C, Frilling A, Broelsch CE *et al* (2005). Silencing of the maternally imprinted tumor suppressor ARHI contributes to follicular thyroid carcinogenesis. *J Clin Endocrinol Metab* **90:** 1149-1155.

Weber JL, May PE (1989). Abundant class of human DNA polymorphisms which can be typed using the polymerase chain reaction. *Am J Hum Genet* **44:** 388-396.

Weller M, Felsberg J, Hartmann C, Berger H, Steinbach JP, Schramm J *et al* (2009). Molecular predictors of progression-free and overall survival in patients with newly diagnosed glioblastoma: a prospective translational study of the German Glioma Network. *J Clin Oncol* **27:** 5743-5750.

Wennerberg K, Rossman KL, Der CJ (2005). The Ras superfamily at a glance. *J Cell Sci* **118:** 843-846.

Wick W, Weller M (2009). Classification and management of anaplastic gliomas. *Curr Opin Neurol* **22:** 650-656.

Wittinghofer A, Nassar N (1996). How Ras-related proteins talk to their effectors. *Trends Biochem Sci* **21:** 488-491.

Wolter M, Reifenberger J, Blaschke B, Ichimura K, Schmidt EE, Collins VP *et al* (2001). Oligodendroglial tumors frequently demonstrate hypermethylation of the CDKN2A (MTS1, p16INK4a), p14ARF, and CDKN2B (MTS2, p15INK4b) tumor suppressor genes. *J Neuropathol Exp Neurol* **60:** 1170-1180.

Wyllie AH, Kerr JF, Currie AR (1980). Cell death: the significance of apoptosis. *Int Rev Cytol* **68:** 251-306.

Yin D, Ong JM, Hu J, Desmond JC, Kawamata N, Konda BM *et al* (2007). Suberoylanilide hydroxamic acid, a histone deacetylase inhibitor: effects on gene expression and growth of glioma cells in vitro and in vivo. *Clin Cancer Res* **13:** 1045-1052.

Yoon YS, Choo JH, Yoo T, Kang K, Chung JH (2007). RhoB is epigenetically regulated in an age- and tissue-specific manner. *Biochem Biophys Res Commun* **362:** 164-169.

Yu Y, Xu F, Peng H, Fang X, Zhao S, Li Y *et al* (1999). NOEY2 (ARHI), an imprinted putative tumor suppressor gene in ovarian and breast carcinomas. *Proc Natl Acad Sci U S A* **96:** 214-219.

Yuan J, Luo RZ, Fujii S, Wang L, Hu W, Andreeff M *et al* (2003). Aberrant methylation and silencing of ARHI, an imprinted tumor suppressor gene in which the function is lost in breast cancers. *Cancer Res* **63:** 4174-4180.

Zhao X, Li J, Zhuo J, Cai L (2010). Reexpression of ARHI inhibits tumor growth and angiogenesis and impairs the mTOR/VEGF pathway in hepatocellular carcinoma. *Biochem Biophys Res Commun* **403:** 417-421.

Zou CF, Jia L, Jin H, Yao M, Zhao N, Huan J *et al* (2011). Re-expression of ARHI (DIRAS3) induces autophagy in breast cancer cells and enhances the inhibitory effect of paclitaxel. *BMC Cancer* **11:** 22.

Zucman-Rossi J, Legoix P, Thomas G (1996). Identification of new members of the Gas2 and Ras families in the 22q12 chromosome region. *Genomics* **38:** 247-254.

9 Danksagung

Mein besonderer Dank gilt Herrn Prof. Dr. Guido Reifenberger für die Möglichkeit, meine Promotion am Institut für Neuropathologie der Heinrich-Heine-Universität Düsseldorf durchführen zu können sowie für die freundliche Unterstützung und fundierte Beratung bei der Durchführung dieser Arbeit.

Mein weiterer großer Dank gilt Herrn Prof. Dr. Markus Riemenschneider für die Überlassung des interessanten Promotionsthemas und seine Betreuung während der gesamten Promotion sowie für die motivierende Beratung und Unterstützung dieser Arbeit.

Bei Herrn Prof. Dr. Dieter Willbold bedanke ich mich besonders für die freundliche Übernahme der Betreuung meiner Dissertation seitens der Mathematisch-Naturwissenschaftlichen Fakultät der Heinrich-Heine-Universität Düsseldorf und die Erstellung des Korreferats.

Ich möchte auch der gesamten Arbeitsgruppe am Institut für Neuropathologie für die praktische Unterstützung der experimentellen Arbeiten und für die zahlreichen Ratschläge, die wesentlich zum Gelingen der Arbeit beigetragen haben, Dank sagen. Insbesondere gilt mein Dank

… Nadine Lottmann für ihre Hilfsbereitschaft im Labor

… Franziska Liesenberg, die mit mir die Höhen und Tiefen der Doktorandenzeit durchlebt hat und mir immer mit Rat und Tat zu Seite stand

… Dr. Marietta Wolter für ihre Hilfsbereitschaft in allen Belangen

… Dr. Daniela Karra für ihr großes Engagement und ihre immer sinnvollen Tipps zu meiner Arbeit

…Nina Graffmann und Isabelle Messner für die freundliche Unterstützung und die Bereitstellung der Laborgeräte

Dem ganzen Institut möchte ich für die angenehme Arbeitsatmosphäre und die großartige Hilfsbereitschaft danken.

Mein herzlicher Dank gilt meinen Eltern, die mich von Anfang an bedenkenlos unterstützten und immer an mich geglaubt haben sowie meiner Schwester für ihre stets aufbauenden Worte und dafür, dass sie mir immer zur Seite stand.

Meinem Freund Gregor Hansen danke ich von ganzem Herzen, für seine Geduld, sein Verständnis und seinen starken Rückhalt, vor allem in der letzten Phase meiner Dissertation.

10 Ehrenwörtliche Erklärung

Hiermit erkläre ich, dass ich die vorliegende Dissertation eigenständig und ohne unerlaubte Hilfe angefertigt und diese in der vorgelegten oder in ähnlicher Form noch bei keiner anderen Institution eingereicht habe.

Ort, Datum Unterschrift